nagra
National Cooperative for the
Disposal of Radioactive Waste

TECHNICAL REPORT 01-05

Indications for self-sealing of a cementitious repository for low- and intermediate-level waste

September 2001

W. Pfingsten

Labor für Endlagersicherheit (LES/PSI)

Hardstrasse 73, CH-5430 Wettingen/Switzerland, Telephone +41-56-437 11 11

nagra
National Cooperative for the
Disposal of Radioactive Waste

TECHNICAL REPORT 01-05

Indications for self-sealing of a cementitious repository for low- and intermediate-level waste

September 2001

W. Pfingsten

Labor für Endlagersicherheit (LES/PSI)

Hardstrasse 73, CH-5430 Wettingen/Switzerland, Telephone +41-56-437 11 11

This report was prepared on behalf of Nagra. The viewpoints presented and conclusions reached are those of the author(s) and do not necessarily represent those of Nagra.

PREFACE

The Laboratory for Waste Management at the Paul Scherrer Institut is performing work to develop and test models as well as to acquire specific data relevant to performance assessments of planned Swiss nuclear waste repositories. These investigations are undertaken in close co-operation with, and with the financial support of, the National Co-operative for the Disposal of Radioactive Waste (Nagra). The present report is issued simultaneously as a PSI-Bericht and a Nagra Technical Report.

ISSN 1015-2636

ABSTRACT

Repositories for low and intermediate level nuclear waste contain large amounts of cementitious material. As a consequence of the interaction with formation waters, the cement will be degraded forming secondary minerals. The amount of precipitating secondary minerals depends on the chemical composition of the formation water. Furthermore, in the vicinity of the repository the hydraulic conditions and the parameters describing mass (radionuclide) transport will change with time during the cement degradation phase. As a result, porosity changes due to mineral and cement reactions will influence permeability and diffusivity: formation water rich in CO_2 will lead to calcite precipitation in the water conducting zones surrounding the cementitious waste repository and, therefore, will have an impact on the radionuclide release from the cementitious repository into the host rock environment.

Laboratory column experiments showed concurrent porosity and permeability changes during degradation of porous cement discs. However, very different quantitative results have been observed when CO_2-rich or pure water were used. The sequentially coupled flow, transport and chemical reaction code, MCOTAC, is used to include such observations in the modelling. A porosity-permeability and a porosity-diffusivity relation are used for describing cement degradation and related secondary mineral precipitation. For these complex coupled processes one-dimensional modelling has reached its limits of applicability. Therefore, two-dimensional model calculations are used to predict the temporal evolution of transport parameters for radionuclides within a “small scale” near-field of a cementitious waste repository. Mineral reactions influence hydraulic and transport parameters within such a near-field, causing reduced solute transport in the vicinity of the repository due to porosity and permeability changes at the rock-repository-interface. Also, the transport of radionuclides from the repository may be drastically reduced by porosity and permeability decreases. This is especially important for those radionuclides which show little or no sorption, since only the transport parameters (water flow velocity, dispersion and diffusion) will influence their migration behaviour. Within the “small scale” porous medium approach, coupling of chemical reactions and hydrodynamic parameters indicates a self sealing barrier at the host rock-repository interface for several scenarios. This barrier might persist for very long times and effectively contain radionuclides within the engineered repository system.

ZUSAMMENFASSUNG

Endlager für schwach- und mittelradioaktiven Abfall werden zu einem Grossteil aus Zement bestehen. Aufgrund der Wechselwirkung mit dem Wirtsgestein wird der Zement langsam degradiert und Sekundärminerale werden ausfallen. Das Ausmass dieser Ausfällungen hängt dabei von der chemischen Zusammensetzung des Wassers im Wirtsgestein ab. Darüber hinaus werden sich während der Zementdegradierung die hydraulischen und physikalischen Transportbedingungen für Radionuklide in der Umgebung des Endlagers mit der Zeit verändern. Porositätsänderungen sind die Folge der Zement- und Mineralreaktionen, wobei diese die Permeabilität und Diffusivität beeinflussen: CO_2-reiches Gesteinswasser führt zu Calcitausfällungen in den wasserführenden Zonen um das zementhaltige Endlager, was die Freisetzung von Radionukliden vom Endlager in das umgebende Gestein beeinflusst.

In Kolonnenexperimenten im Labor wurden Porositäts- und Permeabilitätsänderungen während der Alterierung von porösen Zementscheiben beobachtet. Dabei gab es deutliche Unterschiede bei der Verwendung von CO_2-haltigem bzw. CO_2-freiem Wasser. Der sequentiell gekoppelte Strömungs-Transport-Chemie Code MCOTAC wurde benutzt, um dieses beobachtete Verhalten zu modellieren. Porositäts-Permeabilitäts- und Porositäts-Diffusivitäts-Beziehungen werden für die Modellierung der Zementalterierung und Ausfällung von Sekundärphasen benutzt. Unter Berücksichtigung dieser komplexen gekoppelten Prozesse werden die Grenzen für die Anwendung eindimensionaler Modelle deutlich. Deshalb wurden hier zweidimensionale Modellrechnungen durchgeführt, die die Entwicklung der Transportparameter in einem kleinskaligen, zementhaltigen Endlager-Nahfeld beschreiben. Die Rückkopplung von chemischen Reaktionen auf die hydraulischen und Transportparameter im Nahfeld hat aufgrund von Porositäts- und Permeabilitätsänderungen im Grenzbereich Gestein-Endlager einen verminderten Transport der Radionuklide in der Nähe des Endlagers zur Folge. Der Transport von Radionukliden weg vom Endlager kann durch Porositäts- und Permeabilitätsverringerung drastisch reduziert sein. Dies ist speziell für die Radionuklide wichtig, die nicht oder nur wenig sorbieren, da nur die Transportparameter (Wasserfliessgeschwindigkeit, Dispersion und Diffusion) ihr Migrationsverhalten beeinflussen. Mit diesem kleinskaligen Ansatz für ein poröses Medium führt die Kopplung zwischen chemischen Reaktionen und hydrodynamischen Parametern für verschiedene Szenarien zu einer selbstschliessenden Barriere an der Grenze Wirtsgestein-Endlager. Diese Barriere kann über grosse Zeiträume beständig sein und Radionuklide effektiv innerhalb des Endlagers einschliessen.

RESUME

Les dépôts pour les déchets nucléaires de faible et de moyenne activité contiennent de grandes quantités de matériau cimenté. Par suite de l'interaction avec l'eau de formation, le ciment sera dégradé et formera des minéraux secondaires. La quantité de minéraux secondaires précipités dépend de la composition chimique de l'eau de formation. De plus, au voisinage du dépôt, les conditions hydrauliques et les paramètres décrivant le transport de masse (des radionucléides) évolueront avec le temps pendant la phase de dégradation du ciment. En conséquence, les changements de porosité dus aux réactions des minéraux et du ciment influenceront la perméabilité et la diffusion: une eau de formation riche en CO_2 conduira à la précipitation de calcite dans les zones conductrices d'eau entourant le dépôt de déchets cimenté et aura ainsi un impact sur le relarguage des radionucléides issus du dépôt cimenté dans l'environnement rocheux hôte.

Des expériences en colonne au laboratoire ont montré des changements simultanés de la porosité et de la perméabilité pendant la dégradation de disques de ciment poreux. Des résultats quantitativement différents ont été obtenus pour l'interaction avec de l'eau enrichie en CO_2 et pure. Le code séquentiellement couplé d'écoulement, de transport et de réaction chimique, MCOTAC, est utilisé pour inclure de telles observations dans la modélisation. Des relations porosité-perméabilité et porosité-diffusion sont utilisées pour décrire la dégradation du ciment et la précipitation consécutive de minéraux secondaires. Pour ces procédés couplés complexes, la modélisation à une dimension a atteint ses limites d'application. Donc, des calculs avec des modèles à deux dimensions ont été utilisés pour prédire l'évolution temporelle des paramètres de transport des radionucléides à l'intérieur d'une "échelle réduite" d'un champ proche d'un dépôt de déchets cimenté. Le feedback des réactions de chimie minérale sur les paramètres hydrauliques et de transport à l'intérieur d'un tel champ-proche produit un transport réduit des solutés dans le voisinage d'un site de stockage à cause des changements de porosité et de perméabilité à l'interface roche-site de stockage. Le transport des radionucléides issus du site de stockage pourrait donc être drastiquement réduit par la porosité et la diminution de perméabilité. Ce phénomène est particulièrement important pour les radionucléides qui montrent peu ou pas de sorption, car seuls les paramètres de transport (vitesse d'écoulement d'eau, dispersion et diffusion) influenceront leur comportement migratoire. A l'intérieur de l'approche "échelle réduite" en milieu poreux, le couplage des réactions chimiques et des paramètres hydrodynamiques indique une barrière autobloquante à l'interface roche-site de stockage simulée pour plusieurs scénarios. Cette barrière pourrait perdurer pour des temps très longs et contenir efficacement les radionucléides à l'intérieur du système de stockage ouvragé.

TABLE OF CONTENTS

LIST OF FIGURES

LIST OF TABLES

LIST OF SYMBOLS

A	cross section [m^2]
A_{ij}	stoichiometric coefficient matrix used to form all complexes *i* by the set basis species *j*
A1, A2, A3, A4	weighted areas for interpolation [m^2]
B_{jk}	stoichiometric coefficient matrix used to form solids *k* by the set of basis species *j*
c	empirical constant within the Kozeny-Carman equation [m/s]
$C(x,t)$	solute concentration depending on location and time [mol/l]
C_i	concentration of the complex *i* [mol/l]
C_i^t	concentration of complex *i* at time *t* [mol/l]
$\hat{C}_i$	concentration of the complex *i* [mol]
C_i'	concentration of the complex *i* within an iteration [mol/l]
$\{C_i\}$	activity of the complex *i* [mol/l]
$\mathbf{D}$	hydrodynamic dispersion tensor
D_{xx},,D_{yy},,D_{xy},,D_{yx}	components of the hydrodynamic dispersion tensor $\mathbf{D}$ [m^2/s]
D	(constant) dispersion coefficient [m^2/s]
D_e	effective diffusion coefficient [m^2/s]
D_i	dispersion coefficient for complex *i* [m^2/s]
D_j	dispersion coefficient for species *j* [m^2/s]
D_L, D_T	longitudinal and transversal dispersion coefficients [m^2/s]
$\mathbf{D}_{\text{mech}}$	mechanical dispersion tensor [m^2/s]
D_{m_j}	molecular diffusion coefficient for species *j* [m^2/s]
D_{m0}	diffusion coefficient in pure water [m^2/s]
D_p	diffusion coefficient in a porous medium [m^2/s]
F	the formation factor
h	hydraulic head [m]
i	index of complex species
j	index of basis species
k	index of solid species
$\boldsymbol{K}$	hydraulic conductivity tensor
K	component of the hydraulic conductivity tensor [m/s]
K_i	equilibrium constant for complexation reaction *i*
K_{so}^k	solubility product for the *k*th precipitation/dissolution reaction
k_1, k_2, k_3	dissociation or dissolution constants
L	domain length of a model [m]
M	aquifer thickness [m]
M_0	tracer mass [mol]
m	cementation exponent", empirical constant ranging between 1.3 and 2.5
m	index of a cell
m	mass [mol]
n	index
$nb(m)$	number of particles in cell *m*
$\vec{n}$	particle mass vector for particle *n*
N_c	number of complexed species (or complexes)
N_j	number of basis species
N_k	number of solid phases
N_{max}	maximum number of particles in the model area
P_k	concentration of the solid phase *k* [mol/l_{fluid}]
$\overline{P}_k$	concentration of the solid phase *k* [mol/l]
q	volumetric flow rate [m^3/m^3/s]
q^{extern}	pumping or injection rate [m^3/s]
r_j^{ch}	source/sink term for species *j* due to chemical reactions [mol/l/s]
r_j^q	source/sink term for species *j* due to external pumping [mol/l/s]
S_x, S_y	random diffusive-dispersive step in *x*- and *y*-direction [m]

t	time [s]
$\mathbf{T}$	tortuosity tensor
T	scalar tortuosity in an isotropic medium
v	(constant) effective flow velocity [m/s]
v_{Darcy}	Darcy velocity in one dimension [m/s]
v_D	is specific discharge , Darcy flux [m/s]
v_i	effective flow velocity for complex i [m/s]
v_j	effective flow velocity for species j [m/s]
V	volume related to a grid cell [m^3]
V_k	molar volume of the reactive solid k [m^3/mol]
x	co-ordinate in x direction [m]
$\underline{x_n}$	location of particle n [m]
$\bar{x}$	mean movement of a particle ensemble [m]
X_j	concentration of the species j [mol/l]
$\{X_j\}$	activity of the basis species j
$\vec{X}$	vector of the independent variables (basis species and solids)
Z_n	normally distributed random number
α_j	dispersivity for species j [m]
α_L, α_T	longitudinal and transversal dispersion length [m]
γ_j	activity coefficient of species j
ΔP_k	mass transfer from the solid into the liquid phase with respect to solid k
Δt	time step [s]
Δt_{max}	maximum time step [s]
Δx	cell width, grid spacing in x direction [m]
Δy	cell width, grid spacing in y direction [m]
Δm	tracer mass [mol]
$\Delta s_a(n)$	advective movement of a particle n [m]
Δx_n	displacement of particle n [m]
ΔX_j	component j of a vector $\vec{X}$
$\Delta\varepsilon$,	change in porosity
ε_m	volume fraction of the non-reactive solids
ε_f	volume fraction of the fluid phase
ε_p	pore space of the reactive solids
ε_g	volume fraction of a gas phase
$\bar{\varepsilon}$	error tolerance for iteration procedure
ε_f	porosity of a porous medium [-]
λ_j	decay constant for species j [1/s]
ρ	density, mass per unit volume of fluid [kg/m^3]

1 INTRODUCTION

The isolation of radioactive waste from the biosphere is one of the central issues for the design of a repository. For performance assessment purposes, the potential for mobilisation of radionuclides as dissolved or colloidal species in groundwater has to be addressed: How long will it take for radionuclides to reach the accessible environment and at what concentration levels? Time scales considered are typically much longer than 10'000 years and for such long time scales, processes become important that are less relevant for shorter time scales and are hard to investigate in short-term experiments. In such short-term experiments, kinetic reactions are often investigated that are less relevant for long-term processes, and extrapolation to long time scales seems doubtful. Further means to get long-term system understanding are natural analogue observations. Their histories cover similar time scales as necessary for long-term prognoses of repository behaviour. However, the boundary conditions, responsible for the actual stage of a natural analogue system, have to be estimated for interpretation of its long-term development and they are generally not well known.

Mineral dissolution and precipitation are important processes in the long-term description of repository behaviour. They affect the porosity available for the aqueous phase (groundwater), that is the dominant path for radionuclides migrating from the repository to the biosphere. Groundwater interacts with and alters the repository components and is also the transport medium for radionuclides (Fig. 1.1). Cement and concrete, as the main repository components, will be degraded by groundwater because of the large chemical gradient between the waters in the cementitious near-field (pH > 12.5) and in the surrounding host rock (pH~ 8). Ca-rich cement water in contact with CO_2-rich groundwater may then precipitate calcite at the repository-host rock interface, changing the hydraulic properties of individual repository components and the host rock. Therefore, a coupled description of hydraulic, transport and chemical processes is necessary for a comprehensive performance assessment of nuclear waste repositories. Porosity changes due to mineral precipitation can be detrimental or beneficial with respect to transport of radionuclides from a repository. If precipitation takes place predominantly in the rock matrix of a fractured medium, a porosity reduction is not desirable since it reduces retardation [Steefel and Lichtner 1994]. However, if diffusion is the dominant transport process and chemical reactions decrease diffusion porosity (as if advective flow paths do seal), the radioactive waste would be isolated more efficiently.

One major process which might also be important in the repository environment is the precipitation of calcite. If CO_2 (within the atmosphere but also dissolved in the groundwater) reacts with calcium, which is a degradation product of cement, calcite precipitates[1]. This has been observed for "old concrete and mortar" exposed to atmosphere or groundwater [Lagerblad and Traegardh 1996] as well as in everyday life, when boiling water[2] or in recent large scale environmental experiments[3].

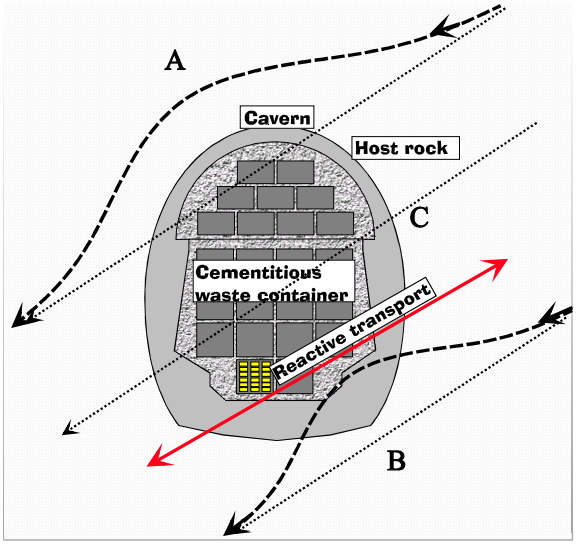

Fig. 1.1: Cross-section through a cementitious repository near-field. The dotted lines indicate an initial background groundwater flow field that might be changed due to mineral reactions and porosity and hydraulic conductivity changes. A: Sealing of the cement so that groundwater flow will be diverted around the cavern. B: Porosity and hydraulic conductivity increase allows for additional groundwater flow through the cavern. C: Initial flow field.

Another observation of calcite precipitation has been observed in several laboratories working on cement degradation. In flow-through and in-diffusion experiments, sealing of cement was observed that prevented further water flow or diffusion through samples

---

[1] A CO_2-uptake from air or from degradation processes of organic material and related calcite precipitation is likely during a long-term observation period of an open cementitious repository for L/IL waste until it will be closed. Latter long-term observations are proposed within the new (modified) concept for disposal of radioactive waste in Switzerland [Wildi et al. 2000].

[2] When boiling water for coffee in an old pot under atmospheric conditions, the inner walls are covered with calcite. After cleaning such pots, the calcite will again very soon be visible on the walls, indicating a fast precipitation process.

[3] Within the large scale Biosphere-II experiment, the calculated CO_2 balance did not meet researchers expectations [Broecker 1996]. The missing CO_2 was found to be within the concrete walls. The Portland cement used for constructions contains 15% $Ca(OH)_2$, which upon exposure to carbon dioxide is converted to $CaCO_3$, calcite, (CO_2 in - H_2O out, with respect to the generalised reaction $Ca(OH)_2 + CO_2 \rightarrow CaCO_3 + H_2O$). A 2 cm thick $CaCO_3$ saturated rind was observed inside the building's walls. Outside, this rind was about 0.2 cm. The difference was explained by the fact that the CO_2 content of the air inside the Biosphere-II building was about eight times of that outside, and the rate of CO_2-uptake should be roughly proportional to the CO_2 content of the air in contact with the concrete. From these measurements the amount of $CaCO_3$ within the inside rind of the wall accounted for the missing CO_2.

when working under atmospheric conditions. Therefore, experiments have been performed in glove boxes under CO_2-free conditions [Reardon 1992; Wieland 1997; Bateman et al. 1998; Pfingsten and Shiotsuki 1998; Jakob et al. 1999]. Most of these studies have been performed to investigate radionuclide migration processes (advection, diffusion, sorption) in cements. Often pure water was used in one-dimensional experimental set-ups to keep the interaction with the complex cement system as simple as possible so as to identify individual processes. The results may be quite different when using different groundwaters. Investigations of interactions with real groundwater are in progress in a second step, e.g. in in-situ experiments performed in rock laboratories where more complex reactions will happen [Frick et al. 1992; Pfingsten and Soler 2001].

To take into account such coupled processes, which become especially important at long time scales where mineral alteration can be significant, the existing one-dimensional model and code MCOTAC was extended to a two-dimensional description of reactive transport and to the coupling of reactive transport to hydraulics in a heterogeneous porous medium. A verification of the code is shown in App. A for a simple two-dimensional reactive transport problem where an analytical solution can be deduced. The model includes the description of porosity changes due to mineral reactions that define the transport parameters, such as hydraulic conductivity, water flow velocity or diffusivity. A decrease of porosity in a certain volume may decrease the hydraulic conductivity leading to a reduced local groundwater flow. Locally increasing porosity will locally decrease the hydraulic pressure and will increase the water flow towards the volume of increased porosity. Both processes will occur in the quite heterogeneous environment of a cementitious L&ILW (low and intermediate level waste) repository.

The investigation and quantification of such processes and their impact on the performance of a repository will increase the system understanding for scenario analysis purposes. Some observations and calculations indicate a possible self-sealing of a cementitious repository within its host rock environment which would be a benefit for the general safety of this repository type. However, a sufficient proof for its occurrence is still not possible because these fully coupled approaches are rare and still deal with simplified model scenarios, e.g. not taking into account the more complex geometry of the near-field (heterogeneous fractured media) or by assuming oversimplified boundary conditions for modelling the long-term behaviour.

Coupled modelling may also help to identify open questions that have to be investigated by carefully directed, well-aimed experiments, possibly long-term experiments. Such coupled modelling approaches should not be ignored. Their applicability is growing with ongoing increasing computer performance [Van der Lee and De Windt 2000], which is a necessary condition for applying such models to complex hydro-geochemical systems such as the degradation of a L&ILW repository and related radionuclide leaching and migration. Modelling this in its full complexity is still a challenge although computer resources and available data are still looked at as the limiting factors of fully coupled code applications.

2 MOTIVATION

In general, simple transport models are used for performance assessment purposes. Although these model approaches have shown to be robust and useful, they cannot be applied for certain scenarios and processes. For example, the pH plume propagation from a cementitious repository and its influence on radionuclide migration is still not known in all details. In addition, the limitation to one-dimensional descriptions in space makes it impossible to explain or investigate processes which are really two-dimensional (local porosity and permeability changes and related changes of the spatial groundwater flow field). Consequences may be qualitatively estimated from one-dimensional modelling, but two-dimensional modelling is necessary for quantitative predictions[4].

2.1 Experimental results during cement degradation

When trying to produce artificially altered cement under well defined laboratory conditions in order to investigate radionuclide transport and sorption behaviour on altered cement [Sarott et al. 1992], some preliminary experiments showed clogging of the cement specimen within a few weeks of water penetration. The experiments (see Fig. 2.1) were performed on identically produced cement disks. Several disk-like specimens with thicknesses of 0.5 and 1.0 cm and a diameter of about 2 cm were cut from a cementitious cylinder. Such cylinders were produced in the past using sulphate-resistant Portland cement. Further details concerning the production of these highly porous (about 65% porosity) cement pastes can be found in [Doehring et al. 1994].

In flow-through experiments under constant hydraulic head condition, pure (distilled, Millipore water, $CO_2 < 2.2 \cdot 10^{-6}$ mol/l [Stumm and Morgan 1996]) water flowed through the cement specimen with an initially constant rate. Calcite was precipitated at the inlet surface of the cement specimen when a similar experiment was performed under atmospheric condition in the laboratory. Inspection by eye indicated a calcite layer with a thickness of less than one mm [Wieland 1997] - enough to decrease the porosity of the hardened cement paste specimen to such low values that no further water flow could be measured (Fig. 2.2). The initial hydraulic conductivity of the artificially produced

[4] Three-dimensional modelling should be the final goal but up to now two-dimensional reactive transport modelling already consumes a huge amount of computer resources.

hardened cement paste sample was measured to be 10^{-10} m/s by the same experimental set-up [Pfingsten and Shiotsuki 1998]. This high value was expected because of the artificially high porosity of the hardened cement paste, selected to accelerate the degradation process (less solid has to be dissolved) and decrease the experimental time. The initial water flow rate was in the range of 0.1 ml/h, resulting in a water flow velocity of about $3.3 \cdot 10^{-8}$ m/s (~1 m/yr).

When the same experiment was performed under CO_2-free conditions, the precipitation of calcite was avoided. In this case, the experimental degradation of the cement disks could be performed for three years, until the disk became highly permeable to the water (Fig. 2.2). The degradation experiment was modelled successfully by a coupled code approach [Pfingsten and Shiotsuki 1998] taking into account the dissolution of the main cement minerals, related porosity and hydraulic permeability changes and chemical reactions induced by large chemical gradients between inflowing fluid and cement pore water. A chemical equilibrium model was applied to describe the mineral dissolution. This was justified by the experimental results: The portlandite buffers the pH of the outlet fluid at a level of 12.5 indicating that the leaching pore water was in equilibrium with portlandite (that means that the dissolution of portlandite by inflowing water is a fast process), at least after a migration distance of 1 cm, that is the thickness of the sample.

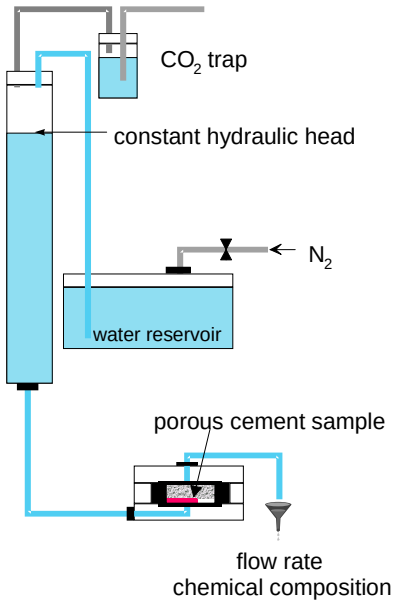

Fig. 2.1: Experimental set-up for the degradation of a porous cement disc by pure water under atmospheric and nitrogen (CO_2-free) conditions [Pfingsten and Shiotsuki 1998].

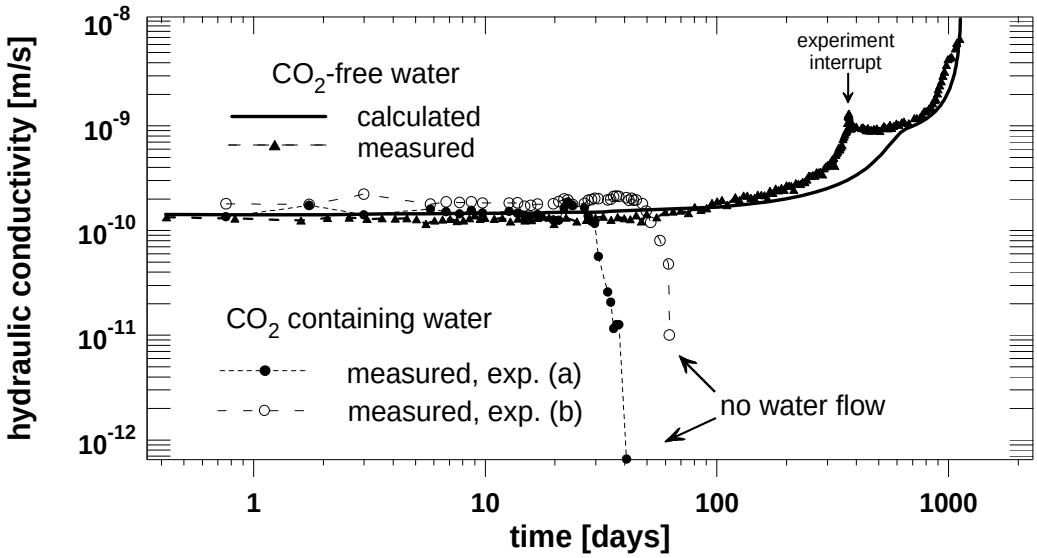

Fig. 2.2: Hydraulic conductivity during degradation of highly porous cement paste specimen by pure water under CO_2-containing and CO_2-free conditions. Its value was deduced from the constant hydraulic head conditions applied to the sample and the water flow measured through the specimen (see Fig. 2.1). The CO_2-free degradation experiment was compared to a fully coupled modelling approach including the cement degradation of the main cement components [Pfingsten and Shiotsuki 1998].

Moreover, as indicated by the clogging experiments, the carbonation of the surface of the cement disk was a fast process, too. Therefore, equilibrium precipitation was assumed also for the modelling of the clogging experiments. However, mass balance calculations assuming advective water flow through the porous cement disk showed that the amount of precipitated calcite is not enough to account for the observed clogging. Assuming that the calcite production is limited by the carbonate content in the inlet solution and the related carbonate flux through the specimen's cross section, a time span of 30 to 60 days would be too short to precipitate enough calcite to clog the near-surface pores. Assuming that the clogging might be caused by only a 0.1 mm thin calcite layer on top of the open pores, an area of 13.2 cm^2 (the cross section of the cement specimen) multiplied by its porosity 0.65 must be covered by calcite[5].

[5] The area of open pores at the surface of the specimen may be deduced from the volumetric property of the specimen, porosity, for the limit of zero thickness. One can also argue that not all open pores have to be covered with calcite, only the larger, water conducting pores; or that for clogging a much thinner layer would be enough. But neither of these points change the general result, because the thickness of the calcite layer calculated for pure advective flow is too thin (orders of magnitude) to clog the system (see Table 2.1).

A simple calculation allows one to roughly estimate a value for the observed time until clogging. CO_2 enters the sample by advective water flow ($v_{water} = 3.3 \cdot 10^{-8}$ m/s) with an assumed time-dependent concentration $C_{carbonate}$[6]. 65% of the surface area of the cement disk, *A*, (that is the area of open pores at the surface, or porosity) is assumed to be clogged by calcite precipitation. Calcite has a molar weight of 100.09 g/mol and a solid density of 2.72 g/cm^3 giving a molar volume of 36.8 cm^3/mol ($V_{mol}^{calcite}$). If all carbonate is used to precipitate calcite (that might be an overestimation because calcium may be limited, too), a linear function results for the growth of the calcite layer with time *t*:

$$x_{calcite} = \frac{v_{water} \; t \; C_{carbonate} V_{mol}^{calcite}}{A \varepsilon} \qquad (2.1)$$

Table 2.1: Thickness of a calcite layer on top of a highly porous hardened cement paste specimen limited by advective flow through the specimen during 60 days as a function of carbonate content (see Eq. 2.1).

t [d]	$C_{carbonate}$ [mol/l]	$x_{calcite}$ [m]
60	10^{-2} ($NaHCO_3$-type Wellenberg water)	$6.2 \cdot 10^{-5}$
60	10^{-3}	$6.2 \cdot 10^{-6}$
60	10^{-4}	$6.2 \cdot 10^{-7}$
60	10^{-5} (distilled water in contact with atmosphere)	$6.2 \cdot 10^{-8}$

The calculated thickness of the calcite layer is too thin (62 nm, Table 2.1) to account for the clogging because pores sizes of the cement sample were measured up to 400nm [Doehring et al. 1994]; furthermore, the calcite layer was visible by eye after the experiment. Therefore, additional processes, other than advective transport of carbonate within the water, must have been responsible for the clogging. A possible process might be diffusion. In the experiment the water enters the cement specimen in the degradation cell via a small water volume (with porosity 1) at the inlet interface of the sample (Fig. 2.3). Carbonate diffusion may take place from this water volume to the surface of the sample. To evaluate this hypothesis, the diffusive mobility of carbonate and calcium ions in the water and their mass balances should allow for clogging pores with calcite.

[6] CO_2 content might be time-dependent within the laboratory experiment but will be also different for different host rock waters surrounding potential repository.

Using an effective diffusion coefficient D_e of $5 \cdot 10^{-10}$ m^2/s, measured for diffusion of a non-sorbing species within highly porous cement [Sarott et al. 1992][7], a mean diffusion path length, Δx_m, into the cement during time span Δt, can be calculated for pure diffusion [Pfingsten 1994]:

$$\Delta x_m \approx \sqrt{2\, D_p\, \Delta t}\ , \tag{2.2}$$

where D_p is the pore diffusion coefficient in a porous medium, defined by:

$$D_p = D_w \cdot \tau = \frac{D_e}{\varepsilon}\ , \tag{2.3}$$

D_w is the diffusion coefficient in pure water and τ is the tortuosity and ε the porosity of the porous medium. The mean diffusion path length would be about the maximum distance (or the diffusive mobility) within which calcite is able to precipitate. A mean diffusion length for carbonate of 0.1 mm is calculated for about 10 s and 1 mm is reached after 1000 s. Therefore, ion mobility due to diffusion would be high enough to precipitate calcite near the surface. The total amount of calcite precipitated is limited by the diffusive carbonate flux to the cement interface and the availability of calcium, which is assumed to be present in excess due to portlandite dissolution.

To estimate whether the mass balance would allow for calcite precipitation, the CO_2 transfer at the interfaces air-water and water-cement has to be calculated. [Stumm and Morgan 1996] estimated the rate at which carbonate went through a thin film ($40 \cdot 10^{-6}$ m) at the gas (atmosphere)-water interface for a similar CO_2 gradient to be $6 \cdot 10^{-9}$ mol cm^{-2} s^{-1} for a diffusion coefficient of $2 \cdot 10^{-9}$ m^2 s^{-1} in the film. That means that in about 60 days ($5.2 \cdot 10^6$ s) about 0.03 mol cm^{-2} CO_2 may enter the water via a surface in contact with the atmosphere. Assuming that the gas-water interface area is the same as the water-cement interface area (13.2 cm^2), about 0.4 mol CO_2 would be able to enter the water within 60 days. A calcite layer of 1.1 cm could grow, if the whole amount of CO_2 was precipitated as calcite at the surface of the specimen. Although, the gas-water interface area is not known, a much smaller interface area would allow for a calcite

[7] [Frick 1993] gives a diffusion coefficient in water for Ca^{2+} and CO_3^{2-} of $7.93 \cdot 10^{-10}$ and $9.55 \cdot 10^{-10}$m^2/s, respectively.

cover of the specimen, provided that the carbonate enters the specimen's surface fast enough.

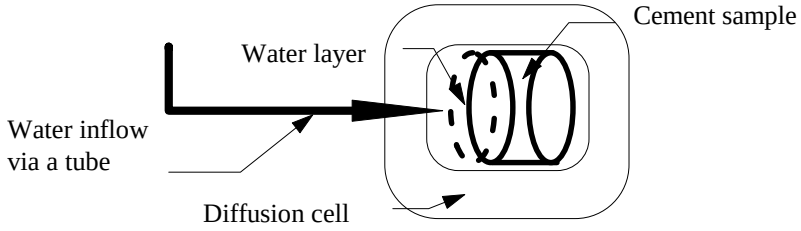

Fig. 2.3: Sketch of the interface water-cement specimen within the diffusion cell.

Another estimation seems possible for the carbonate that diffused to the water-cement interface. [Jakob et al. 1999] estimated the mass that diffused through a porous medium as a function of time by an analytical expression:

$$m(L,t) = \frac{C_0\, A}{L} D_e\, t \left\{ 1 - \frac{\alpha\, L^2}{6 D_e\, t} \left[1 + \frac{12}{\pi^2} \sum_{n=1}^{\infty} (-)^n \frac{1}{n^2} \exp\left(-\pi^2 n^2 \frac{D_e}{\alpha\, L^2} t \right) \right] \right\} \qquad (2.4)$$

where C_0 is the constant solute concentration at the "high concentration side" and a constant zero boundary condition is assumed for the "low concentration side". Initially, zero concentration is assumed within the sample of length L, α is the rock capacity factor[8], and A is the cross section. At the "high concentration side" C_0 is $6.3 \cdot 10^{-5}$ mol/l (pure water at pH 7 in contact with the atmosphere). The concentration at the "low concentration side" would be about 10^{-6} mol/l (carbonate content in the cement water) and is assumed to be zero for simplicity reasons and to apply Eq. 2.4). Then, Eq. 2.4 yields about $4 \cdot 10^{-4}$ mol carbonate diffused through a layer of about 1 mm thickness within 60 days allowing for a $1.7 \cdot 10^{-3}$ cm thick layer over the surfaces of all the open pores of the specimen. Therefore, diffusive processes at the air-water and water-cement

[8] The rock capacity factor α of a porous medium with a solid density ρ [kg/m^3] and a (connected) porosity ε is defined by:

$$\alpha = \varepsilon + (1 - \varepsilon)\, \rho\, k_D \qquad \text{(fe-1)}$$

It is equal to the porosity of the medium in the case of a non-sorbing solute with zero linear equilibrium sorption distribution coefficient [m^3/kg].

interfaces would allow enough calcite to precipitate for clogging of the cement surface. A final quantitative explanation seems to be impossible here, due to the uncertainty in the experimental set-up with respect to the amount of carbonate entering the cement specimen. Also further detailed modelling of these clogging experiments seems to be difficult and maybe not worthwhile because too many important questions concerning the experimental boundary conditions were not addressed. For example, the carbonate concentration in the inlet water at the cement surface and the air-water interface area that allows air born carbonate to enter the water are unknown. Hence, a kinetic formulation might be necessary for a quantitative description of the rate at which CO_2 enters the water.

The investigation of the degradation of the artificially produced, highly porous hardened cement paste gives indications of the dissolution (perturbation) or clogging of the cement depending on the experimental boundary conditions. However, to describe the behaviour of a heterogeneous cementitious waste repository one has to keep in mind that the cement and concrete that will be used for a real repository, as well as the waste containers, will be of a different composition from those used in the experiments. The cementitious repository will be quite heterogeneous with respect to cement and concrete used[9]. A general degradation behaviour can hardly be deduced from the degradation of the homogeneous hardened cement pastes. However, parts of the repository may behave similarly to the hardened cement paste, e.g. some waste forms may be produced homogeneously. The complex transient behaviour will depend on the degree of heterogeneity. In addition, degradation by pure water is also a further simplification. This was done, in a first step, to better understand and analyse the individual degradation processes; however, site specific groundwater may induce quite different degradation processes. An example has already been shown in Fig. 2.2, where two “pure waters” with different carbonate saturation levels induce complementary behaviour, from “nearly complete dissolution” to “complete clogging” of the cement specimen. The implication of the results obtained for the artificially produced highly porous cement paste for application to cementitious repository relevant cement pastes, mortars and concrete, and extrapolation from these results is not unique. Small changes in site specific properties, whether due to their structural or chemical nature (host rock and

[9] Backfill mortar will be a highly porous material with a porosity of 27% and with a high permeability (hydraulic conductivity greater than 10^{-4} m^2/s), whereas cavern liner or some cementitious wastes will be of low porosity (6%) and low hydraulic conductivity ($<10^{-12}$ m^2/s) [Pfingsten 1998].

water composition), can lead to completely opposite results and consequences. A time scale for clogging due to calcite precipitation and/or other secondary mineral precipitation is therefore difficult to deduce without detailed near-field knowledge.

Nevertheless, there are some results that can be used to describe scenarios more like the repository. During the early, hyper-alkaline degradation phase, where the pH decreases from about 13.5 to 12.5, the changes in porosity and hydraulic permeability of the cement paste are negligible. Later on, the portlandite solubility limit buffers the pH of the outlet fluid, or calcite precipitates at the cement surface. Both phenomena indicate the assumption of chemical equilibrium conditions is valid for these processes, at least for the experimental conditions chosen (temperature, pressure, water flow velocities, etc.). Therefore, assuming chemical equilibrium for the cement degradation in a similar near-field environment is also applicable for similar hydraulic and geochemical parameters.

2.2 Results from reactive transport modelling using a simplified geometry

Several approaches have been presented in the literature that describe the migration of a hyper-alkaline plume into a host rock accompanied by mineral dissolution or secondary mineral precipitation [Steefel and Lichtner 1994; Lichtner and Eikenberg 1995; Bateman et al. 1998; Lichtner et al. 1998]. Mostly, the obtained results were direct consequences of the chosen boundary conditions or modelling conditions, rather than the chosen type of geometry or the set of “allowed” mineral reactions. For example, it is questionable to take into account mineral reactions deduced from short-term laboratory experiments representing meta-stable conditions and extrapolating these mineral reactions to long-term repository conditions with characteristic time spans which are longer by several orders of magnitude. The same doubts arise for model boundary conditions, possibilities, capabilities with respect to processes and coupling included in the model and their applications. It seems equivocal to set-up a geochemical system with steep chemical gradients where strong precipitation and dissolution reactions will change the local porosity tremendously without evaluating how a varying porosity and related hydraulic conductivity affect solute transport. Using one-dimensional simplifications of such chemical reactive, heterogeneous near-field systems for long-term simulations might be inappropriate. They may be applicable to describe column experiments of simple geometry – a first step, in addition to batch experiments, to gain dynamic system and process understanding, but it should not be the last. One-

dimensional models are often motivated by limited computer resources. A lot of approaches deal with constant inlet conditions that give results hard to transfer to real near-field conditions. For example, a constant chemical composition at the boundary may continuously generate steep chemical gradients in the water composition, leading to “accelerated migration”, simply induced by the choice of this boundary condition.

Other problems occur when modelling the leaching of a high pH plume from a cementitious repository and related interactions with the host rock. Here, the assumption of a constant water and solute flux [Steefel and Lichtner, 1998a, Steefel and Lichtner, 1998b] from the repository into the host rock, maybe with a transient phase for the pH and other solutes, is a simplification that ignores mineral reactions upstream, which will occur in a real repository. Cement dissolves within the repository and causes porosity and hydraulic conductivity changes which will define the water flux through the repository. The transient water flux may be beneficial or disadvantageous for the performance assessment and, therefore, should be taken into account.

Nevertheless, these modelling approaches for simple systems or geometry lead to an increased understanding of coupled processes. Furthermore, chemically reactive, hydraulic systems need to be described in at least 2D to account more accurately for the complex system behaviour. The selection of appropriate boundary conditions, in both, 1D as well as in 2D, is important for the system under consideration. An example is presented in Appendix B. There, differences are compared and quantified between a cement-host rock interface, where in one case the interface was assumed to be directly at the boundary, and in the other case where the interface is set at the centre of the model domain. The second case is the more appropriate approach, where the interfaces between the cement and the host rock are described by a cement completely surrounded by the host rock. The first case might be appropriate for describing cement degradation by an inlet solution in a column like experiment.

3 TWO-DIMENSIONAL HYDRAULIC, TRANSPORT AND CHEMICAL DESCRIPTION, EQUATIONS AND THEIR COUPLING

A modular structure of hydraulic, transport and chemical models (codes) is chosen, where the modules are coupled sequentially with the option of iteration in between the modules[10]. This allows for description of a complex near-field scenario, involving steep chemical gradients together with hydraulic conditions that may change as the system evolves.

The individual modules and their properties are described below. The hydraulic module describes stepwise stationary flow (it is assumed that the hydraulic gradients in a repository near-field are small, or change slowly with time) including sources and sinks in a heterogeneous porous medium. Transport takes into account advection, dispersion, diffusion and linear sorption in a heterogeneous porous medium as well as decay for a single species and source and sink terms due to external pumping and/or chemical reaction. The chemistry module includes a chemical equilibrium description for complexation, sorption and mineral reactions including an incongruent dissolution model for solids, especially CSH. Groundwater flow (Darcy flux) is non-linearly coupled to mineral dissolution (precipitation) and consequent porosity and hydraulic conductivity changes are then back-coupled with changed transport parameters to the migration of solutes (Fig. 3.1)

[10] The individual modules for flow, transport and chemical calculations contain their individual iteration criteria for accuracy or error tolerance, respectively, for example, hydraulic head or species concentration distribution calculated during iteration. In addition, according to the coupling of modules by exchange terms and dependency of parameters, iteration is also foreseen between calculations of the different modules. Defining tolerances or upper limits for the values of the exchange terms and their changes with time, these iterations influence the time stepping. The latter is also modified, if individual module iterations do not converge properly.

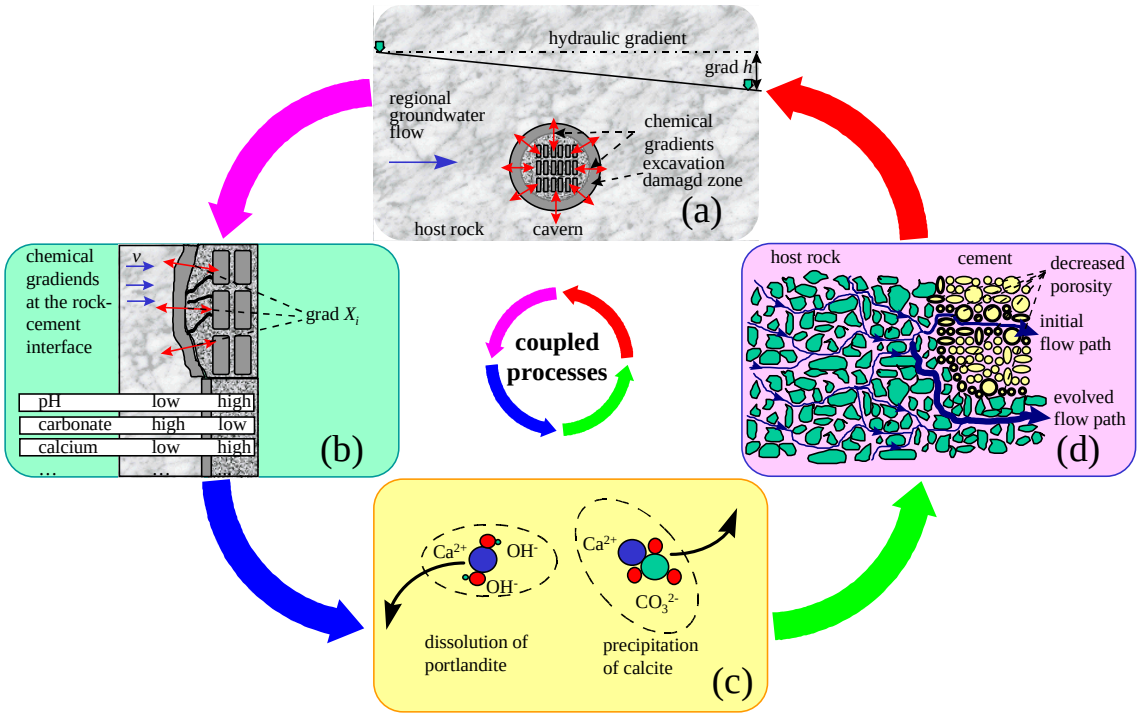

Fig. 3.1: Coupled hydraulic, transport and geochemical processes in a repository near-field environment. **(a)** Background groundwater flow induces advective-dispersive transport in the near-field. **(b)** Chemical gradients cause diffusion of solutes at the host rock-cement interface. **(c)** Mineral reactions result, accompanied by porosity and hydraulic permeability changes in the near-field, and solute transport parameters evolve with time **(d)**.

3.1 Flow equation

Groundwater flow may be described by two equations (see e.g. [de Marsily 1986; Yeh and Tripathi 1989]). First, the mass balance

$$div(\rho\,\vec{v}_D) + \frac{\partial}{\partial t}(\rho\varepsilon_f) + \rho q = 0\ , \qquad (3.1)$$

where ρ is the mass of the liquid phase per unit volume of fluid [kg/m^3] which is assumed to be constant, $\vec{v}_D$ is specific discharge (Darcy flux in m/s), ε_f is the porosity of the medium [-], and q is the volumetric flow rate of fluid per unit volume of rock withdrawn (or added, if it is negative) in the porous medium [m^3/m^3/s].

The second equation is Darcy's law:

$$\vec{v}_D = -K \cdot grad\ h\ , \tag{3.2}$$

where K is the hydraulic conductivity tensor (tensor elements in [m/s]) and h the hydraulic head [m]. A model for stationary hydraulic flow conditions in two dimensions was chosen:

$$div(-\frac{K}{M} grad\ h) + q = 0\Big|_{\Delta t}\ , \tag{3.3}$$

where M is the aquifer thickness [m]. To describe the transient behaviour of the hydraulics a sequence of stationary states is used. M and q are distributions of parameters in space, representing varying aquifer thickness, pumping rates of field or laboratory experiments, or volume changes due to chemical reactions. They are calculated for initial conditions, and then subsequently recalculated by the other modules fulfilling fluid and mass balances. The solution of the two-dimensional flow problem is done by a finite differences procedure for steady state conditions. This means constant head or flux conditions at the boundaries, constant external sources or sinks as well as constant porosity, and hydraulic conductivity during a single time step. Time dependence, as for example induced by chemical reactions and related porosity and hydraulic conductivity changes, can be described by an appropriate discretisation in time (time stepping). The finite differences grid is related to the chemical grid system by the distribution of minerals in the modelling area. External sources, q^{extern}, as pumping rates of wells, and volume changes, q^{ε}, due to porosity changes $\Delta\varepsilon_f$, are calculated from the chemical module (see below) and enter the mass balance Eq. 3.1 by the value of q defined by:

$$q = q^{extern} + q^{\varepsilon}(x, y, \Delta t, \Delta\varepsilon_f, ..) \tag{3.4}$$

It is defined for a certain location (x, y) which is related to a finite differences grid.

The hydraulic conductivity is calculated using the Kozeny-Carman equation that relates directly the hydraulic conductivity to the porosity ε_f, as it was deduced in [Pfingsten and Shiotsuki 1998] for a hardened cement paste[11]:

$$K = c \cdot \frac{\varepsilon_f^{\,3}}{(1-\varepsilon_f)^2} \ . \tag{3.5}$$

The constant c has to be deduced from initial conditions for porosity and hydraulic conductivity and depends on the solid composition and structure. The Kozeny-Carman equation is highly non-linear as shown in Fig. 3.2 for different values of c.

The water flow velocity, $\vec{v}$, used for solute transport modelling is calculated from the Darcy flux:

$$\vec{v}_D = \varepsilon_f \cdot \vec{v} \ . \tag{3.6}$$

The flow porosity ε_f is a space- and time-dependent function of the changes in mineralogy (precipitation/dissolution of solids) influencing the flow velocity and yielding an additional coupling between fluid flow and solute transport. With the concept of modular coupling hydraulic, transport and chemical calculations are separated from each other and already existing modules can be used.

[11] A number of empirical relations are available to relate values of porosity to (local) hydraulic conductivity $K(\varepsilon_f)$, one is the Kozeny-Carmen equation [Bear 1972]. Other relations take into account porosity and effective mineral surface areas that are often not well defined for such complex systems as is a cement. In a first step, it is adequate to use this simple expression for the hydraulic conductivity as a function of porosity.

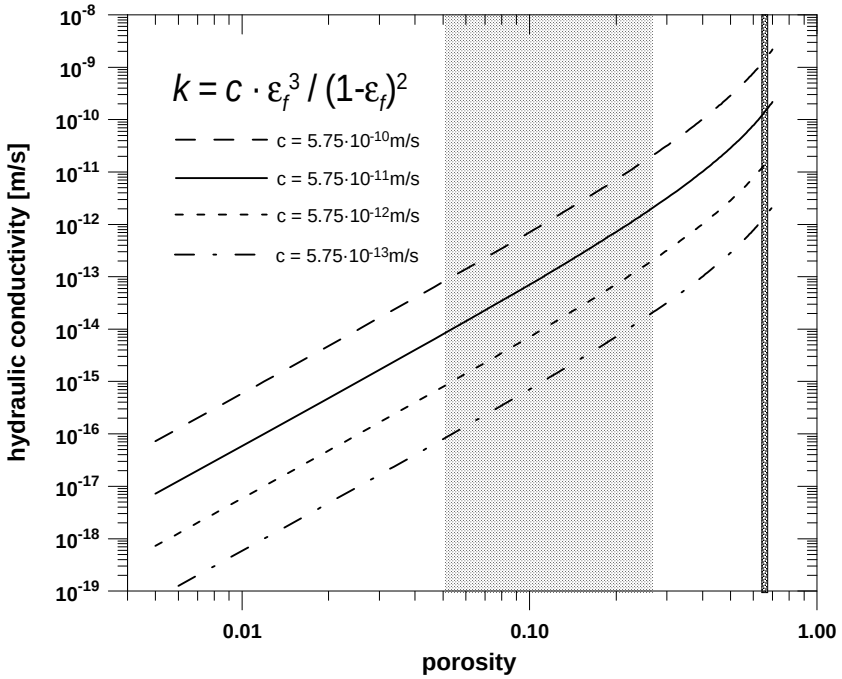

Fig. 3.2: Hydraulic conductivity as a function of porosity (Kozeny-Carman). The curve for $c = 5.75 \cdot 10^{-11}$ m/s was deduced from an experiment where highly porous hardened cement paste (porosity of 65%, indicated by the bold vertical line) was degraded by pure water [Pfingsten and Shiotsuki 1998]. Porosities of repository-relevant cement and mortar are in the range of 5% to 27% (indicated by the dotted area). Hydraulic conductivities were estimated in the range of 10^{-12} to $>10^{-4}$ m/s [NAGRA 1993; NAGRA 1994; Pfingsten 1998].

3.2 Solute transport equation

The transport equation of an ideal tracer including advection, hydrodynamic dispersion, decay and external sources and sinks may be written as:

$$\frac{\partial(\varepsilon_f X)}{\partial t} + \nabla \cdot \varepsilon_f \vec{v}\, X - \nabla \cdot \left((\varepsilon_f \mathbf{D}) \cdot \nabla X\right) + \varepsilon_f \lambda\ X - r = 0\ , \qquad (3.7)$$

where λ is the decay constant of the tracer and r indicates sources and sinks of the tracer. It can be rewritten to:

$$X\frac{\partial \varepsilon_f}{\partial t}+\varepsilon_f\frac{\partial X}{\partial t}+\left(\nabla\cdot\varepsilon_f\vec{v}\right)X+\varepsilon_f\vec{v}\cdot\nabla X-\left((\nabla\varepsilon_f)\cdot\mathbf{D})\right)\cdot\nabla X-\left(\varepsilon_f(\nabla\cdot\mathbf{D})\cdot\nabla X\right)$$

$$+\varepsilon_f\lambda\ X-r=0 \qquad (3.8)$$

If terms including deviations of the porosity are summed up in an additional source term, a standard transport equation results which can be solved by several numerical methods. Here, a Random-Walk of multi-species particles is used[12]:

$$\varepsilon_f\frac{\partial X}{\partial t}+\varepsilon_f\vec{v}\cdot\nabla X-\left(\varepsilon_f(\nabla\cdot\mathbf{D})\cdot\nabla X\right)+\varepsilon_f\lambda\ X-r-r^{\varepsilon}=0\ , \qquad (3.9)$$

where

$$r^{\varepsilon}=-X\frac{\partial \varepsilon_f}{\partial t}-\left(\nabla\cdot\varepsilon_f\vec{v}\right)X+\left((\nabla\varepsilon_f)\cdot\mathbf{D}\right)\cdot\nabla X\ . \qquad (3.10)$$

Assuming that transport parameters are the same for all N_j (j=1,…,N_j) species in solution ($v_j(x,y)=v(x,y)$ and $D_j(x,y)=D(x,y)$[13]), and in analogy to the one-dimensional transport equation used for reactive transport within MCOTAC [Pfingsten 1996], the equation in two dimensions is:

---

[12] It is assumed that porosity changes due to chemical reactions are small compared to transport processes (solute mass has to be transported to "create " or "destroy" at a certain location much denser solid mass). In addition, it is assumed that the properties of the porous medium, such as porosity, do not change abruptly in space so that their spatial gradients are small, or that medium properties evolve slowly with time. Both are restrictions with respect to discretisation in space and time. Otherwise, other approaches, like a dual porous medium approach, have to be applied for the description of flow and transport processes (see e.g. Jakob, 1997). For solution of the transport equation it is assumed that the porosity, elements of the dispersion tensor, flow velocity, and the source terms are constant in time. They are approximated by mean values during a time step, and are defined and calculated by other modules (hydraulic and chemical module). The source terms are used to cover these approximations in the transport equation. The source terms are the coupling terms to the hydraulic and chemical modules, and are used to control the iteration between the different modules. The mass balance is fulfilled for the transport module to the level of accuracy chosen for iteration.

[13] This implies that the accessible pore space is equal to all species, and diffusion is independent from species mass and charge. Further on, the porosity is, as a non primary variable within the transport calculation, calculated from the initially known porosity and the accumulated solid precipitation and dissolution reactions, and therefore space and time dependent.

$$\frac{\partial X_j}{\partial t} + v_x \frac{\partial X_j}{\partial x} + v_y \frac{\partial X_j}{\partial y} - \frac{\partial}{\partial x}\left(D_{xx} \frac{\partial X_j}{\partial x} + D_{xy} \frac{\partial X_j}{\partial y} \right) - \frac{\partial}{\partial y}\left(D_{yx} \frac{\partial X_j}{\partial x} + D_{yy} \frac{\partial X_j}{\partial y} \right)$$

$$+ \lambda_j X_j - \frac{r_j^{ch}}{\varepsilon_f} - \frac{r_j^q}{\varepsilon_f} - \frac{r_j^\varepsilon}{\varepsilon_f} = 0 \qquad j = 1,..., N_j \ , \tag{3.11}$$

where:

X_j concentration of the basis species j [mol/l] (see Chap. 3.3)
t time [s]
x co-ordinate in x direction [m]
y co-ordinate in y direction [m]
D_{xx}, D_{yy}, D_{xy},$=D_{yx}$ components of the symmetric hydrodynamic dispersion tensor **D**
$\vec{v}$ $\vec{v} = \vec{v}(x, y) = (v_x, v_y)$ effective flow velocity [m/s]
λ_j decay constant for species j [1/s]
r_j^{ch} source/sink term for species j due to chemical reactions [mol/l/s]
r_j^q source/sink term for species j due to external pumping (injection, extraction) [mol/l/s]
r_j^ε source/sink term for species j due to temporal and spatial porosity changes [mol/l/s]

The hydrodynamic dispersion **D** is a tensor defined by, e.g. in [Bear 1979]:

$$\mathbf{D} = \mathbf{D}_{mech} + \mathbf{D}_p \ , \tag{3.12}$$

where $\mathbf{D}_p = D_p \cdot \mathbf{T}$, **T** is the tortuosity (tensor) of a porous medium and D_p is the diffusion coefficient in a porous medium for an isotropic medium the (scalar[14]) tortuosity is usually admitted as:

$$T = \frac{D_p}{D_{m0}} = \frac{1}{\varepsilon_f \ F} \ , \tag{3.13}$$

where D_{m0} is the diffusion coefficient in pure water. F, the formation factor, relates the resistivity of the saturated porous medium to the resistivity of the pore solution alone [de Marsily 1986]. The factor F, is defined in numerous ways [Dullien 1979] though [Steefel and Lichtner 1994] used a definition based on Archie's Law that gives the formation factor as:

$$F = \varepsilon_f^{-m} \ , \tag{3.14}$$

where m is the "cementation exponent", ranging between 1.3 and 2.5 [Dullien 1979]. When choosing a value of 2 for m, a linear expression in ε_f for D_p results:

$$D_p = D_{m0}\varepsilon_f \ . \tag{3.15}$$

Since ε_f is a space and time dependent function of the mineralogy changes, an additional coupling results between mineral reactions and solute transport. The linear relationship (Eq. 3.15) allows an explicit calculation of the molecular diffusion coefficient in a porous medium as a function of porosity. An example is given in Fig. 3.3.

For a two-dimensional problem in space, the (mechanical) dispersion tensor $\mathbf{D}_{\text{mech}}$ is defined by its components:

$$\mathbf{D}_{mech} = \begin{pmatrix} D_{xx} & D_{xy} \\ D_{xy} & D_{yy} \end{pmatrix} \ , \tag{3.16}$$

which degenerates to:

$$\mathbf{D}_{mech} = \begin{pmatrix} D_L & 0 \\ 0 & D_T \end{pmatrix} \ , \tag{3.17}$$

[14] Tortuosity in bedded sediments or other structured minerals may be extremely anisotropic and would need a tensor description of tortuosity. This is not looked at in this context.

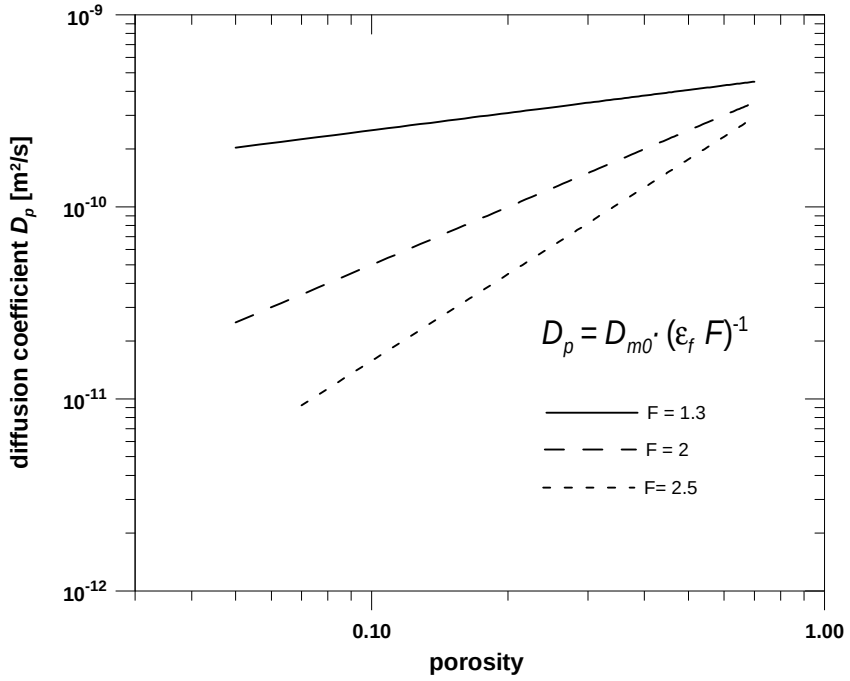

Fig. 3.3: Diffusion coefficient D_p in a porous medium as a function of porosity and "cementation exponent" as given in Eqs. 3.13 to 3.15 (D_{m0} is assumed to be $5 \cdot 10^{-10} m^2/s$).

if the water flow is in x-direction, and D_L and D_T are the longitudinal and transversal dispersion coefficients. For an arbitrary flow field, $\mathbf{D}$ is given by [Bear 1979][15]:

$$\mathbf{D} = \begin{pmatrix} \alpha_L \frac{v_x^2}{|\vec{v}|} + \alpha_T \frac{v_y^2}{|\vec{v}|} + D_p & (\alpha_L - \alpha_T) \frac{v_x v_y}{|\vec{v}|} \\ (\alpha_L - \alpha_T) \frac{v_x v_y}{|\vec{v}|} & \alpha_T \frac{v_x^2}{|\vec{v}|} + \alpha_L \frac{v_y^2}{|\vec{v}|} + D_p \end{pmatrix}, \qquad (3.18)$$

with

[15] v_x *and* v_y are components of the two-dimensional flow field which is calculated by a finite differences hydraulic model. Therefore, values for v_x *and* v_y are mean values related to the finite differences grid. The same applies for D_m as a function of porosity, since porosity is defined by the solid distribution in space which is also related to the finite differences grid. Nevertheless, particle related transport parameters are interpolated from the finite differences grid to the location of the particle.

$$|\vec{v}| = \sqrt{v_x^2 + v_y^2} \quad . \tag{3.19}$$

The transport of solutes (basis species X_j) during a time step Δt is then calculated by the Random-Walk of multi-species particles (particles represent a mass vector with vector components X_j , [Pfingsten 1994]) as a sum of an explicitly defined advective step in two dimensions in space with flow velocity $\vec{v}'$, including the counter terms described in App. C:

$$\Delta\vec{s}_a(n) = \vec{v}' \cdot \Delta t \tag{3.20}$$

and an explicit random diffusive-dispersive step in *x*- and *y*-direction ($S_{D,x}$ and $S_{D,y}$, respectively) calculated for each particle [Kinzelbach and Uffink 1991, p. 231]:

$$S_{D,x} = Z_1 \cdot \sqrt{2 \cdot (\alpha_L \cdot |v| + D_p) \cdot \Delta t} \cdot \frac{v_x}{|v|} - Z_2 \cdot \sqrt{2 \cdot (\alpha_T \cdot |v| + D_p) \cdot \Delta t} \cdot \frac{v_y}{|v|} \ , \tag{3.21}$$

$$S_{D,y} = Z_1 \cdot \sqrt{2 \cdot (\alpha_L \cdot |v| + D_p) \cdot \Delta t} \cdot \frac{v_y}{|v|} + Z_2 \cdot \sqrt{2 \cdot (\alpha_T \cdot |v| + D_p) \cdot \Delta t} \cdot \frac{v_x}{|v|} \ , \tag{3.22}$$

where Z_n is a two-dimensional vector of normally distributed random numbers related to the individual random diffusive-dispersive step of particle *n* in two dimensions.

Then, the new particle positions x_n for particles n = 1, ..., $N_{\max}$ are given by:

$$x_n = x_{n,old} + \Delta s_a(n) + \Delta s_D(n) \quad . \tag{3.23}$$

After a transport step *Δt*, particles have been moved to new positions. Then, the species concentrations in solution are given by summing up particle masses within the spatial grid (sum over individual mass vector components, each representing a solute) and the source and sink terms (see below). The latter include the correction terms which take

into account deviations of porosity and dispersivity in time and space[16]. All these terms are calculated according to the spatial grid. The new concentration distribution in solution may be not in equilibrium with the spatial distribution of the solids and has to be re-equilibrated by means of the chemical module.

Radioactive decay during a time step Δt is taken into account by:

$$X_j(t+\Delta t) = X_j(t) \cdot e^{-\lambda_j \cdot \Delta t} \tag{3.24}$$

It can be applied either to species concentrations X_j (as shown in the equation above) or directly to related particle mass vector components m_j.

3.3 Chemical equations

The chemical module is similar to that used for the 1D MCOTAC version as it calculates the chemical equilibrium in a volume of water and solid material for a total mass of individual components[17] given in the solid and liquid phase [Pfingsten 1994]. For simplicity of presentation, the spatial index (x,y) is left out in the following for solutes, solids and porosities or volume fractions although they are handled grid specifically in the modelling. Chemical equilibrium reactions in solution for N_c complexes are described by N_j basis species X_j:

$$\{C_i\} = K_i \cdot \prod_j^{N_j} \{X_j\}^{A_{ij}} \quad , \tag{3.25}$$

---

[16] Other methods to include these terms are described in [LaBolle et al., 1996] using modified Random-Walk particle tracking methods and several interpolation procedures. For large discontinuities they recommend the use of a carefully chosen interpolation scheme or reflection principle.

[17] The total mass of a basis species X_j is defined by:

$$X_{j,total} = X_j + \sum_{i=1}^{N_c} A_{ji} C_i + \sum_{k=1}^{N_k} B_{jk} P_k \quad \cdot \tag{fe-2}$$

Depending on the mathematical set-up of the basis species, complexes and solids, the total mass can have a negative value [Pfingsten 1994]. Individual concentrations X_j, C_i and P_k are always positive.

where K_i is the equilibrium constant for complex i, $\{C_i\}$ and $\{X_j\}$ are the activities of the complexes and basis species in solution with $\{X_j\} = \gamma_j X_j$; γ_j is the activity coefficient, and A_{ji} are stoichiometric coefficients[18].

Precipitation and dissolution reactions are described for N_k solid phases (k=1,…, N_k):

$$K_{so}^k = \prod_{j=1}^{N_j} \{X_j\}^{B_{jk}} \quad , \tag{3.26}$$

where K_{so}^k is the solubility product and B_{jk} are stoichiometric coefficients. The species concentrations as well as solid composition are calculated in a defined x-y grid initially and sequentially after transport calculations that may have disturbed the chemical equilibrium within individual grid volumes. Sources and sinks due to mineral reactions for the species X_j during time step Δt (Eq. 3.11) are given by [Pfingsten 1994]:

$$r_j^{ch} = \varepsilon_f \cdot \sum_{k=1}^{N_k} B_{jk} \frac{\Delta P_k}{\Delta t} \quad . \tag{3.27}$$

The mineral composition defines the porosity that is used to recalculate the porosity in the volume, the hydraulic conductivity and the fluid volume that may be pressed out or sucked in. If the porosity decreases, fluid will be pressed out, and if porosity increases fluid will be sucked in. This fluid volume is explicitly calculated from the difference in solid composition and related porosity changes (see Eqs. 3.4 and 3.30). Its chemical solute composition is assumed to be in chemical equilibrium within the related volume. Solute mass and fluid conservation are guaranteed with this procedure. It is more than a porosity update, since for a pure porosity update, volume differences ($\partial \varepsilon_f / \partial t$, Eq. 3.4) are neglected and therefore solute and fluid mass conservation is not fulfilled.

Taking into account different volume fractions, the fluid porosity is defined by:

---

[18] In addition, any other equilibrium reaction that can be formulated as described in Eq. 3.25 can be included in the chemical equilibrium model provided that the definition of related K_i and activity coefficients are appropriate; e.g. linear sorption may be included as a chemical reaction defined by $K_{Di} = \{S_i\}/\{X_i\}$, where K_{Di} is the equilibrium distribution coefficient between sorbed, $\{S_i\}$, and mobile, $\{X_i\}$, amounts of a species given in related units. A sorbed species can also be handled as immobile complex or, alternatively, a "retarded" species can be described by a second set of particles (with related mass vector components) that are moving with modified transport parameters $\vec{v}' = \vec{v} / R$ and $D_p' = D_p / R$.

$$1 = \varepsilon_m + \varepsilon_f + \varepsilon_p + \varepsilon_g \ , \tag{3.28}$$

where ε_m is the volume fraction of the non-reactive solids, ε_f is the volume fraction of the fluid phase, ε_p is the pore space of the reactive solids, and ε_g is the volume fraction of a gas phase. The pore space of the N_k reactive solids is given by:

$$\varepsilon_p = \sum_{k=1}^{N_k} V_k \cdot \overline{P}_k \ , \tag{3.29}$$

where $\overline{P}_k = \varepsilon_f \cdot P_k$ is in mol/l and V_k is the molar volume of the reactive solid *k* which is assumed to be constant. If the non-reactive solid volume fraction ε_m and the gas phase volume fraction ε_g are assumed to be constant then, after a time step Δt, changes in the fluid phase volume fraction are given by changes of the reactive solids[19]:

$$\Delta\varepsilon_f \Big|_{\Delta t} = -\Delta\varepsilon_p = -\varepsilon_f \Big|_t \cdot \sum_{k=1}^{N_k} V_k \cdot \Delta P_k \Big|_{\Delta t} \ . \tag{3.30}$$

The amount of minerals *k* dissolved (precipitated), ΔP_k, increases (decreases) the fluid porosity ε_f by a mineral volume fraction $\Delta\varepsilon_p$. The molar volume V_k [l/mol] of mineral *k* is calculated from molar weight [kg/mol] divided by its solid density [kg/l]. For each grid volume, $V_{cell\ x,y}$, the changes of the porosity during Δt and the related spatial gradients are calculated and transferred to the hydraulic module as an internal source or sink defined by Eq. 3.4. The related species mass flux r_j^{ch} is transferred to the transport module (Eq. 3.11) as a constant average species source/sink term within a grid cell during the next time step.

---

[19] Porosity changes in a spatial volume are calculated by chemical re-equilibration between solids and solutes in that volume, whereas the solutes induce the non-equilibrium due to transport processes. The solute masses m_j (sum of particle mass vector components) that are present in the volume V with porosity ε_f after time step Δt leads to a concentration $X_j = m_j / (\varepsilon_f \cdot V)$. The solid remains constant during solute transport calculation. Only re-equilibration of X_j [mol/l_{fluid}] with $P_k(t)$ [mol/l_{fluid}] changes the solid concentration to $P_k(t+\Delta t)$ [mol/l_{fluid}] to $\overline{P}_k(t+\Delta t) = \varepsilon_f(t) \cdot (P_k(t+\Delta t) - P_k(t)) = \varepsilon_f(t) \cdot \Delta P_k$.

$$r_j^{\varepsilon}\Big|_{cell\,x,y} \approx \left(-\frac{\Delta \varepsilon_f \Big|_{\Delta t}}{\Delta t} - \nabla \cdot \varepsilon_f \vec{v}(x,y) \right) X_j + \left((\nabla \varepsilon_f) \cdot \mathbf{D} \right) \cdot \nabla X_j \ . \qquad (3.31)$$

The first two terms are related to an accompanied local water flux $q^{\varepsilon}\big|_{cell\,x,y}$ (compare Eq. 3.1):

$$q^{\varepsilon}\Big|_{cell\,x,y} \approx -\frac{\Delta \varepsilon_f}{\Delta t}\Bigg|_{cell\,x,y}^{\Delta t} \cdot \varepsilon_f \ \Delta x \Delta y M\Big|_{cell\,x,y}^{t} \ . \qquad (3.32)$$

which is induced by porosity changes. The last term is related to pure solute mass flux. All terms are calculated from grid specific values at time *t* (see App. 3) to be taken into account during calculations for time $t + \Delta t$. Their values are controlled during iteration by defined limits.

3.4 Coupling by a sequential iterative procedure between flow, transport and chemical equilibrium module

The individual code modules, their physical background and their dependencies are already mentioned in the chapters above. In order to take into account their interaction, it is quite common to sequentially couple individual model codes by introducing exchange terms. This allows for using existing codes. Solution of the whole set of equations given in chapters 3.1 to 3.3 leads to a complete solution for the “fully coupled hydro-geochemical reactive transport description” by complex mathematics and codes. It has been shown that an operator splitting method, or the sequential coupling approach will give good results compared to an iterative approach, whereas the sequential coupling approach consumed less computing time, which is a major aspect for code applicability [Frind et al. 1994; Van der Lee and De Windt 2000 and references therein]. When solving the hydraulic, transport and chemical equations separately, with certain independent parameters in one module kept constant in the other modules by using an averaged value during a time step, additional focus must be taken on the consequences of such an approximation approach. This is done by controlling the changes of the calculated time averaged values in subsequent time steps. If, e.g. porosity changes and related hydraulic conductivity and water flow velocity exceeds a given value, indicating

large amounts of mineral turnover, time step reduction is used to ensure that time averaged parameters follow a smooth curve. Further, calculated porosity changes are taken into account within the fluid mass balance by defining external, grid specific sources or sinks q^{ε}, depending on increasing or decreasing porosity, as mentioned above.

The coupling of the hydraulic, transport and chemical equilibrium module is shown in Fig. 3.4. Each module includes its own iteration procedure, whereas the coupling terms are responsible for their mutual interaction. In case of convergence problems of individual modules, generally, a time step reduction is sufficient. Iteration between chemical and transport modelling or (optional) hydraulic modelling depends on the change of coupling terms. For example, in a pure diffusive driven system, the hydraulic model becomes unnecessary, whereas precipitation and dissolution reactions, calculated within the chemical module may induce strong changes of the hydraulic parameters. Hence, the iteration has to include the hydraulic modelling where transport parameters are calculated.

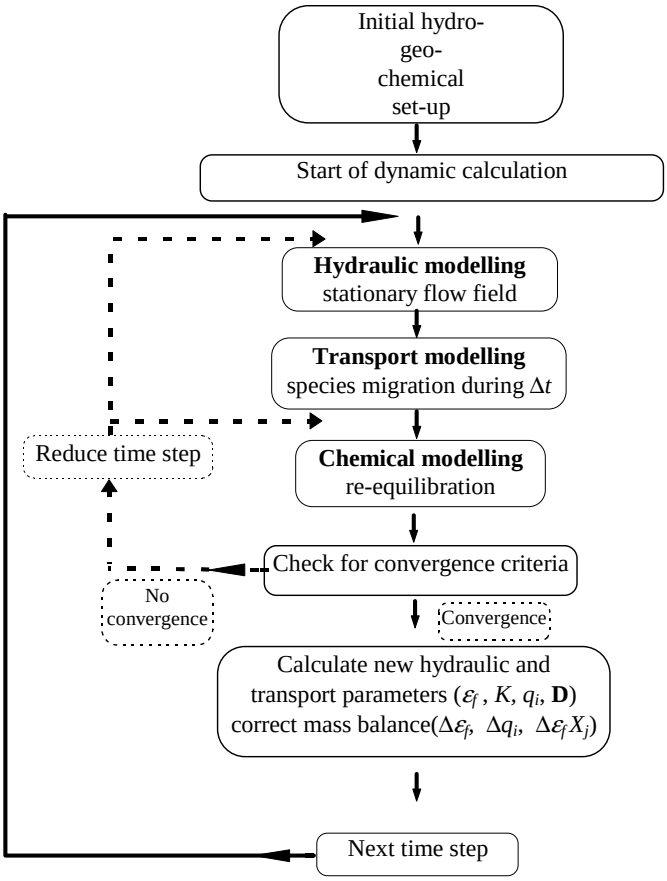

Fig. 3.4: Coupling procedure and modules used during "fully coupled" simulations.

A verification for the coupling procedure used in MCOTAC is shown in Appendix A for the coupling of two-dimensional reactive transport including chemical equilibrium reactions between three basis species (X_j), two complexes (C_i) and one solid (P_k), but within a simple flow field where an analytical solution exists. The coupling of precipitation and dissolution reactions to hydraulics including an explicit porosity-permeability relationship was done by successfully applying MCOTAC to a one-dimensional cement degradation experiment [Pfingsten and Shiotsuki 1998]. For a verification of a fully coupled, heterogeneous system in two spatial dimensions including hydraulics, transport and chemical reactions, no other computer code seems to be available[20]. Only simplified model approaches may serve for code comparison at the moment. In the following the influence of such coupling was investigated for two-

[20] Several code applications to reactive transport problems are published in the literature using codes that are used as research codes, often under construction and not free available. A benchmark exercise with respect to coupled codes would be helpful for further improvement of the applicability and building of confidence in coupled codes.

dimensional systems which are related to the interaction of a cementitious repository in a host rock environment.

For applications, shown in the next chapters, a simplified initial geometry has been chosen with respect to heterogeneity of the initial hydro-geochemical parameters (porosity, hydraulic permeability, chemical composition of the solutes and solids etc.). Then, the discretisation in space and time caused little problems with convergence, especially, if a small time steps were chosen. Optimising for convergence and computing time was not investigated here. The optimisation seems to be problem dependent and is left to further investigations. They should focus on an optimised coupling, to save computing time, but also to include heterogeneity more properly. For example, a realistic repository near-field modelling should include the structure of the cementitious repository with respect to the cement and concrete structures used (cavern liner, backfill, waste forms), their composition and a proper model for the host rock including EDZ and fractures. In addition, flow path geometry (fractured and/or porous medium) may have also an impact on the coupling terms[21] and the temporal development of the chemical fronts [Steefel and Lichtner, 1998a, Steefel and Lichtner, 1998b] and should be investigated because this will finally allow to predict the degradation and migration behaviour in a realistic repository near-field.

[21] Coupling or cross terms may become more relevant in this case and a dual porous medium approach for transport might be more appropriate to overcome discretisation problems.

4 APPLICATIONS TO TWO-DIMENSIONAL SMALL SCALE CEMENTITIOUS NEAR-FIELD SCENARIOS

To investigate processes ongoing in the near-field of a cementitious repository in its host rock environment, coupled modelling was performed for an abstraction of the near-field as depicted in Fig. 4.1. A simplified geometry, a two-dimensional cross section, of the near-field was chosen in order to include the description of several processes, for example porosity and permeability changes due to mineral reactions and related flow field changes. The simplification includes also the homogenisation of the structured repository and its environment by using mean values for chemical composition of all the repository components and their hydraulic and transport properties, as well as mean parameters for the adjacent host rock. In a first approach, these simplifications are based on the fact that a large fraction of a cementitious repository consists of highly porous backfill mortar. Transport will take place predominantly within this repository component due to its high porosity and hydraulic conductivity. Similarly, an excavation damaged rock zone (EDZ) created by the excavation procedure will develop, where hydraulic conductivity will be increased compared to the undisturbed host rock. Therefore, ongoing coupled processes will dominate in those parts of the repository with increased transport parameters, driven by diffusion (chemical gradients) or advection-dispersion (flow field). In addition, the backfill mortar and the EDZ are looked at as porous media.

In order to have a minimum discretisation necessary to describe the repository-host rock interactions and the evolving system in some temporal and spatial resolution, the spatial dimensions of the repository have been decreased compared to the actual size planned. Instead of the realistic repository cross section of about 10 to 16 m^2 plus several 10 m^2 adjacent host rock, a 1 m^2 “small scale repository near-field” was modelled here. This permits modelling of several coupled processes at the same time with an appropriate resolution in time and space[22], and within a reasonable computing time (reactive transport calculations are still CPU and memory intensive). The down-scaling of repository size should not influence the description of the general system behaviour. The steep chemical gradients between repository and host rock environment are present on the small scale, too; and the background hydraulic field will induce a mean flow through

[22] Spatial discretisation of the model area was done for grids of 20 times 17 nodes up to 80 times 50 nodes.

the repository, less influenced by its spatial dimensions than its hydraulic properties (predominant flow through porous, high conductive mortar). Therefore, important reactions occurring at the cement-host rock interface will be taken into account correctly, whereas processes that are important for the whole volume of the repository, e.g. total amount of the cement dissolved, or the amount of radionuclides in the pore water of the backfill, have to be scaled with respect to the surface or volume of a real repository[23].

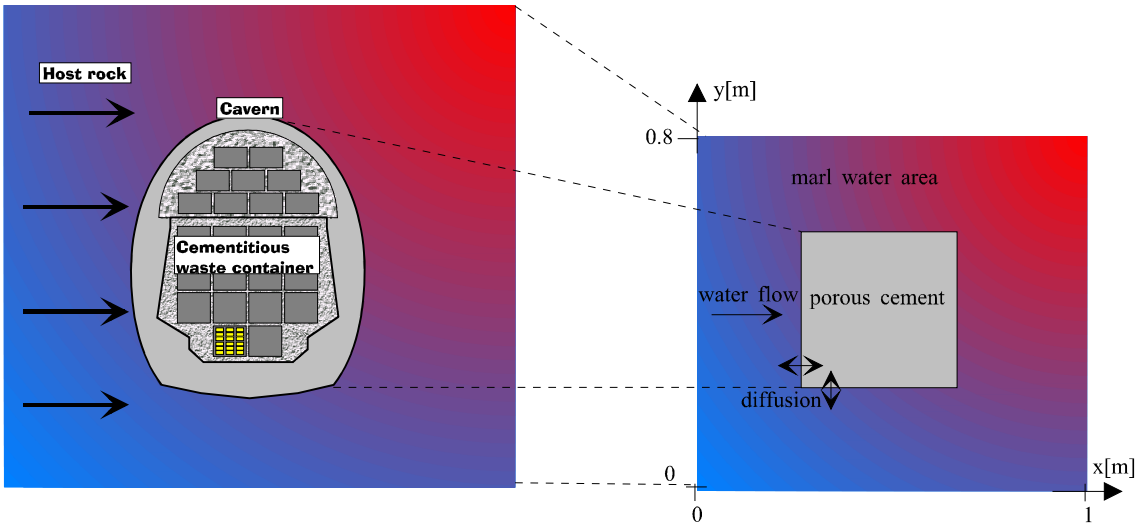

Fig. 4.1: Cross-section through the near-field within a host rock environment (left) and its simplified representation in the model (right). Groundwater flow is defined by a hydraulic gradient. Model boundaries used in Chap. 4.1 and Chap. 4.2 are: Constant head at left and right and no-flow on top and at the bottom of the model area. A constant head boundary condition all around the model area and zero gradient was used in Chap. 4.3.

In order to achieve some system understanding, several hydraulic and transport scenarios are investigated within this “small scale repository near-field”. The hydraulic parameters are related to parameters estimated for the Wellenberg. In Chap. 4.1 and Chap. 4.2, a constant hydraulic background gradient of 0.4 [NAGRA 1994] is assumed across the repository site. Two initial values for the hydraulic conductivity for repository and host rock were chosen, $K = 1 \cdot 10^{-8}$ m/s and $K = 1 \cdot 10^{-12}$ m/s, respectively. Mean parameter values are chosen for the hydraulic properties of the cement and the surrounding rock related to values given in [Neall 1994]. Background water flux

[23] However, a more sophisticated system description should include the real dimensions of a repository as well as the heterogeneity of the repository (cavern liner, waste container, backfill) and the adjacent host (increased fracturing in EDZ compared to host rock).

through the “small scale repository” is calculated from the regional background hydraulic gradient, mean hydraulic conductivities and a mean porosity of 17% for the repository and its host rock environment[24]. Transport parameters are assumed to be the same for all solutes and related to site specific values given in [NAGRA 1993; NAGRA 1994]. In Chap. 4.3, a no flow environment is investigated that would be favourable for the choice of a real repository site.

For the initial geochemical composition of the repository and the host rock averaged values are chosen to describe water and mineral composition. The water composition was deduced from [Neall 1994] and [Baeyens and Bradbury 1994]. For the cement, representing the repository, the hardened cement paste composition was chosen as described in Table 4.5. The early, high pH phase of the cement degradation (alkali leaching) was neglected. This is because first, the description of the alkali leaching is still vague: [Reardon 1992] and [Taylor 1987] mentioned that it is not possible to reliably predict mineral alteration products, e.g. the formation of zeolites. The alteration products observed mainly originate from short-term laboratory experiments, with timescales not relevant to repository timescales [Thoenen 1996]. Second, it is unclear if the leachate will have a pH of 13.5 measured for the pore water directly leached from the cement. Dilution by host rock water or mixing of host rock water in the highly conductive repository backfill mortar will cause a lower pH buffered by “main” cement components like portlandite [Reardon 1992; Pfingsten 1998]. Even if a plume with pH above 13.5 leaches from the repository into the surrounding near-field, this transient time period will be small compared to the period where portlandite will buffer the leachate at pH 12.5 [Neall 1994]. And third, short-term laboratory experiments generally showed a porosity reduction when a so-called ‘young fluid’ at pH 13.3 enters columns filled with different repository relevant minerals (pure minerals, synthetic mixes of pure minerals and real marl and granite samples), due to secondary mineral precipitation, mainly precipitation of CSH, CSAH phases and zeolites [Bateman et al. 1999; Bateman et al. 2000]. This means that taking into account the early leaching of a high pH solution (pH >13) from the cementitious repository would imply a decrease of porosity in the

[24] Also geometrical structures of the water conducting features are important for solute transport and degradation behaviour, especially if fractures are present in hard rock formations, the near-field may be considered as a single porous cement in a porous host rock environment (EDZ), ignoring additional structures. For simplicity reasons, the same averaged porosity was chosen for the porous cement as well as for the host rock environment. In a further study the fully coupled code will be developed for fractured, heterogeneous or dual porous media applicable to real repository scale as it should be for performance assessment purposes.

adjacent host rock, similarly to the results calculated for a solution of pH 12.5 as shown below.

The geochemical set-up for the host rock and the porous cement composition is summarised in Tables 4.1 to 4.5. It is related to the L/ILW repository site foreseen at Wellenberg. Two major possible groundwater compositions at the repository side are distinguished. Here the $NaHCO_3$-Type [Neall 1994] was chosen to interact with a homogeneous porous cement, represented by its major components. The modelling includes nine basis species (Na^+, Ca^{2+}, $H_2SiO_4^{2-}$, OH^- CO_3^{2-}, F^-, Cl^-, Mg^{2+}, Al^{3+}), twenty-two complexes and five minerals, three used within CSH-gel model for incongruent dissolution [Berner 1988] and two allowing for precipitation of the calcite and fluorite. Initial and boundary conditions are given in Fig. 4.1 and Table 4.4. The geochemical set-up for the cement-host rock interaction is the same for all scenarios modelled within Chap. 4. and App. B.

Table 4.1: Chemical reactions in solution and log*K* values used to model cement-Wellenberg water interaction.

Reaction	log*K*
$H_2O - OH^- \leftrightarrow H^+$	-14
$Ca^{2+} + OH^- \leftrightarrow CaOH^+$	1.22
$H_2SiO_4^{2-} + H_2O - OH^- \leftrightarrow H_3SiO_4^-$	-0.67
$H_2SiO_4^{2-} + 2H_2O - 2OH^- \leftrightarrow H_4SiO_4(aq)$	-4.86
$Ca^{2+} + CO_3^{2-} \leftrightarrow CaCO_3(aq)$	3.22
$Ca^{2+} + CO_3^{2-} + H_2O - OH^- \leftrightarrow CaHCO_3^-$	-2.56
$Ca^{2+} + F^- \leftrightarrow CaF^+$	0.94
$Na^+ + OH^- \leftrightarrow NaOH(aq)$	-0.18
$Na^+ + CO_3^{2-} \leftrightarrow NaCO_3^-$	1.27
$Na^+ + CO_3^{2-} + H_2O - OH^- \leftrightarrow NaHCO(aq)$	-3.92
$Na^+ + F^- \leftrightarrow NaF(aq)$	-0.24
$CO_3^{2-} + H_2O - OH^- \leftrightarrow HCO_3^-$	-3.67
$2F^- + H_2O - OH^- \leftrightarrow HF_2^-$	-10.38
$F^- + H_2O - OH^- \leftrightarrow HF(aq)$	-10.82
$CO_3^{2-} + 2H_2O - 2OH^- \leftrightarrow H_2CO_3(aq)$	-11.32
$Mg^{2+} + CO_3^{2-} \leftrightarrow MgCO_3(aq)$	2.98
$Mg^{2+} + CO_3^{2-} + H_2O - OH^- \leftrightarrow MgHCO_3^+$	-2.6
$Mg^{2+} + F^- \leftrightarrow MgF^+$	1.82
$Mg^{2+} + OH^- \leftrightarrow MgOH^+$	2.56
$Al^{3+} + 4OH^- \leftrightarrow Al(OH)_4^-$	33.34
$Al^{3+} + 3OH^- \leftrightarrow Al(OH)_3(aq)$	25.06
$Al^{3+} + 2OH^- \leftrightarrow Al(OH)_2^+$	17.89

Table 4.2: Mineral reactions used to model cement-Wellenberg water interaction.

Precipitation- dissolution reaction	$\log K_{so}$
$Ca(OH)_2(s) \leftrightarrow Ca^{2+} + 2OH^-$	f(C/S)*
$CaH_2SiO_4(s) \leftrightarrow Ca^{2+} + H_2SiO_4^{2-}$	f(C/S)*
$SiO_2(s) \leftrightarrow H_2SiO_4^{2-} - 2OH^-$	f(C/S)*
$CaCO_3(s) \leftrightarrow Ca^{2+} + CO_3^{2-}$	-8.48
$CaF_2(s) \leftrightarrow Ca^{2+} + 2F^-$	-10.6

(* see Table 4.3)

Table 4.3: Solubility product as a function of calcium to silica in the solid phase (C/S) as used by [Berner 1988] for the modelling of CSH dissolution.

C/S region	Component	$\log K_{so}$
$\frac{C}{S} = 0$	$SiO_2(s) \leftrightarrow H_2SiO_4^{2-} - 2OH^-$	2.34
$0 \le \frac{C}{S} \le 1$	$SiO_2(s) \leftrightarrow H_2SiO_4^{2-} - 2OH^-$	$3.0 + \frac{0.792}{C/S - 1.2}$
	$CaH_2SiO_4(s) \leftrightarrow Ca^{2+} + H_2SiO_4^{2-}$	$-8.16 - \frac{1 - C/S}{C/S} \cdot (0.78 + \frac{0.792}{C/S - 1.2})$
$1 \le \frac{C}{S} \le 2.5$	$Ca(OH)_2(s) \leftrightarrow Ca^{2+} + 2OH^-$	$-4.945 - \frac{0.338}{C/S - 0.85}$
	$CaH_2SiO_4(s) \leftrightarrow Ca^{2+} + H_2SiO_4^{2-}$	-8.16
$\frac{C}{S} > 2.5$	$Ca(OH)_2(s) \leftrightarrow Ca^{2+} + 2OH^-$	-5.15
	$CaH_2SiO_4(s) \leftrightarrow Ca^{2+} + H_2SiO_4^{2-}$	-8.16

Table 4.4: Simplified Wellenberg water and initial cement (CSH-gel) water composition. Concentrations are in [mol/l] [25].

	Wellenberg water		Cement water	
Basis species	Total concentration	Species concentration	Total concentration	Species concentration
Na^+	$1.7561 \cdot 10^{-2}$	$1.7401 \cdot 10^{-2}$	$1.7564 \cdot 10^{-2}$	$1.7163 \cdot 10^{-2}$
Ca^{2+}	$5.7250 \cdot 10^{-5}$	$4.6516 \cdot 10^{-5}$	$1.1939 \cdot 10^{-2}$	$8.5957 \cdot 10^{-3}$
$H_2SiO_4^{2-}$	$1.7400 \cdot 10^{-4}$	$6.0834 \cdot 10^{-11}$	$1.5268 \cdot 10^{-5}$	$4.1568 \cdot 10^{-6}$
OH^-	$-1.6390 \cdot 10^{-2}$	$1.9551 \cdot 10^{-6}$	$5.6873 \cdot 10^{-2}$	$5.3119 \cdot 10^{-2}$
CO_3^{2-}	$1.6099 \cdot 10^{-2}$	$1.8519 \cdot 10^{-4}$	$7.7716 \cdot 10^{-6}$	$1.9896 \cdot 10^{-6}$
F^-	$9.5553 \cdot 10^{-4}$	$9.4700 \cdot 10^{-4}$	$1.0402 \cdot 10^{-4}$	$1.0006 \cdot 10^{-4}$
Cl^-	$6.3921 \cdot 10^{-4}$	$6.3921 \cdot 10^{-4}$	$6.3921 \cdot 10^{-4}$	$6.3921 \cdot 10^{-4}$
Mg^{2+}	$3.2819 \cdot 10^{-5}$	$2.7815 \cdot 10^{-5}$	$3.2800 \cdot 10^{-5}$	$3.4563 \cdot 10^{-6}$
Al^{3+}	$3.7343 \cdot 10^{-7}$	$5.6439 \cdot 10^{-17}$	$3.7000 \cdot 10^{-7}$	$2.4932 \cdot 10^{-34}$

Table 4.5: Model solids present in the Wellenberg water area and in the initial cement composition (CSH-gel).

	Wellenberg area	Cement area		
Solid phase	Concentration [equiv. mol/l_{fluid}]	Concentration [equiv. mol/l_{fluid}]	Specific density [kg/l]	Molar weight [g/mol]
$Ca(OH)_2(s)$	0	48.491	2.25	74.09
$CaH_2SiO_4(s)$	0	29.547	2.48	134.18
$SiO_2(s)$	0	0	2.22	60.09
$CaCO_3(s)$	0	$1.6091 \cdot 10^{-2}$	2.72	100.09
$CaF_2(s)$	0	$4.2149 \cdot 10^{-4}$	3.18	78.08
inert solids[26]			-	-

[25] A negative total concentration is the consequence of the definition of the total concentration within the numerical description of aqueous and solid species (see Eq. fe-2). Also the number of digits and obviously very low concentration levels are a consequence of the chemical model and module used and do not suggest the degree of chemical system accuracy.

[26] Inert solids do not participate in chemical reactions but are used to represent host rock and cement properties, like porosity, correctly.

4.1 A diffusion-dominated near-field scenario

A diffusion-dominated scenario results from the assumption of low hydraulic conductivity for host rock and cement block. The rectangular model area is divided into an inner part, the cement area, surrounded by an outer part, the host rock (Fig 4.1). Water flow is induced by an applied hydraulic gradient in x-direction. Low flow velocities ($v = 2.3 \cdot 10^{-12}$ m/s) result from the assumed low value for the hydraulic conductivity of cement and host rock. Mechanical dispersion and diffusion are in *x*- and *y*-direction.

Modelling results are shown in Figs. 4.2 to 4.6 for the calculated solid distribution as a function of time. Fig. 4.2 represents about the initial solid and porosity distribution within the model area (see Table 4.5). The cement dissolves all around its interface to the host rock, scarcely affected by the water flow which is in *x*-direction. The CSH model solids dissolve (build up of SiO_2) in their sequence as time evolves[27]. In parallel, a carbonate front (calcite and fluorite) precipitates around the cement. After one hundred years of interaction, there is already an increase in the amount of carbonate calculated at the interface with the host rock. The temporal evolution of the solutes in the water in the cement and host rock area is related to the solid distributions calculated. An example for the pH and calcium concentration is calculated across the cement-rock water interface (see App. B). In the initial phase of the cement rock water interaction modelled, the edges of the cement block are degraded more than the sides parallel to the *x*- and *y*-direction because of the two dimensional steep gradients at the edges (Fig. 4.4). However, along the side, only one-dimensional gradients are active. The slightly asymmetric shapes of the calculated solid distributions are due to the Random-Walk transport calculations where particles are moved statistically. This leads to Random-Walk-typical, scattered concentration distributions of species all around the cement if they are not buffered by a solid. Due to the coupling of hydraulic, transport and chemical processes these scattered concentrations distributions may generate non-linear changes of the hydraulic and transport parameters. Within 2000 years the model solid $Ca(OH)_2$ has nearly been dissolved or transferred to the model solid CaH_2SiO_4 (Fig. 4.6). Comparison of calcite precipitation at 1000 and 2000 years (Figs. 4.5 and 4.6)

[27] The used dissolution model for CSH phases [Berner 1988] allows $logK_{so}$ being a function of the calcium to silica ratio (C/S) within the solid (see Table 4.3) This is similar to a solid solution description of a CSH. Therefore, $Ca(OH)_2$ and CaH_2SiO_4 are dissolving according to the C/S ratio that defines their $logK_{so}$. $Ca(OH)_2$ dissolution directly at the interface to the host rock (node *n*) will not prevent $Ca(OH)_2$ dissolution further inward the cement area (node *n*+1) because it is used as a model solid together with CaH_2SiO_4 and SiO_2; their solubility products are varying in space according to the spatial calcium to silica distribution.

shows that the amount of calcite precipitate in the first 1000 years is larger than for the second 1000 years. An explanation is that, although inside the cement the porosity is still increased compared to initial conditions, the calcite precipitation around the cement serves as a “barrier” for migrating solutes and a circumferential trench of low porosity evolves around the cement (Fig. 4.6). The calcite precipitation reduces locally the porosity all around the cement and also decreases the diffusion coefficient (Eq. 3.15). Chemical gradients are the driving force for transport in this example. A further explanation for the reduction in calcite precipitation calculated is the decreasing of chemical gradients from cement area to the host rock area during the second half period, since the initially steep gradients at the cement host rock interface become flatten. As porosity decreases to nearly zero in the calcite precipitation ring, the transport (diffusion) will become infinitely slow in this area slowing down any further reaction between host rock water outside and cement water inside the “vulcano”.

Also porosity and herewith hydraulic conductivity increase and decrease locally, the flow field is less influenced because of its minor importance for the assumed low hydraulic conductivity for host rock and cement. The symmetric dissolution and precipitation patterns calculated for the solid distributions show only small deformations. These are due to the small background flow field in *x*-direction. The porosity distribution shows an asymmetry along a slice (parallel to background flow) through the model area containing the cement. Lower porosity has been calculated at the upstream boundary of the cement indicating a larger amount of precipitation, since at the upstream side more “fresh” rock water enters the interface to the cement due to advection/dispersion compared to the downstream boundary. The small background flow “compresses” the precipitation zone at the upstream interface, whereas it increases the precipitation zone at the downstream interface, where the porosity is higher but dispersed in a wider zone (Fig. 4.7). The porosity distribution along a slice perpendicular to the background flow is shown in Fig. 4.8. Here, the porosity distribution is symmetric relative to the centre of the cement area. The porosity decreased to nearly zero after 2000 years of interaction. Along this cross section the advection-dispersion acted equally to both interfaces due to symmetric flow conditions. After 2000 years of interaction the model solid portlandite is nearly dissolved, and the porosity is increased. Looking at the time intervals of 500 years (Figs. 4.7 and 4.8), total porosity in the cement area increases slightly during the first 500 years. Then, the increase of total porosity is maximal in between 500 and 1000, and 1000 and 1500 years. Later on, the total porosity decreases again. This behaviour is partly due to the mineral reactions but also due the incongruent dissolution model where model solid

portlandite is partly transferred to CaH_2SiO_4 during dissolution[28]. Altogether, such a system behaviour is beneficial for a cementitious repository in the assumed host rock environment as the repository will isolate itself from the host rock by precipitation and dissolution reactions. The same would be the case for cementitious radioactive waste which would be located in less permeable parts of a repository. Nevertheless, one has to carefully consider the model assumptions. The porous and homogeneous cement and host rock structure are simplifications as well as the main but simplified chemical descriptions of the cement and the host rock composition and their waters. A fractured host rock together with a hydraulically heterogeneous (and fractured) cementitious repository may lead to a different system behaviour from that described here and should be thoroughly investigated. Another question is the relationship between porosity and diffusion coefficient. The linear relationship (Eq. 3.15) used here may not be valid if porosity becomes quite small, or if minerals, very different in molar volume or structure, dissolve and precipitate. However, until realistic cement and host rock properties, their dependence on porosity, and their heterogeneity are taken into account, the time scale for clogging reactions will be uncertain. The result of "porosity nearly zero at the cement-host rock interface after 2000 years" is a consequence of chemical gradients at the interface and related transport parameters used for the modelling. Other transport parameters or heterogeneity of the cementitious repository with respect to cement composition and structure may influence the temporal evolution but not the general trend of the cement-host rock interaction, because the responsible and important reactions always will happen first at the interface cement-host rock[29]. These are mineral reactions that decrease porosity for the diffusion dominated scenario. In the next chapter a scenario is investigated with the same geochemical system but with different transport parameters.

[28] Although model solids were used to describe the cement dissolution, values for molar volumes of the real solids were used.

[29] The generation of cracks is possible due to mechanical stress, hydraulic or gas pressure build-up, but it is not included in these considerations.

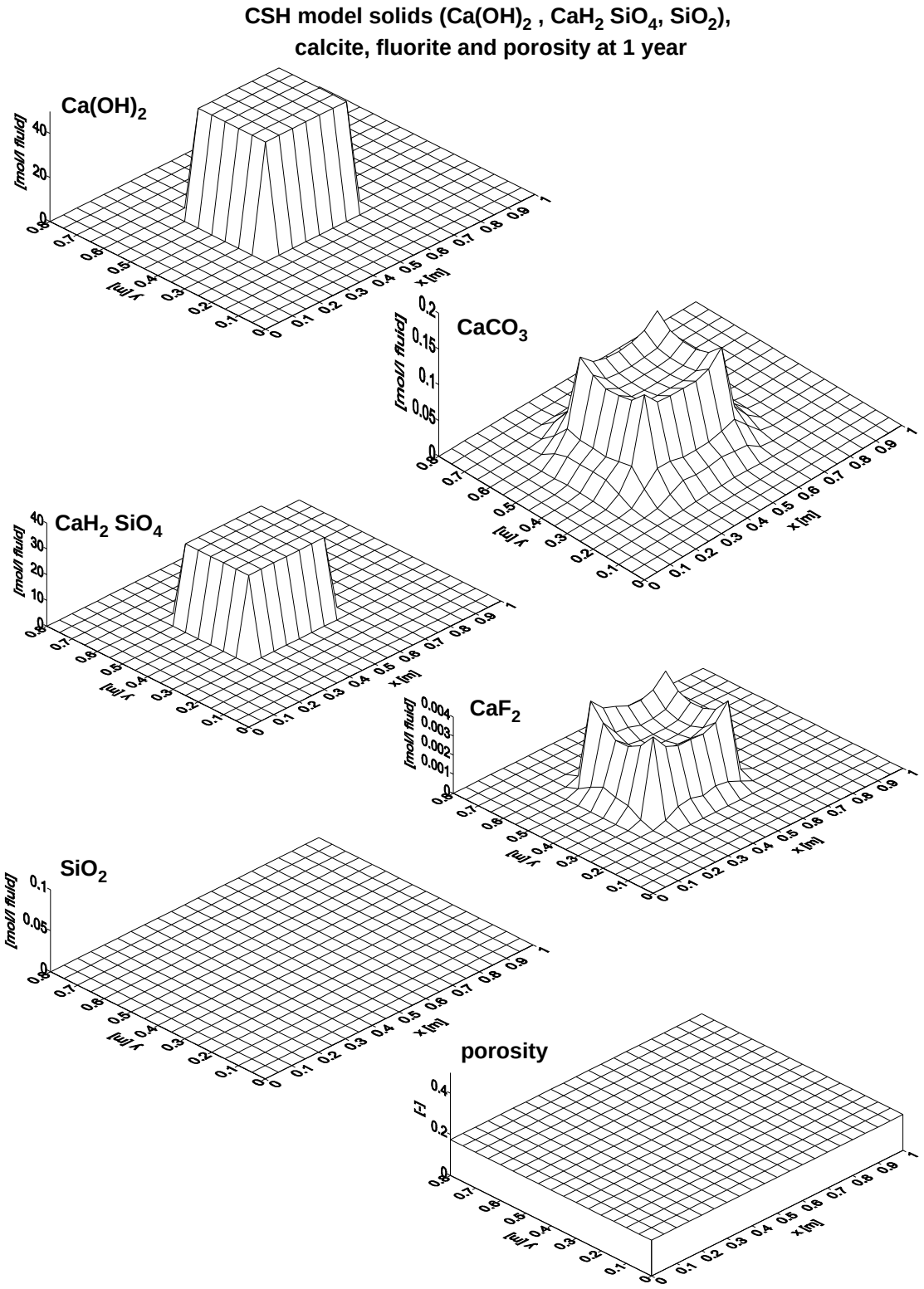

Fig. 4.2: Concentration of model solids calculated for 1 year of interaction of a cement "area", in the middle of the modelling area, surrounded by Wellenberg water and the resulting porosity changes due to mineral reactions (diffusion dominated case).

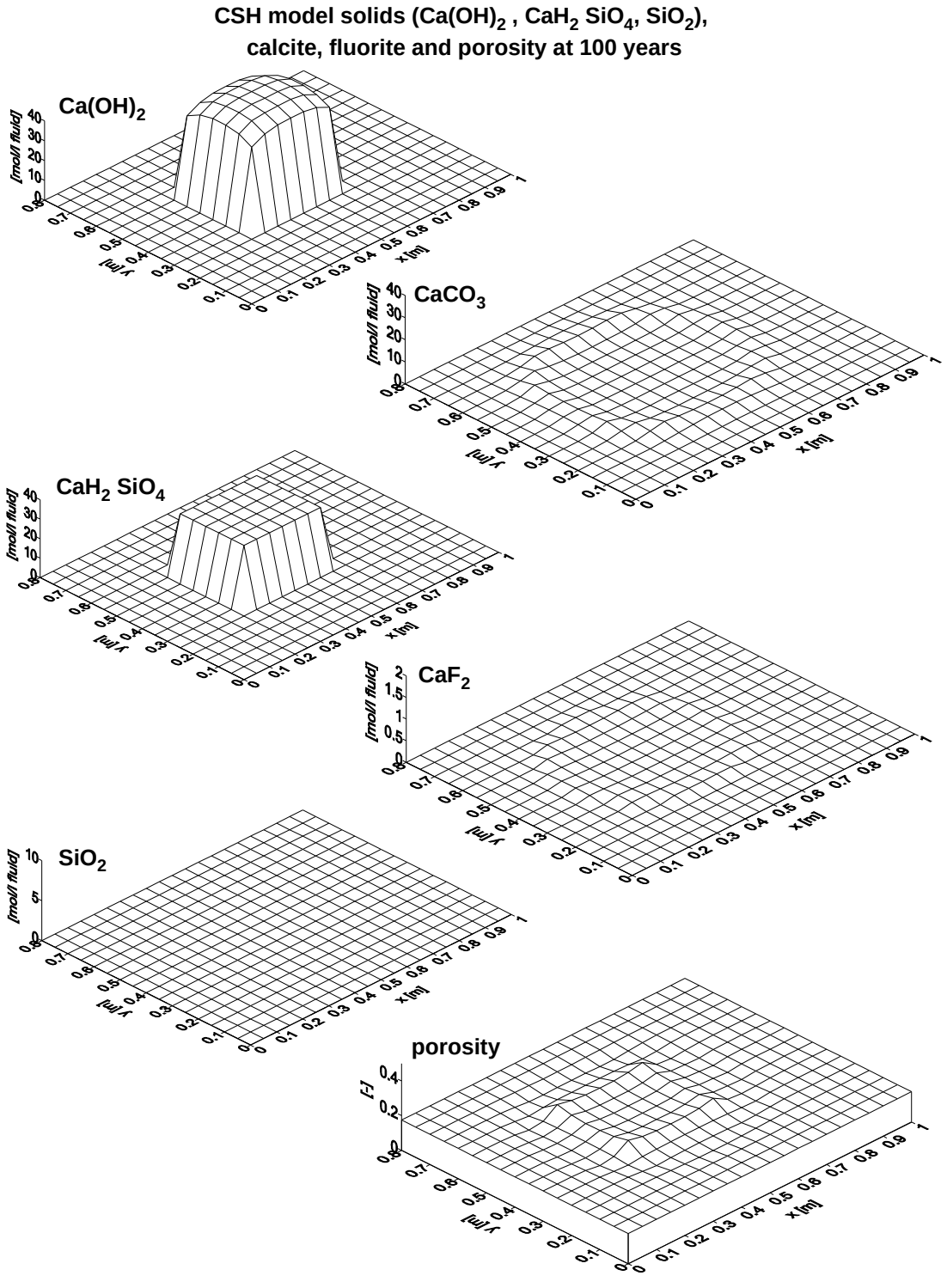

Fig. 4.3: Concentration of model solids calculated for 100 years of interaction of a cement "area", in the middle of the modelling area, surrounded by Wellenberg water and the resulting porosity changes due to mineral reactions (diffusion dominated case).

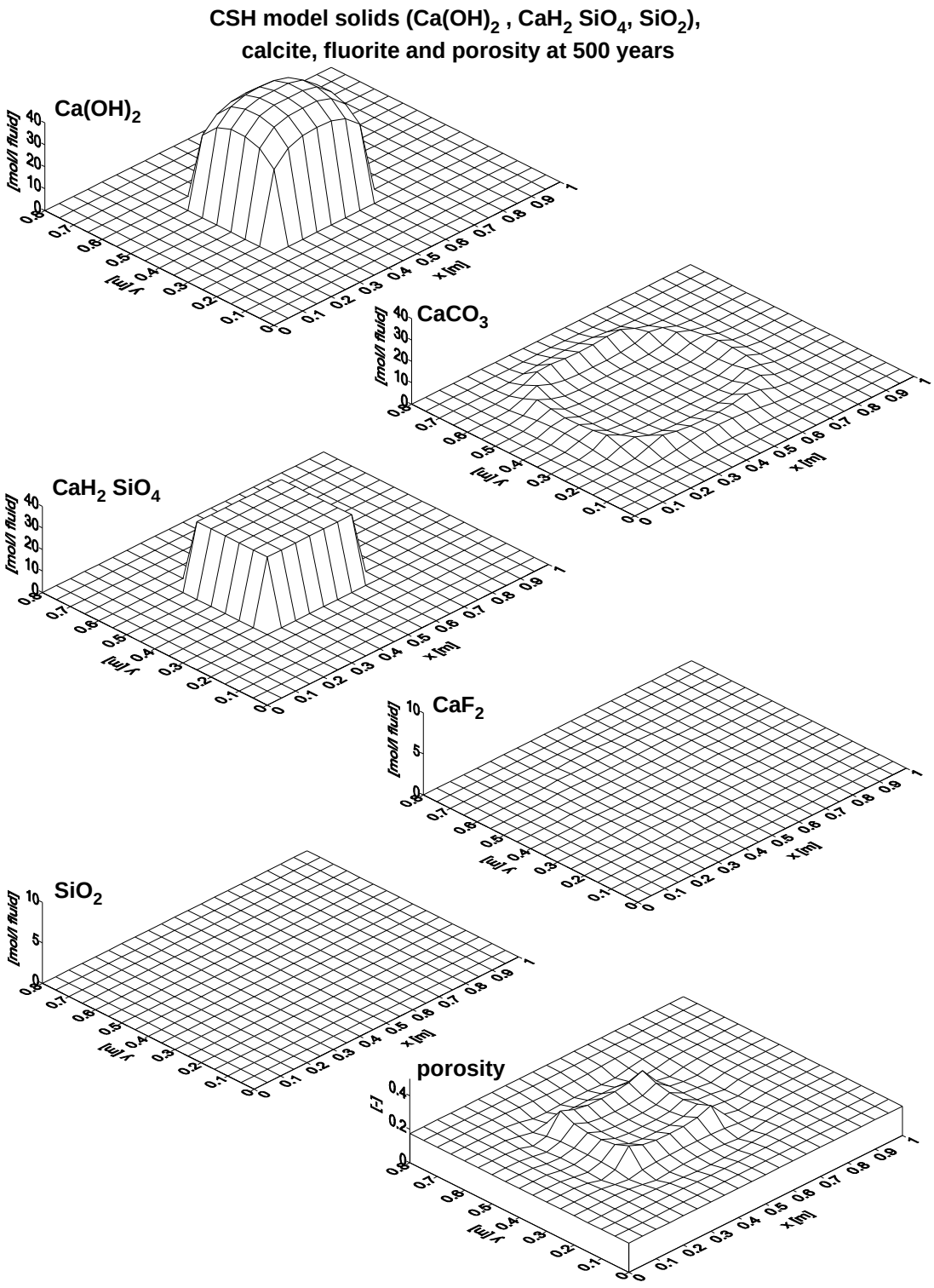

Fig. 4.4: Concentration of model solids calculated for 500 years of interaction of a cement "area", in the middle of the modelling area, surrounded by Wellenberg water and the resulting porosity changes due to mineral reactions (diffusion dominated case).

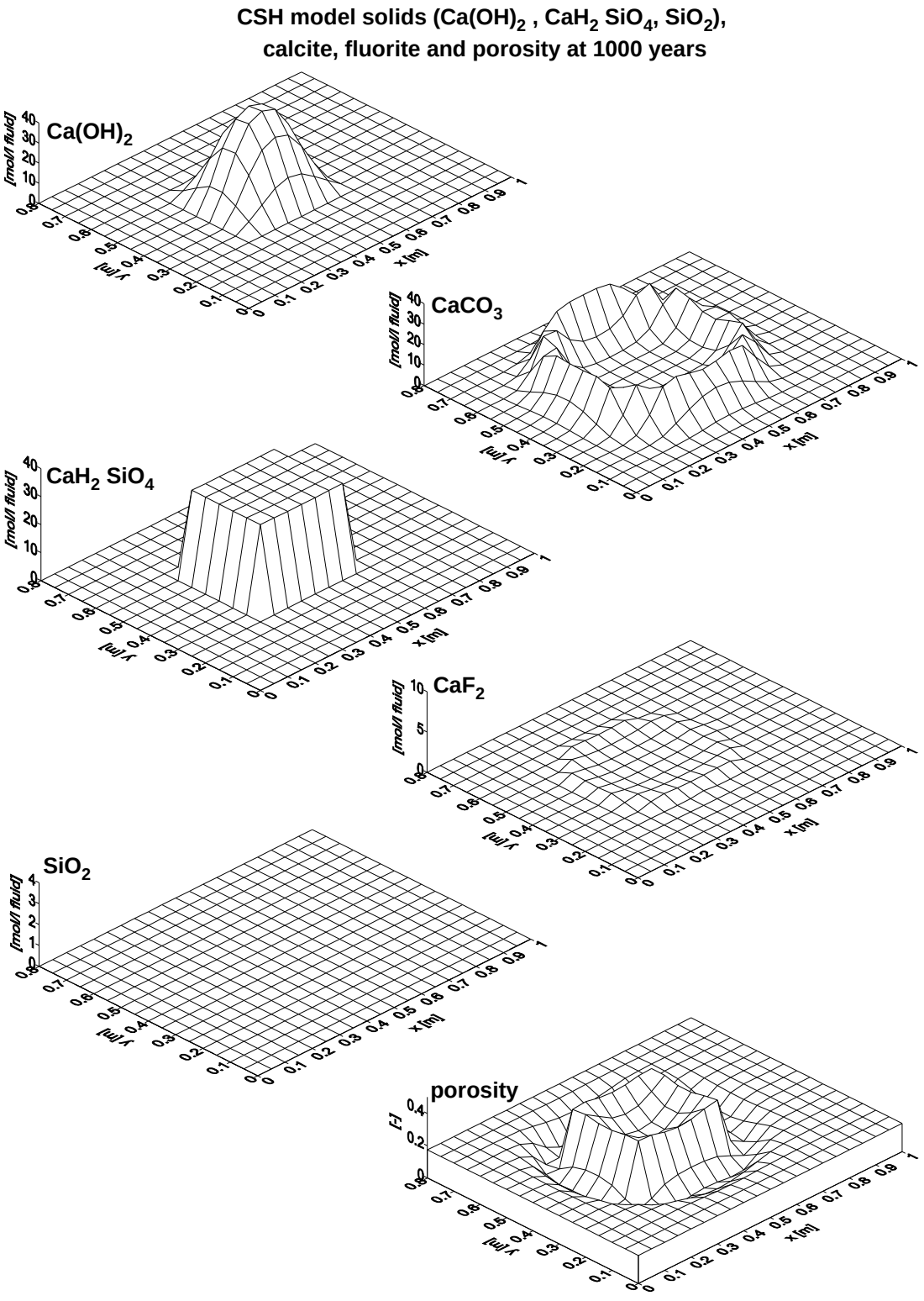

Fig. 4.5: Concentration of model solids calculated for 1000 years of interaction of a cement "area", in the middle of the modelling area, surrounded by Wellenberg water and the resulting porosity changes due to mineral reactions (diffusion dominated case).

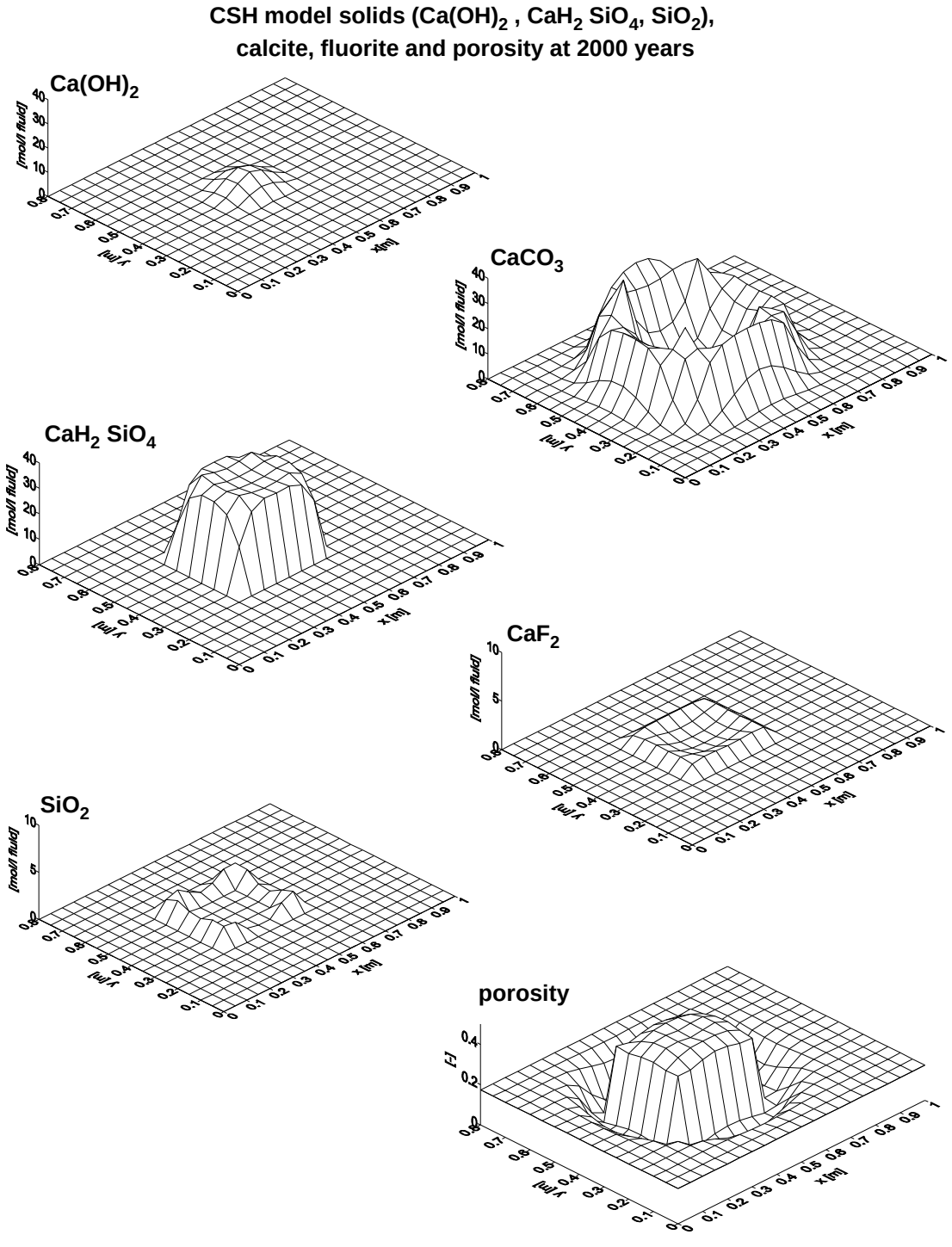

Fig. 4.6: Concentration of model solids calculated for 2000 years of interaction of a cement “area”, in the middle of the modelling area, surrounded by Wellenberg water and the resulting porosity changes due to mineral reactions (diffusion dominated case).

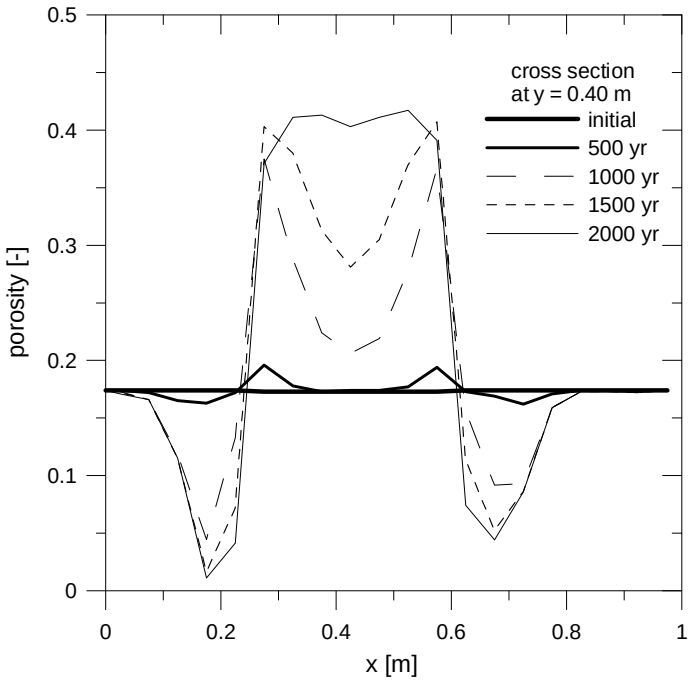

Fig. 4.7: Porosity distribution along a cross section in direction of the background water flow.

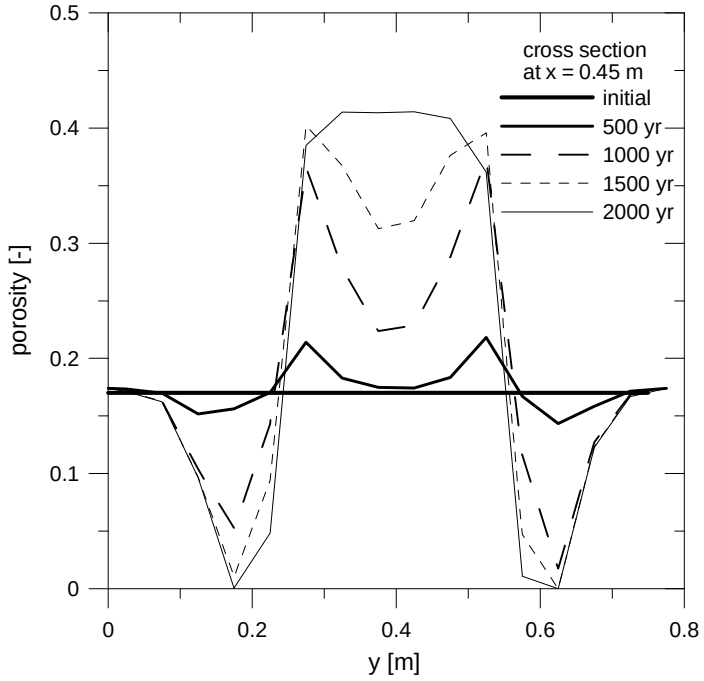

Fig. 4.8: Porosity distribution along a cross section perpendicular to the direction of the background water flow.

4.2 A diffusion-advection-dispersion near-field scenario

For this scenario the initial hydraulic conductivity is increased to $K = 10^{-8}$ m/s and all other parameters are as defined for Chap. 4.1. The initial background flow is increased by a factor of 10000 to $v = 2.3 \cdot 10^{-8}$ m/s. This scenario is related to the "pessimistic" value of 10^{-8} m/s for the hydraulic conductivity of the cementitious repository [NAGRA 1994]. The increased background water flow deforms the spatial distribution of solids dissolved and precipitated compared to the system described in Chap. 4.1. Results are shown in Figs. 4.9 to 4.13. The tendency in forming a calcite precipitation front is still dominating because porosity still decreases locally. This means that the cementitious repository would be isolated from the host rock environment directly at the upstream interface, and at some distance in the downstream area within the host rock. Compared to the scenario modelled in Chap. 4.1, the increased advective/dispersive flux yields an accelerated and more asymmetric dissolution of the model solid $Ca(OH)_2$. After one hundred years of interaction, this asymmetry is obvious in the spatial distribution of calcite and fluorite (Fig. 4.9). The increased background water flux causes increased dissolution but also increased precipitation at the upstream interface of the cement. This asymmetry is amplified for the solid distributions as time evolves. When comparing solid distributions at 500 years (Fig. 4.10), the $Ca(OH)_2$ is more dissolved at the upstream interface of the cement than for the pure diffusion scenario. In parallel, CaH_2SiO_4 is increased and SiO_2 is already present as a model solid at the upstream interface indicating there an accelerated dissolution. Increased calcite and fluorite precipitation occurs also at the upstream interface, whereas lower levels are reached for areas more downstream of the cement within the host rock and near the downstream model boundary. Fig. 4.11 illustrates that already after 100 years of cement-host rock water interaction a marked porosity decrease was calculated near the downstream boundary. The increased groundwater flow and the downstream concentration boundary condition chosen are mainly responsible for this decrease in porosity. The constant concentration boundary condition chosen may be justified by assuming a fast groundwater flow directly at the boundary. Then, the chemical gradients between water leaching from the cement and water at the downstream boundary will increase as the leaching front arrives at the boundary. Calcite precipitation will continue, because these chemical gradients will remain steep between boundary and cement leachate water composition (mixed composition of cement and host rock water). Porosity will decrease

to zero near the downstream boundary provided that enough calcium from the cement dissolution will reach this boundary[30].

The hydraulic conductivity distribution calculated from the porosity distribution at 500 years according to the Kozeny-Carman equation (Eq. 3.5) is shown in Fig. 4.12. After 500 years of interaction the variability in hydraulic conductivity has changed to values between 10^{-12} m/s and 10^{-7} m/s within the model domain, a variation where hydraulic codes may get into trouble with regard to numerical convergence. The hydraulic head distribution and related flow field is shown in Fig. 4.13. It differs from the initially homogeneous flow field in the x-direction. At the upstream interface of the cement, there is a lower conductivity zone with smaller values for water velocity (small arrows in Fig. 4.13). Directly along the sides of the cement area parallel to *x*-direction, there are high conductivity zones and faster water flow. At some distance from the sides slower water flow is observed due to smaller hydraulic conductivities (Figs. 4.12 and 4.13). Because hydraulic conductivity depends non-linearly on porosity, these flow patterns will change, especially for the areas where a porosity reduction occurs. The steep gradients in the hydraulic conductivity distribution, together with the decrease of porosity near the downstream boundary, caused slow convergence, especially in the hydraulic module, and calculations were stopped after 500 years.

When looking at the “small scale repository”, the same conclusions can be drawn as in Chap. 4.1. The reactions at the upstream cement-host rock interface will decrease the porosity there, reducing the values for the hydraulic conductivity and diffusivity. This will increase the water flux along the cement-rock interface in flow direction. In the downstream region a calcite precipitation front will develop on a lower and slower level. The tendency here is to clog the cement from further interaction with the host rock by decreasing the solute transport parameters. This clogging will be more effective when steep chemical gradients remain constant as for the constant concentration boundary condition at the downstream boundary assumed here.

[30] If there is not such a highly conductive zone at the boundary, the model area might be increased, so that there would be no influence of the downstream boundary condition chosen on the calcite precipitation front. Then, the downstream calcite front would be more extended into the host rock area, and the amount of calcite precipitated would be more dispersed but completely within the model area. Another modification would be to change the concentration boundary condition to “free outflow”. This means that the solute concentrations at the boundary will be defined (extrapolated) by concentrations inside the model area. Then, the calcite precipitation front will move across the downstream boundary These scenarios are open to future modelling and comparison.

This diffusion-advection-dispersion scenario might be more sensible to its general trend of evolution - clogging or no clogging, or evolution and extension of the clogging region. If advection-dispersion (slightly) dominates diffusion, then rock water may flow through the degraded cement in the long-term, which means that the cement will be completely dissolved. Such a scenario might be realised by an initially higher hydraulic conductivity and related increased water velocity. If the system was homogeneous, such a scenario might be looked at as a one-dimensional system, where host rock water flows through the cement. The chemical gradient between cement and host rock water is kept steep at the inlet (upstream boundary) for all times. Then, the precipitation and dissolution fronts move through the repository, similar to the fronts described in App. B for a one-dimensional system. As calcite has a lower molar volume than assumed for the model solids portlandite and CaH_2SiO_4[31], the porosity increases at the upstream boundary, because portlandite and CaH_2SiO_4 are successively replaced by calcite. For this pure advective system, the location of the mineral front system might be extrapolated for larger times. If small changes in porosity are neglected, this simple system behaves linearly, due to a constant water flux through the whole system. If the increase of porosity is taken into account, hydraulic conductivity and water flux are increased too, and a faster degradation will occur, if constant hydraulic head conditions are assumed at the model boundaries. As a result, the advection dominated system is characterised by slightly increased porosity in the cement area and a non-sealing behaviour. But when looking at the heterogeneity of a real cementitious repository there will be large compartments where diffusion dominates.

---

[31] As given in Table 4.5 the model solids concentrations of $Ca(OH)_2$ and CaH_2SiO_4 are 48.491 mol/l_{fluid} and 29.547 mol/l_{fluid}, respectively, which results in a C/S of about 2.7. Taking into account these values and the specific density and molar weight of the model solids, the initial volume fraction occupied by the model solids is:

$$initial\ volume = \varepsilon_f \cdot \left(P_{Ca(OH)_2} \frac{\rho_s^{Ca(OH)_2}}{V_{mol}^{Ca(OH)_2}} + P_{CaH_2SiO_4} \frac{\rho_s^{CaH_2SiO_4}}{V_{mol}^{CaH_2SiO_4}} \right) = 0.56 cm^3$$

Assuming that all Ca from the model solids is used to precipitate calcite within the grid cells, the final solid volume - now calcite only - is:

$$final\ volume = \left\{ \begin{matrix} all\ \ Ca\ \ from\ model\ solids\ is \\ used\ to\ \ precipitate\ calcite \end{matrix} \right\} = \varepsilon_f \left(Ca\ in\ Ca(OH)_2 + Ca\ in\ CaH_2SiO_4 \right) \frac{\rho_s^{CaCO_3}}{V_{mol}^{CaCO_3}} = 0.50 cm^3$$

Looking at the sum of the initial volume fractions of the model solids and the final volume fraction of calcite, the porosity increases due to lower molar volume of calcite compared to the mean molar volume of $Ca(OH)_2$ and CaH_2SiO_4 together.

As already mentioned in Chap. 4.1, the results shown here for the diffusive advective-dispersive scenario, depend on the model assumption performed (homogeneous single porous medium, porosity hydraulic conductivity relationship, etc.). Even if modelling starts with “homogeneous parameters” for flow, porosity and hydraulic conductivity, etc. quite heterogeneous parameter distributions are calculated. This has consequences for a heterogeneous cement degradation within such a host rock environment.

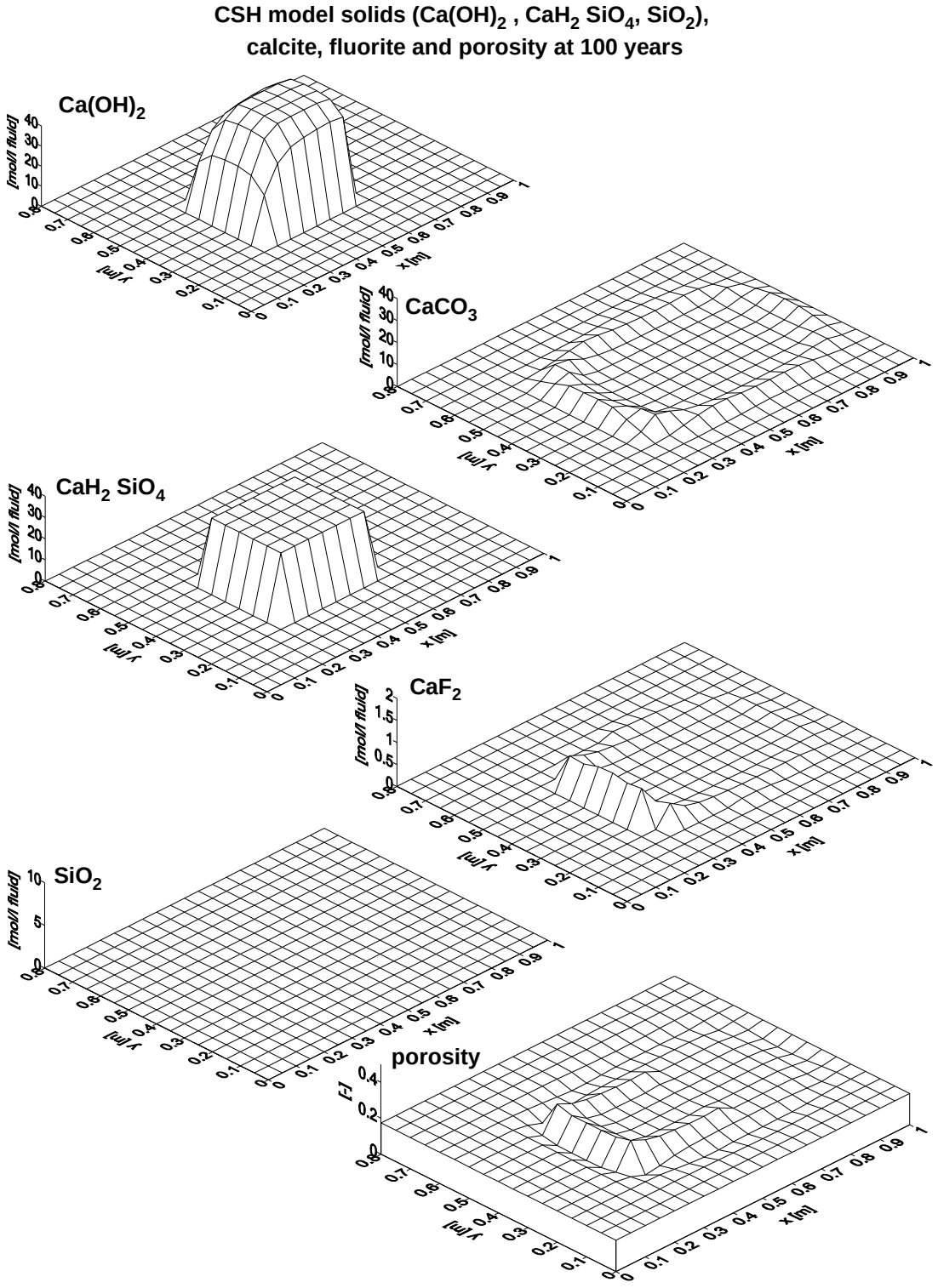

Fig. 4.9: Concentration of model solids calculated for 100 years of interaction of a cement "area", in the middle of the modelling area, surrounded by Wellenberg water and the resulting porosity changes due to mineral reactions (advection-dispersion case, water flow is in *x*-direction).

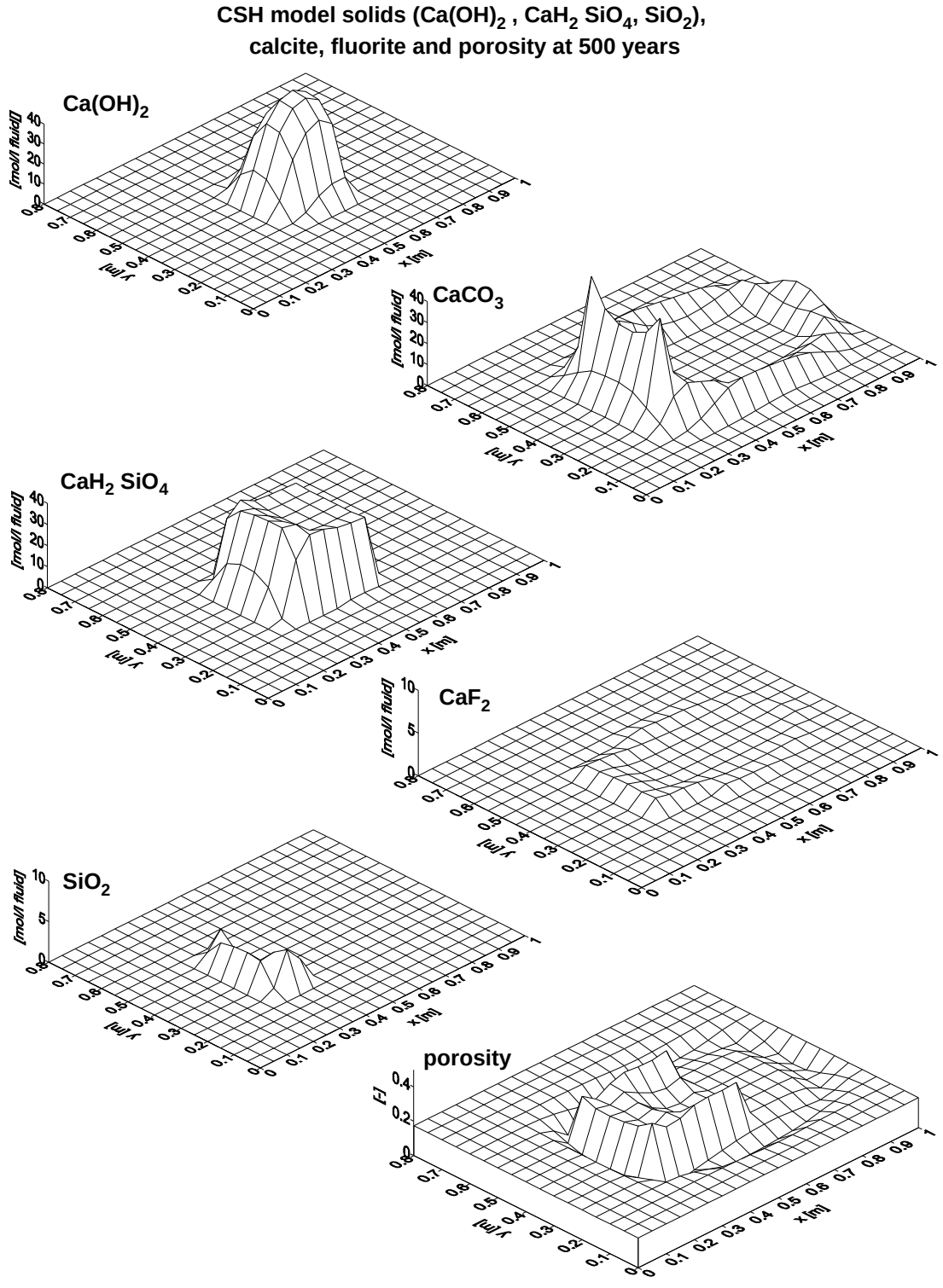

Fig. 4.10: Concentration of model solids calculated for 500 years of interaction of a cement "area", in the middle of the modelling area, surrounded by Wellenberg water and the resulting porosity changes due to mineral reactions (advection-dispersion case, water flow is in *x*-direction).

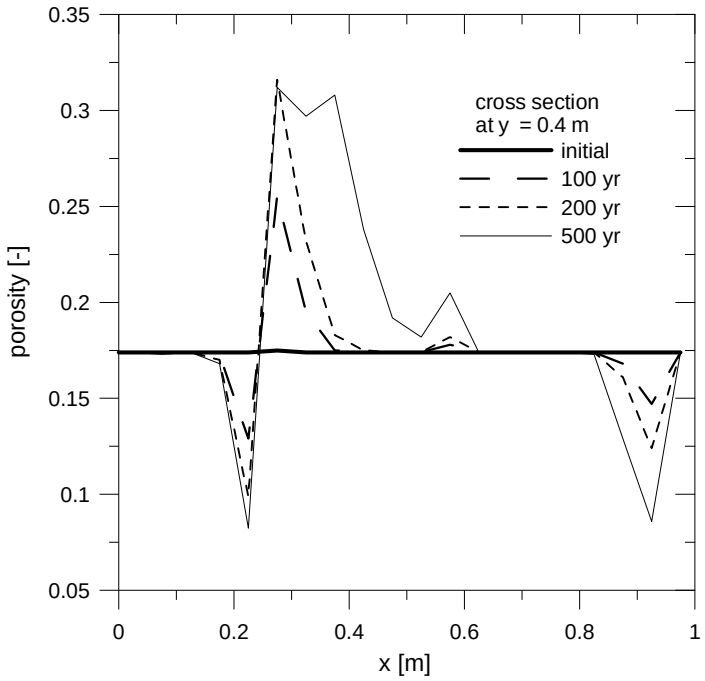

Fig. 4.11: Porosity distribution along a cross section in direction of the background flow.

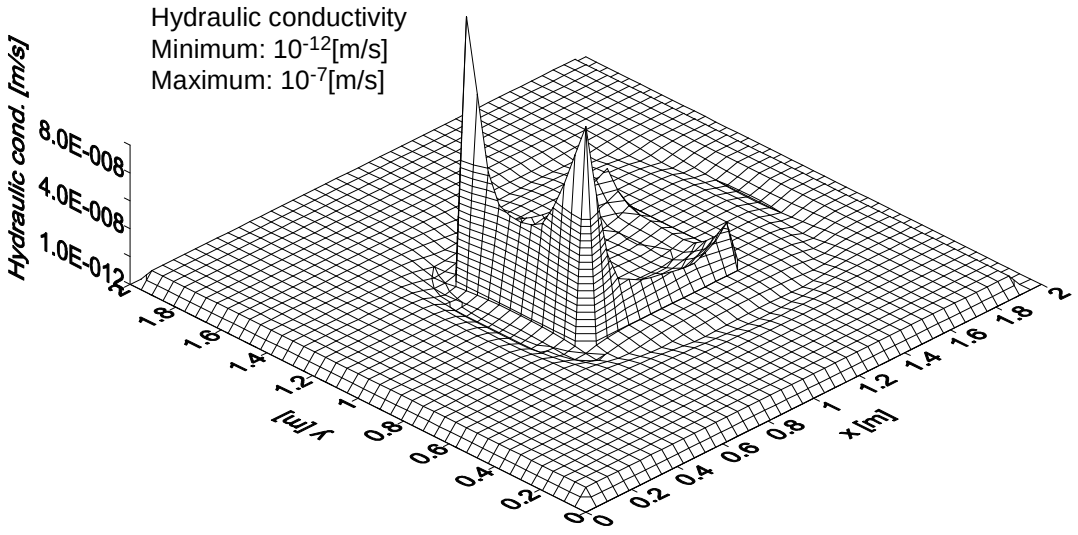

Fig. 4.12: Hydraulic conductivity calculated from porosity (Kozeny-Carman equation) after 500 years cement rock water interaction.

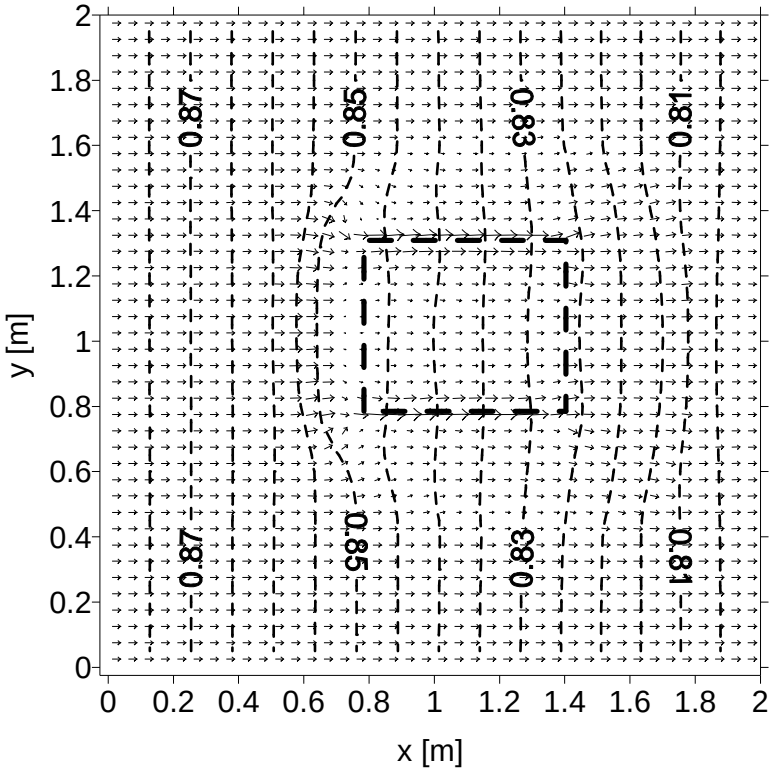

Fig. 4.13: Contour plot of hydraulic heads (dashed lines; levels in m) and related flow field (arrows) calculated for 500 years cement rock water interaction. The initially homogeneous flow field in x-direction is changed due to hydraulic conductivity and porosity changes. The bold dashed line indicates the (initial) boundary of the cement area.

4.3 A diffusion induced flow scenario

The most favourable scenario for a repository would be a zero hydraulic gradient environment without any groundwater flow. Diffusion processes would then dominate solute transport. Although finding such an environment is not very likely, nor can it be guaranteed that it will be stable for long time scales, such a scenario serves for investigation of specific coupled processes. Hydraulic, transport and chemical processes as well as their modular coupling, their interaction, and their exchange terms are tested concerning a correct mass balance for all modules together - not only for an update of parameters between modules. When choosing a scenario without groundwater flow, at first view, one can have the impression that a hydraulic model for such a set-up is not necessary. However, a chemical system with steep chemical gradients induces mineral reactions driven by diffusion in the model area, followed by porosity changes. If the

dissolving and precipitating minerals have different molar volumes, or, if there are developing precipitation or dissolution fronts, local porosity changes will induce additional water flux (and related solute transport) to compensate created or destroyed mineral volume[32].

The induced water flux by mineral reaction is small compared to possible background water flux, and can be at maximum equal to the change in porosity of the whole system from an initial to a final value divided by the time proceeded during this process. However, the induced flow may play an important role in heterogeneous media with steep chemical (reactive) gradients. It may increase locally the hydraulic head gradients (hydrostatic pressure) in a low permeable compartment and therefore, may create cracks - similar to those generated by corrosion processes and organic matter degradation and related gas production (H_2, CO_2 and CH_4 production as described in [NAGRA 1994], p. 40) which can serve for additional fast flow paths for radionuclides. Nevertheless, this example shows that these processes are not ignored in the modular coupling of hydraulics, transport and chemistry.

The following chemical set-up of the system is the same as for the previous applications. The initial transport is by diffusion only (zero hydraulic gradient in *x*- and *y*-direction (Fig. 4.1). Modelling results are shown in Figs. 4.14 to 4.18. The calculated model solid distributions look very similar to those calculated in Chap. 4.1 for the diffusion scenario with a small background groundwater flow in the *x*-direction. Cement is dissolved, especially at the edges, and calcite and fluorite are precipitated around the cement, as shown in Fig. 4.14 for 200 years of interaction. The resulting porosity distribution shows an increased porosity where cement ($Ca(OH)_2$) dissolves and a decreased porosity where calcite precipitates. The porosity changes induce volumetric fluid fluxes according to Eq. 3.4 which affects the hydraulic head distribution in the model area (Eq. 3.3). In addition, the porosity changes induce non-linear hydraulic conductivity changes (Eq. 3.5). The initially assumed smooth hydraulic conductivity distribution becomes quite heterogeneous in the model area. A time series of hydraulic head

[32] If there were only porosity updates from one time step to the next without taking into account the related volume changes, no water flux would be induced in the whole model area by local, chemically born sources and sinks that are related to finite differences grid. Then, the hydraulic conductivity would be recalculated due to the porosity update, but the calculated hydraulic gradient would be different since no changes of water volume (local sources and sinks) would be taken into account. Here, however, the local water volume or porosity changes are taken into account explicitly by the exchange terms, generating water flux from or to the chemical reactive areas in the model domain.

distributions is shown in Figs. 4.15 and 4.16. An initially flat head distribution changes to a mountainous head distribution. Local porosity increase (decrease) generates “sinks” (“sources”) that are taken into account within the hydraulic model. Together, a net flow is produced away from the cement area but on a very small level. At later times this groundwater flow pattern reverses. Groundwater flow is then towards the cement area as illustrated in Figs. 4.17 and 4.18. For the initial flow field (top left in Fig. 4.17), flow velocities are calculated to be on a level of $\pm 10^{-18}$ m/s ($\cong$ 0 m/s) due to the numerical precision chosen for the hydraulic modelling. For the following patterns, the maximum flow velocities are calculated to be on a level of 10^{-14} m/s to 10^{-15} m/s decreasing with increasing time. This is still quite small in comparison to the background flow velocity used in the example described in Chap. 4.1. However, it shows that simple hydraulic, transport and chemical reaction processes generate a complex system behaviour due to their coupling. In the initial phase, mineral reactions driven by diffusion generate a net porosity decrease in the total model area, increasing hydraulic head by “local sources”. Later on, a net increase results, accompanied by a decrease of hydraulic head induced by “local sinks”.

To examine whether this calculated system behaviour is correctly handled in the code, one can compare the porosity changes in the model area within a time period with the resultant hydraulic head distribution, both calculated by different modules. This is shown in Fig. 4.19. Porosity distributions calculated for different times are subtracted from each other. The result is the local, grid related porosity increase or decrease in the model area during a time interval. The total change of porosity in the model area should then result in a decrease or increase in the related hydraulic head distribution. In the initial phase, the total porosity at 1.5 s is larger than that at 0.1 y. Therefore, a porosity decrease results in a head increase in the model area that is due to the additional “local sources”. The picture is different for later times. Comparing porosity distributions at 100 and 200 years leads to a net porosity increase for the total model area. Then the porosity increase causes additional “local sinks” and related hydraulic head reductions as shown in Figs. 4.15 and 4.16. Although diffusion has induced an additional local groundwater flow out or into the model area, this flow is decreasing with time (Figs. 4.17 and 4.18). However, within the region of the cement-host rock interface flow is still induced by the mineral reactions. In cases where porosity becomes quite small, small changes in the porosity lead to fast flow because of high relative porosity changes. These additional “local sources” can generate large hydraulic head differences together with the non-linear dependency of porosity and hydraulic conductivity, so that an influence on the mechanical structure of repository cement or host rock is no longer negligible. These

effects seem to be more important if the heterogeneous cement and host rock structures are taken into account and fracture flow in a steep chemical gradient environment is considered, factors that require a complex future investigation.

Altogether, this example shows that diffusion will remain the dominant transport process in a no-flow environment, also at later times. The same holds for systems, where the diffusion dominates the small background flow field, as described in Chap. 4.1. For those scenarios with background flow field, the local porosity and hydraulic conductivity changes can have a strong influence on the water flow path and their temporal development, the most important feature for the description of radionuclide migration away from a repository. In addition, the diffusion induced flow, although calculated at low levels compared to background flow assumed for Chapts. 4.1 and 4.2, may generate large hydraulic gradients in a low permeable environment. This may cause mechanical stress within the porous medium and additional fractures might be created. These mechanical processes are still not coupled to the hydraulic, transport and chemical processes. It might be worthwhile to investigate rock mechanical stability in the presence of steep chemical gradients and related rock mineral reactions.

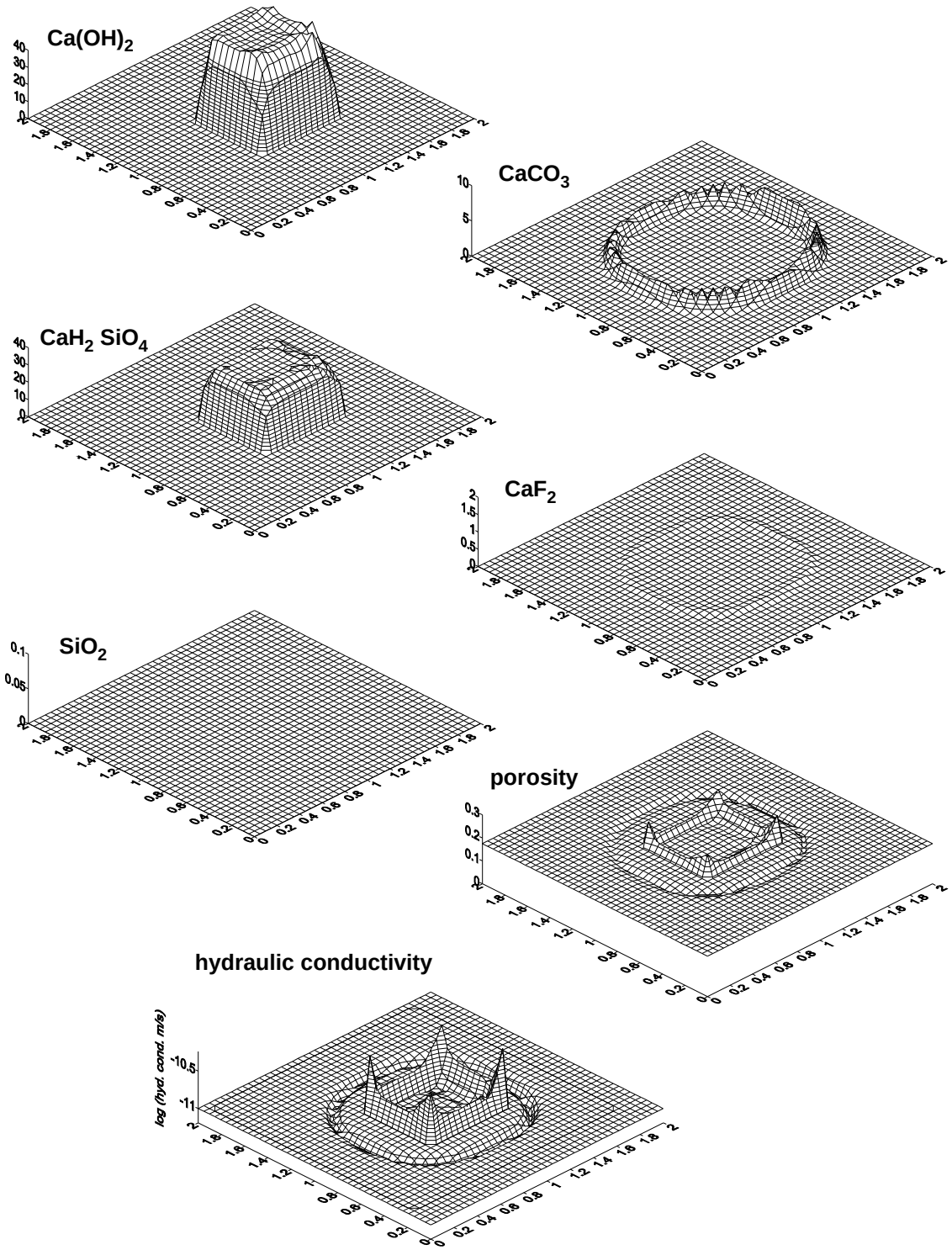

Fig. 4.14: Concentration of model solids [mol/l_{fluid}], porosity and hydraulic conductivity [m/s] calculated after 200 years of interaction of a cement "area", in the middle of the model area (*x*-*y* grid in [m]) surrounded by Wellenberg water and the resulting porosity changes due to mineral reactions (pure dispersion case).

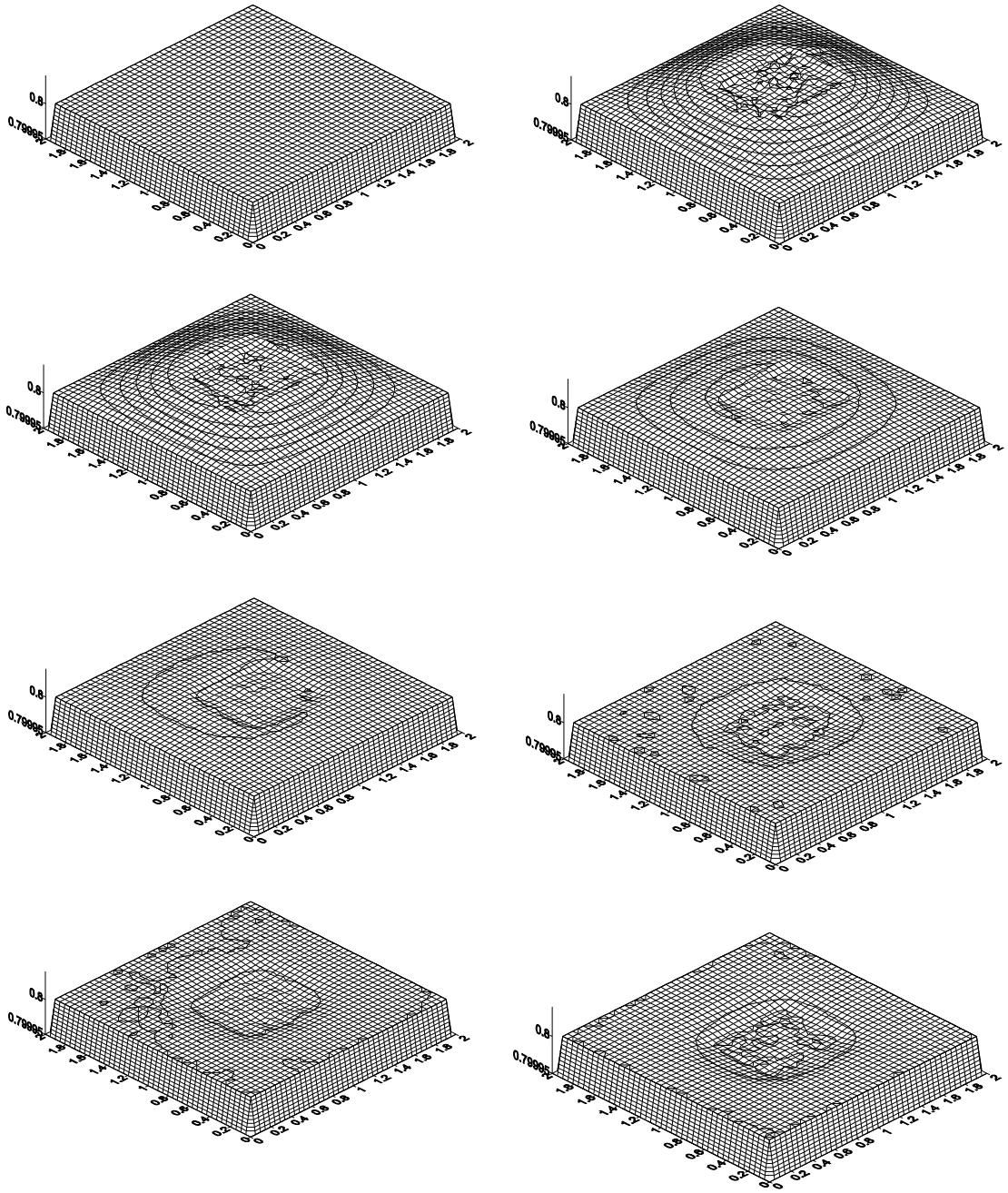

Fig. 4.15: Calculated hydraulic head [m] distributions (surfaces) in the model area (*x*-*y* grid in [m]) for a times of 1.5 s, 0.1 y, 0.2 y, 1 y, 2 y, 10 y, 100 y and 200 y from top left to bottom right.

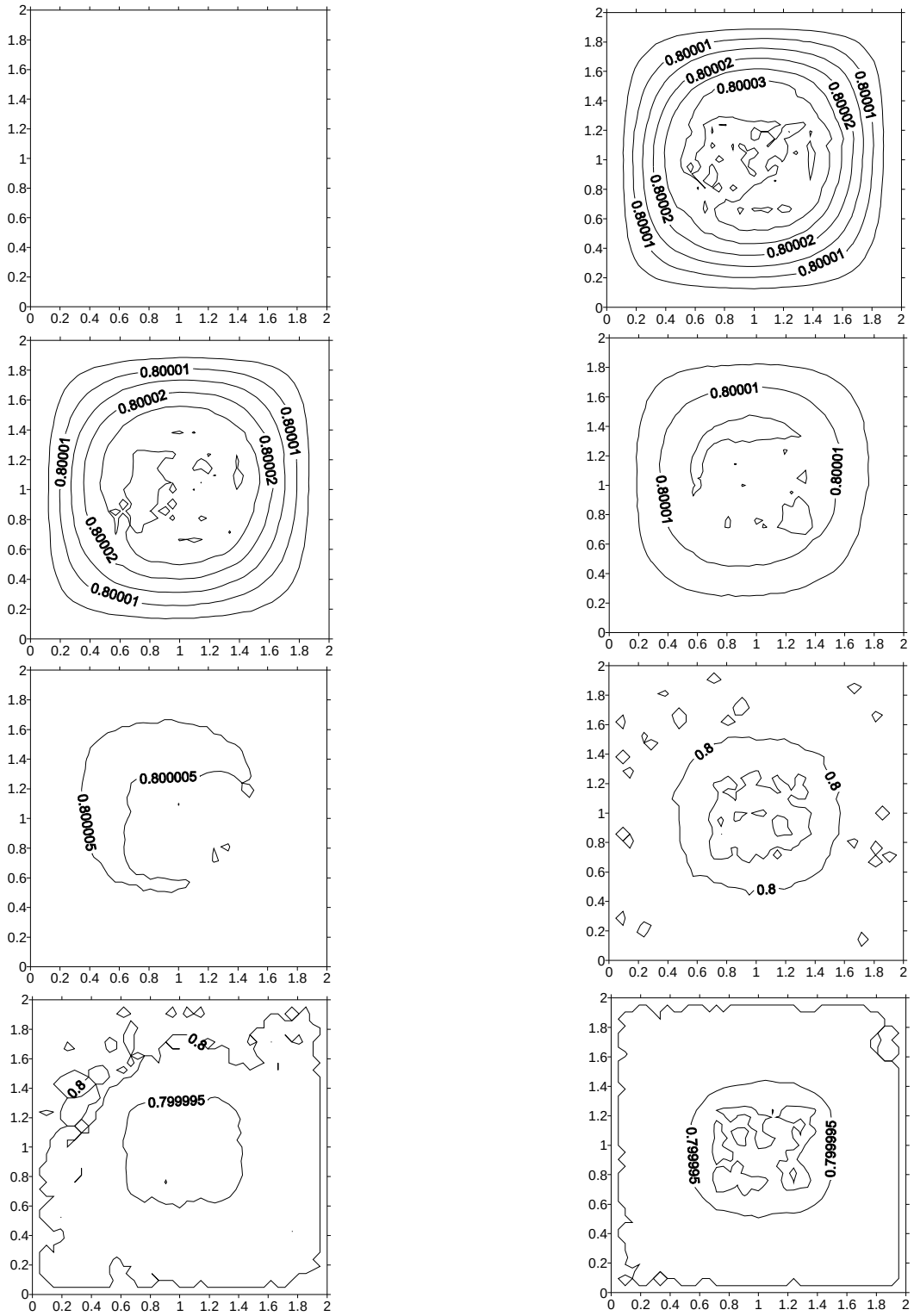

Fig. 4.16: Calculated hydraulic head [m] distributions (lines of equal head level) in the model area (*x-y* grid in [m]) for a times of 1.5 s, 0.1 y, 0.2 y, 1 y, 2 y, 10 y, 100 y and 200 y , top left to bottom right. (The small patterns partly result from the Random-Walk transport description and partly from the numerical interpolation used within the graphics program, and may be considered as artefacts)

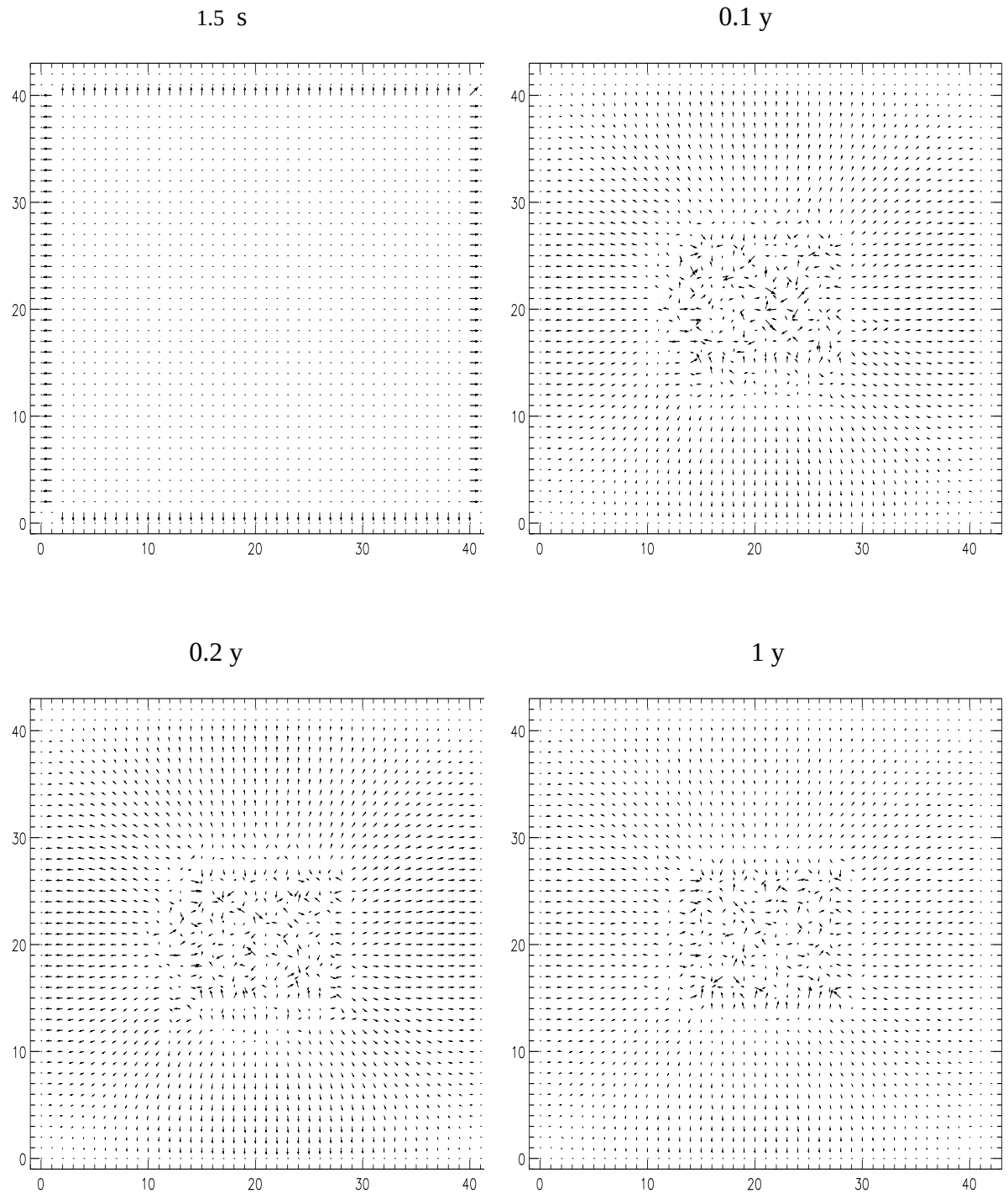

Fig. 4.17: Development of a diffusion and chemical reaction driven groundwater flow field in the model domain (*x-y* grid in [m]).

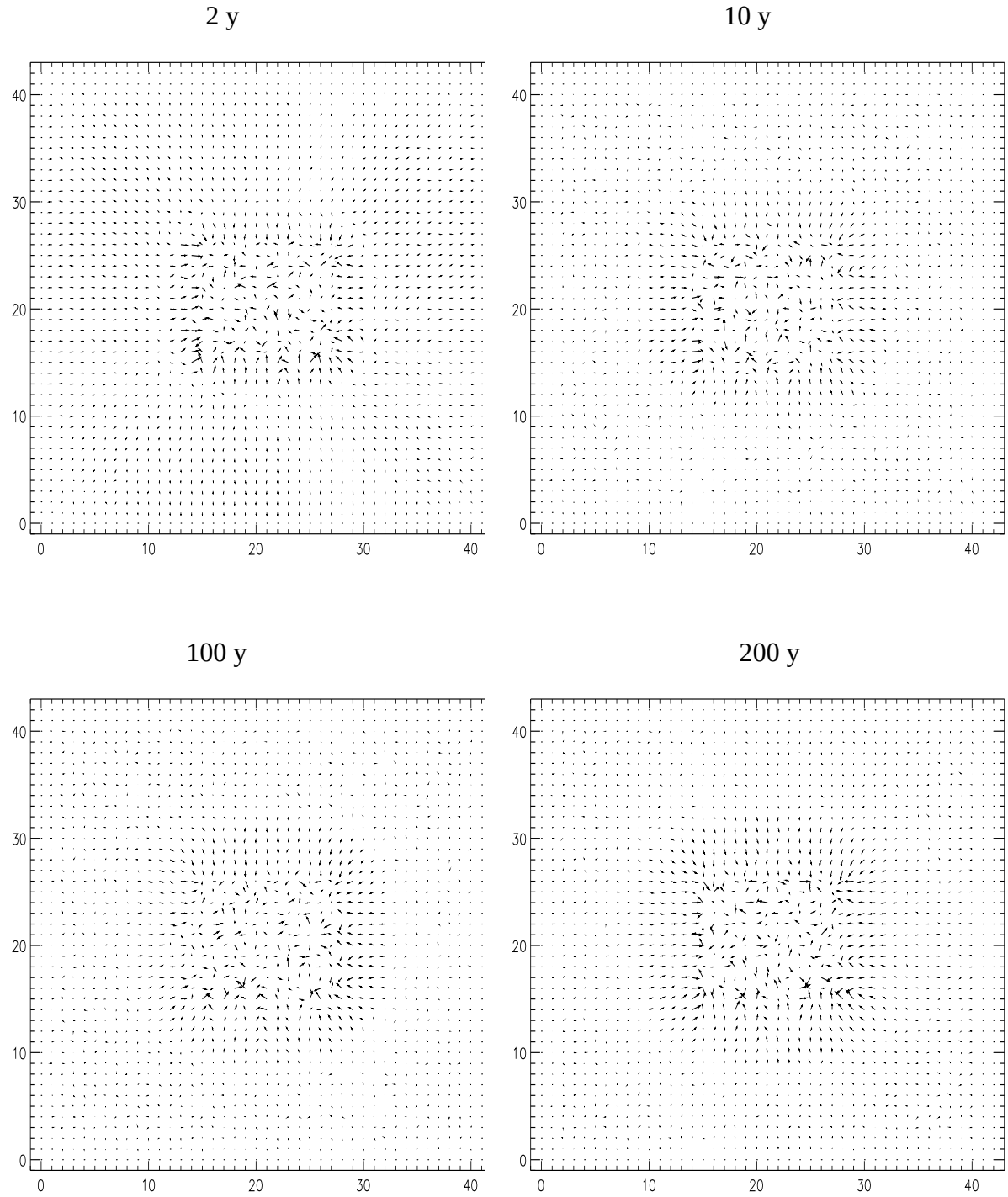

Fig. 4.18: Development of a diffusion and chemical reaction driven groundwater flow field in the model domain (*x*-*y* grid in [m]).

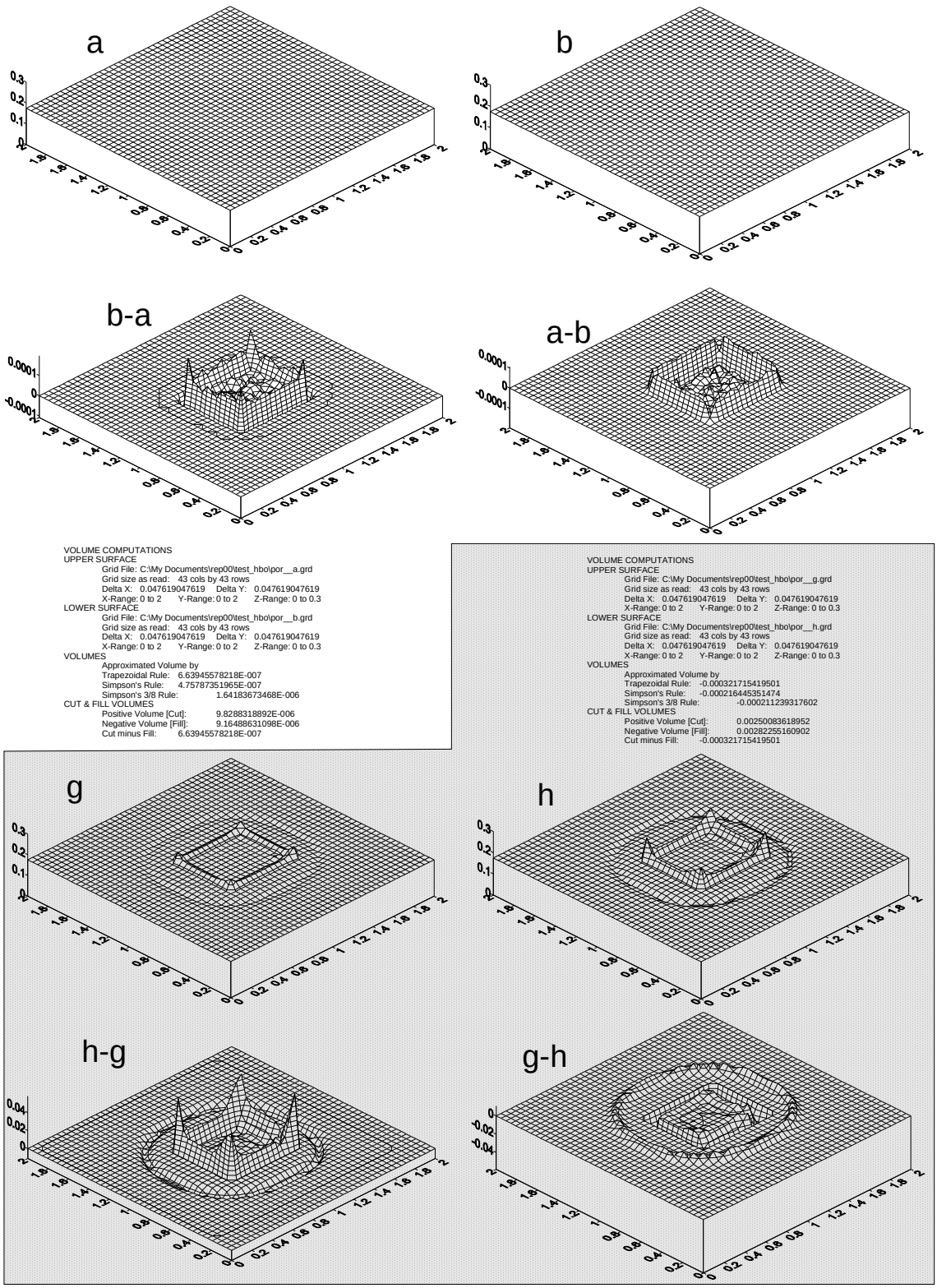

Fig. 4.19: Calculated porosity and porosity differences during initial (a = 1.5s, b = 0.1 s) and later (g = 100 y, h = 200 y) interaction intervals and related volume changes for the total model area (*x*-*y* grid in [m]).

5 CONCLUSIONS

It has been shown that one-dimensional modelling is insufficient for these detailed near-field modelling, especially if large chemical gradients induce mineral reactions and related porosity changes. Although one-dimensional modelling has been applied more or less successfully to several laboratory experiments, the extrapolation from such experiments to multi-dimensional real scenarios in nature is difficult. Results from column experiments and one-dimensional modelling indicated that, due to mineral reactions, hydraulic and transport properties, such as porosity, hydraulic conductivity, flow field and velocity, change with time. It is not possible to rigorously account for these processes in a real repository near-field with one-dimensional modelling, since e.g. the flow field is at least two-dimensional and may change locally from increased flow to zero flow. Here, investigations were also focused on the choice of the boundary conditions assumed within the near-field. A constant concentration boundary chosen at a host rock-cement interface leads to fast degradation of a cement in a diffusion dominated system. If the interface is chosen to be within the model area, the degradation is slower, although the porosity is calculated to be lower for the second case due to spatially separated dissolution and precipitation. The latter is of special interest when investigating clogging processes and the related time scale.

In order to overcome the limitations of one-dimensional modelling, a two-dimensional coupled hydraulic and reactive transport code was developed. The code is described by its individual hydraulic, transport and chemical modules and their coupling. The hydraulic conductivity and diffusion coefficients are described by explicit functions of porosity in order to couple groundwater flow and transport with chemical reactions. The 2D-MCOTAC version was verified by comparison to an analytical solution for a simple hydraulic but reactive transport problem. Code applications to two-dimensional scenarios for cement degradation by a groundwater are relevant to the assessment of long-term performance of a cementitious repository. This modelling shows how the flow field in a “small scale near-field” will change with time due to mineral dissolution and precipitation. In advection-dispersion as well as in diffusion dominated systems, steep chemical gradients cause mineral reactions at the interface cement-host rock. These reactions are accompanied by porosity reductions near the interface and flow field changes, i.e. changes of solute transport parameters. In an initially no flow scenario, the coupling of reactive transport to hydraulic calculations shows that chemical reactions induce flow during interactions between cement and host rock. For this porous medium

approach the induced flow was calculated to be small compared to the assumed background flow at a repository site. However, for another system geometry, e.g. a heterogeneous, fractured cementitious repository, local hydraulic head (stress) build-up may occur generating channelled flow paths for radionuclides. Therefore, calculations assessing the long-term behaviour of cementitious nuclear waste repositories need to include these effects because they affect radionuclide transport from the repository.

So far, the modelling work presented here does not include a complete description of the near-field geometry, structure and geochemical composition. Some consequences resulting from this for hydraulic, transport and chemical processes are included qualitatively in the discussion of the examples and need further investigations. In particular, the influence of heterogeneity is important to investigate, because even thin layers of secondary mineral affect water flow in column experiments. Also not included is the discussion of kinetic reactions and precipitation of metastable minerals, as it is often observed in laboratory experiments. Such experiments have been performed for some months to some years, but their relevance for long-term prediction of several thousands of years needs careful assessment. However, to correctly describe laboratory experiments by coupled modelling such processes have to be included. The systems described here are water saturated systems. Unsaturated systems and additional gas flow, as well as the influences of coupling to mechanical stability of the whole near-field due to mineral reactions were not taken into account. They may be important processes.

Another point should be made on the computer time used for the examples given here. Although computer performance is still increasing, it is easy to get to the limits in increasing spatial dimension or discretisation, in complexity of the chemical system or the degree of coupling of individual models which would be necessary for a full scale heterogeneous representation of the repository near-field. For the examples presented here, the pure runtime on a high end, single processor workstation was in the order of minutes for simple applications, e.g., the verification example, to hours and days for the more complex, more finely discretised, fully coupled systems modelled. In particular, the non-linearity within the coupled description and related slow convergence for iterative coupled modelling can increase computing time. Therefore, an optimisation of the coupling procedure (coupling terms) with respect to runtime is necessary to model more complex systems. In addition, benchmark verification exercises with other codes (or analytical solutions) are necessary, including more complex hydro-geochemical systems, to improve the confidence in results of coupled modelling.

The two-dimensional modelling of coupled hydraulic, transport and chemical processes has improved the understanding of processes occurring in a cementitious repository near-field. The simplified geometry and composition used for the cement and host rock showed a complex system evolution, mainly driven by steep chemical gradients at their interface. Including the detailed geometry and structure of a cementitious repository and the adjacent host rock at scale will further improve the understanding of the near-field allowing for more quantitative predictions concerning self-sealing behaviour and isolation of radionuclides. Further data are required related to the dependence of hydraulic conductivity and diffusion coefficient on porosity, in particular for materials that will be used for the real repository and the site specific host rock. Similar information is necessary on secondary minerals that will form under site specific conditions, i.e. local chemical and mineral compositions, temperature and pressure. Therefore, reactive transport modelling needs additional laboratory and site specific experiments to be applied to a more realistic description of a cementitious waste repository and related radionuclide migration.

6 REFERENCES

Adenot, F. and Buil, M. (1992): *Modelling of the Corrosion of the Cement Paste by Deionized Water*, Cement and Concrete Research, vol. **22**, pp. 489-496.

Baeyens, B. and Bradbury, M.H. (1994): *Physico-chemical characterisation and calculated in situ porewater chemistries for a low permeability Palfris marl sample from Wellenberg*, PSI Bericht 94-19, Paul Scherrer Institut, Villigen, Switzerland.

Bateman, K., Coombs, P., Noy, D.J., Pearce, J.M. and Wetton, P.D. (1998): *Numerical modelling and column experiments to simulate the alkaline disturbed zone around a cementitious radioactive waste repository*, (I. G. McKinley and C. McCombie Eds.) 21st Int. Symp. on the Scientific Basis for Nuclear Waste Management, Davos, Switzerland, Mat. Res. Soc., vol. **506**, pp. 605-611.

Bateman, K., Coombs, P., Noy, D.J., Pearce, J.M., Wetton, P.D., Haworth, A. and Linklater, C. (1999): *Experimental simulation of alkaline disturbed zone around a cementitious radioactive waste repository; numerical modelling and column experiments*, in Chemical containment of waste in the geosphere (R. Metcalfe and C.A. Rochelle Eds.), vol. **157**, Geological Society, London.

Bateman, K., Coombs, P., Pearce, J.M., Noy, D.J. and Wetton, P.D. (2000): *Fluid rock interactions in the disturbed zone: NAGRA/Nirex/SKB column experiments - Phase II*, Interner Bericht, NAGRA, Wettingen, Switzerland.

Bear, J. (1972): *Dynamics of Fluids in Porous Media*, Dover Publications Inc., Dover.

Bear, J. (1979): *Hydraulics of groundwater*, (McGraw-Hill Series in Water Resources and Environmental Engineering (McGraw-Hill Book Company, New York).

Berner, U.R. (1988): *Modelling the Incongruent Dissolution of Hydrated Cement Minerals*, Radiochimica Acta, vol. **44/45**, pp. 387-393.

Broecker, W.S. (1996): *The biosphere and me*, GSA Today, vol. **6**, pp. 1-7.

de Marsily, G. (1986): *Quantitative Hydrogeology - Groundwater Hydrology for Engineers*, Academic Press, San Diego.

Doehring, L., Goerlich, W., Ruettener, S. and Schwerzmann, R. (1994): *Herstellung von homogenen Zementsteinen mit hoher Permeabilitaet*, Internal Report, NAGRA, Wettingen, Switzerland.

Dullien, F.A.L. (1979): *Porous Media*, Academic Press, San Diego.

Fabriol, R., Sauty, J.-P. and Ouzounian, G. (1993): *Coupling Geochemistry with a Particle Tracking Transport Model*, J. of Contaminant Hydrology, vol. **13**, pp. 117-129.

Frick, U. (1993): *An evaluation of diffusion in groundwater of crystalline rocks*, NIB 92-92E, NAGRA, Wettingen, Switzerland.

Frick, U., Alexander, W.R., Baeyens, B., Bossart, P., Bradbury, M.H., Buehler, C., Eikenberg, J., Fierz, T., Heer, W., Hoehn, E., McKinley, I.G. and Smith, P.A. (1992): *The radionuclide migration experiment - overview of investigations 1985-1990*, NTB 91-04, NAGRA, Wettingen, Switzerland.

Frind, E.O., Blowes, D.W., Molson, J.W. and Ptacek, C.J. (1994): *Simulation of Multicomponent Reactive Transport in Groundwater*, in Transport and Reactive Processes in Aquifers (T. H. Dracos and F. Stauffer Eds.), Zürich, Balkema, vol. **5**, pp. 445-450.

Jakob, A. (1997): *Modelling solute transport using the double porous medium approach*, in *Modelling in Aquatic Chemistry*, (I. Grenthe and I. Puigdomènech Eds.) OECD Nuclear Energy Agency, Paris.

Jakob, A., Sarott, F.A. and Spieler, P. (1999): *Diffusion and sorption on hardened cement pastes - experiments and modelling results*, PSI Bericht Nr. 99-05, Paul Scherrer Institut, Villigen.

Kinzelbach, W. (1987): *Numerische Methoden zur Modellierung des Transports von Schadstoffen im Grundwasser*, Schriftenreihe gwf Wasser - Abwasser, vol. **21**, 211ff.

Kinzelbach, W. (1988): *The Random Walk Method in Pollutant Transport Simulation*, in *Groundwater Flow and Quality Modelling*, (E. Custodio, A. Gurgui and J. P. Lobo Ferreira Eds.), D. Reidel, Norwell, Mass., pp. 227-245.

Kinzelbach, W. and Uffink, G. (1991): *The Random Walk Method and Extensions in Groundwater Modelling*, in *Transport Processes in Porous Media*, (J. Bear and M. Y. Corapcioglu Eds.), Kluwer Academic Publishers, The Netherlands, pp. 761-787.

LaBolle, E.M., Fogg, G.E. and Tompson, A.F.B. (1996): *Random-walk simulation of transport in heterogeneous porous media: Local mass-conservation problem and implementation methods*, Water Resources Research, vol. **32**, pp. 583-593.

Lagerblad, B. and Traegardh, J. (1996): *Conceptual model for concrete long time degradation in a deep nuclear waste repository*, CBI report 2:96, Swedish Cement and Concrete Research Institute, Stockholm, Sweden.

Lichtner, P.C. and Eikenberg, J. (1995): *Propagation of a Hyperalkaline Plume into a Geological Barrier Surrounding a Radioactive Waste Repository*, PSI-Report 95-01, Paul Scherrer Institut, Villigen, Switzerland.

Lichtner, P.C., Pabalan, R.T. and Steefel, C.A. (1998): *Model calculations of porosity reduction resulting from cement-tuff diffusive interaction*, (I. G. McKinley and C. McCombie Eds.) 21st Int. Symp. on the Scientific Basis for Nuclear Waste Management, Davos, Switzerland, Mat. Res. Soc., vol. 506, pp. 709-718.

NAGRA (1993): *Beurteilung der langzeitsicherheit des Endlagers SMA am Standort Wellenberg*, NTB 93-26, NAGRA, Wettingen, Switzerland.

NAGRA (1994): *Endlager für schwach- und mittelaktive Abfälle (Endlager SMA). Bericht zur Langzeitsicherheit des Endlagers SMA am Standort Wellenberg*, NTB 94-06, NAGRA, Wettingen, Switzerland.

Neall, F. (1994): *Modeling of the near-field chemistry of the SMA repository at the Wellenberg site*, PSI Bericht 94-18, Paul Scherrer Institut, Villigen, Switzerland.

Pfingsten, W. (1994): *Modular Coupling of Transport and Chemistry: Theory and Model Applications*, NTB 94-19, NAGRA, Wettingen, Switzerland.

Pfingsten, W. (1996): *Efficient Modeling of Reactive Transport Phenomena by a Multispecies Random Walk Coupled to Chemical Equilibrium*, Nuclear Technology, vol. **116**, pp. 208-221.

Pfingsten, W. (1998): *Late 1998 considerations on mortar M1 column experiments and modelling to investigate the degradation of the most permeable component of a L/ILW repository and implications for the pH plume development*, Report TM-44-98-17, Paul Scherrer Institut, Villigen, Switzerland, 33 pp.

Pfingsten, W. and Carnahan, C.L. (1995): *Heterogeneous Redox Reactions in Groundwater Flow Systems - Investigation and Application of two Different Coupled Codes*, PSI-Report 95-08, Paul Scherrer Institute, Villigen, Switzerland.

Pfingsten, W. and Soler, P. (2001): *Hydrogeological and reactive transport modeling of the GTS-HPF experiment (Grimsel Test Site - Hyperalkaline Plume in Fractured Rock, Report (in prep).*

Pfingsten, W. and Shiotsuki, M. (1998): *Modeling a Cement Degradation Experiment by a Hydraulic Transport and Chemical Equilibrium Coupled Code*, (I. G. McKinley and C. McCombie Eds.) 21st Int. Symp. on the Scientific Basis for Nuclear Waste Management, Davos, Switzerland, Mat. Res. Soc., vol. **506**, pp. 805-812.

Prickett, T.A., Naymik, T. and Lonnquist, G. (1982): *A 'Random-Walk' Solute Transport Model for Selected Groundwater Quality Evaluations*, Bulletin 65, Illinois State Water Survey.

Read, D. (1991): *CHEMVAL PROJECT, Report on Stages 3 and 4: Testing of coupled chemical transport models*, EUR 13675, Commission of the European Communities, Brussels.

Reardon, E.J. (1992): *Problems and Approaches to the Prediction of the Chemical Composition in Cement/Water Systems*, Waste Management, vol. **12**, pp. 221-239.

Roach, P.J. (1972): *Computational Fluid Mechanics*, Hermosa Publishers, Albuquerque.

Sarott, F.A., Bradbury, M.H., Pandolfo, P. and Spieler, P. (1992): *Diffusion and adsorption studies on hardened cement paste and the effect of carbonation on diffusion rates*, Cement and Concrete Research, vol. **22**, pp. 439-444.

Steefel, C.I. and Lichtner, P.C. (1994): *Diffusion and reaction in rock matrix bordering a hyperalkaline fluid-filled fracture,* Geochemica et Cosmochemica Acta, vol. **58**, pp. 3595-3612.

Steefel, C.I. and Lichtner, P.C. (1998a): *Multicomponent reactive transport in discrete fractures I: Controls on reaction front geometry*, Journal of Hydrology, vol. **209**, pp. 186-199.

Steefel, C.I. and Lichtner, P.C. (1998b): *Multicomponent reactive transport in discrete fractures II: Infiltration of hyperalkaline groundwater at Maqarin, Jordan, a natural analogue site,* Journal of Hydrology, vol. **209**, pp. 200-224.

Stumm, W. and Morgan, J.J. (1996): *Aquatic Chemistry*, John Wiley & Sons, Inc., New York.

Taylor, H.F.W. (1987): *A method for predicting alkali ion concentrations in cement pore solutions*, Advances in Cement Research, vol. **1**, pp. 5-16.

Thoenen, T. (1996): *Potential alteration minerals formed by a hyperalkaline plume: Status report*, Report TM-44-96-10, Paul Scherrer Institut, Villigen, Switzerland.

Van der Lee, J. and De Windt, L. (2000): *Present state and future directions of modeling of geochemistry in hydrogeological systems*, J. Contaminant Hydrology, vol. **47**, pp. 265-282.

Wieland, E., (1997): Priv. com. related to calcite precipitation on the surface of hardened cement paste specimen.

Wildi, W., Appel, D., Buser, M., Dermange, F., Eckhardt, A., Hufschmied, P., Keusen, H.-R. and Aebersold, M. (2000): *Entsorgungskonzepte fuer radioaktive Abfaelle*, Bundesamt fuer Energie, Bern, Switzerland.

Yeh, G.T. and Tripathi, V.S. (1989): *A Critical Evaluation of Recent Developments in Hydrogeochemical Transport Models of Reactive Multichemical Components*, Water Resources Research, vol. **25**, pp. 93 - 108.

ACKNOWLEDGEMENTS

I would like to thank all colleagues from the Waste Management Laboratory (LES) for discussions and their interest in this work. Special thanks are given to Jörg Hadermann for his valuable comments on the report, to Isabelle Bonhoure for the translation of the abstract into French, and to Jan van der Lee, Vincent Lagneau, Andreas Jakob, Paul Wersin and Lawrence Johnson for their detailed review of the manuscript and their comments and suggestions which helped to improve the quality of the report considerably. Partial financial support by the Swiss National Cooperative for the Disposal of Radioactive Waste (Nagra) is gratefully acknowledged.

APPENDIX A : TWO-DIMENSIONAL CODE VERIFICATION BY COMPARISON TO AN ANALYTICAL SOLUTION

After extending the one-dimensional version of MCOTAC to two dimensions in space, it is necessary to demonstrate that the two-dimensional flow and transport description coupled with chemical reaction solves the equations correctly. Verification can be done by comparing results to other two-dimensional reactive transport applications, or alternatively, to analytical solutions of two-dimensional problems, as it was possible for the one-dimension version of MCOATC [Pfingsten 1994; Pfingsten and Carnahan 1995; Pfingsten 1996; Pfingsten and Shiotsuki 1998]. In the first case, where a comparison is done using other two-dimensional codes, one has to recognise that there are not too many examples in the literature with a defined system of parameters which allows an adequate comparison. This is due to code specific description of processes taken into account and mostly due to the lack of data. For the second type of verification, the comparison to an analytical solution, [Read 1991] proposed a simple two-dimensional geochemical system, where it is possible to reduce the problem to an analytical solution for an instantaneous point injection of a species into a two-dimensional aquifer. The example represents a solution for a reactive transport problem with reduced chemistry within a simple flow field in order to allow a comparison of numerical reactive transport modelling approach with an exact solution for code verification purposes, e.g. done by [Fabriol et al. 1993].

The analytical solution for the concentration of the instantaneously injected species as a function of space (two dimensions) and time is given by [Read 1991]:

$$C(x,y,t) = \frac{M_0}{4\pi\,\varepsilon\,\Delta z\sqrt{D_L\,D_T}\;t}\; e^{-\frac{(x-vt)^2}{4D_L t}-\frac{y^2}{4D_T t}}\;, \qquad \text{(A.1)}$$

where M_0 is the injected mass, Δz is the aquifer thickness, ε is the porosity, D_L and D_T are the longitudinal and the transversal dispersivity ($D_L = \alpha_L \cdot v$, $D_T = \alpha_T \cdot v$) and v is the water flow velocity.

The simulated chemical system is the dissolution of silica by an instantaneous point injection of NaOH into a siliceous aquifer – maybe difficult to perform in reality. Further assumptions are: (a) instantaneous equilibrium, (b) activity of chemical species equal to their concentration, (c) sodium is present as a unique and non-reactive aqueous

species Na^+, and (d) the modelled chemical system consists of four elements H, O, Si, Na, two phases, water and chalcedony (SiO_2), and six aqueous species, H_2O, H^+, OH^-, Na^+, $H_4SiO_4^0$, $H_3SiO_4^-$.

The exact solution for the Na^+ concentration in two dimensions in space is given by the Eq. A.1, and the pH is given by:

$$pH = -\log H^+ = -\log\left[\frac{1}{2}\left(-C_{Na^+} + \sqrt{C_{Na^+}{}^2 + 4\left(k_1 + k_2 k_3\right)}\right)\right], \qquad \text{(A.2)}$$

where k_1, k_2, k_3 are the dissociation constant of water ($k_1 = 10^{-13.998}$), the dissolution constant of chalcedony ($k_2 = 10^{-3.554}$) and the dissociation constant of $H_4SiO_4^0$ ($k_3 = 10^{-9.77}$), respectively. The injected mass of Na^+ and OH^- is 10 mol, leading to an initial concentration of 10^{-2}mol/l, if the reference volume is related to the finite differences flow model discretisation of 10 m by 10 m by 1 m aquifer thickness with a porosity of 0.1.

Calculations were performed for transport parameter v_D = 1m/d, ε = 0.1 ($v = v_D/\varepsilon$) where the flow field is parallel to the x-direction, and D_L = 5 m^2/d, D_T = 1 m^2/d (which both are a factor of 10 higher as referenced in [Fabriol et al. 1993]). A comparison of the results of the analytical solution and the numerical reactive transport modelling is shown in the figures below. The first comparison is made for pure numerical (Random-Walk) transport calculation by MCOTAC according to the instantaneous point injection of tracer Na^+ and OH^- (H^+) and related analytical solutions for Na^+ and H^+. The agreement is excellent for the Na^+ and pH breakthrough curves shown at two locations in the two-dimensional model area in Figs. A.1 and A.2. The same holds for the agreement of the spatial Na^+ distribution in the model area calculated at different times (Fig. A.3). In addition to the pure transport calculated by MCOTAC, a second comparison is made for multiple species reactive transport modelling by MCOTAC. Both approaches differ in modules used, pure Random-Walk transport and reactive transport. In the latter the Random-Walk transport module is coupled to transport, calculating chemical equilibrium among all solute and solid species in between successive transport time steps. Then grid related chemical equilibrium calculations have to be performed for each time step. This is somehow in contradiction to the problem definition for instantaneous point injection, where an analytical solution is available, because after each chemical equilibrium calculation new species concentrations are grid related, leading to a

spreading of the point source just after the instantaneous injection. Therefore, the breakthrough curves of injected tracer (Na^+ and OH^-) should be broader and lower (higher for H^+) for this calculation (Figs. A.5 and A.6) than for the analytical solution for the point source problem. Although these differences exist in the problem definition (analytical solution and numerical reactive transport calculation), the agreement is satisfying and can be improved by decreasing the grid size in order to generate numerically a point source in a grid describing the chemical, multi species (aqueous and solid) system.

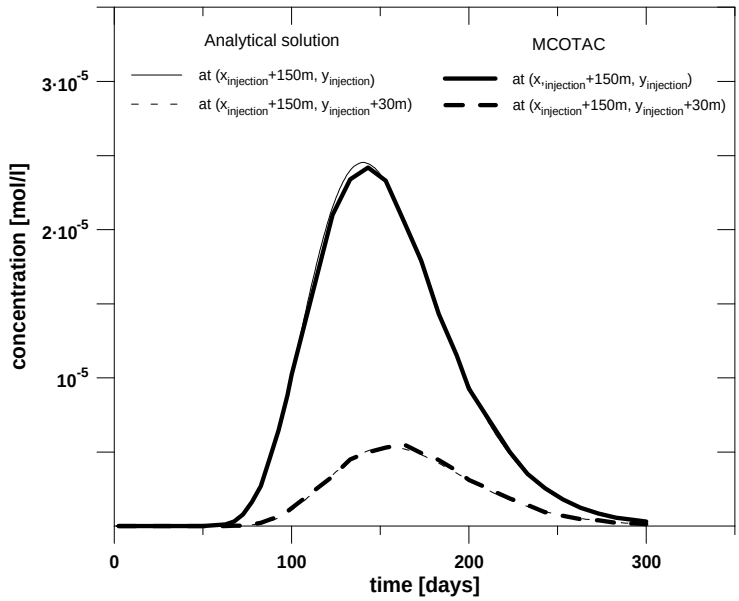

Fig. A.1: Comparison of MCOATC 2D-simulation (pure Random-Walk transport) and a related 2D-analytical solution for a special reactive transport problem proposed by [Read 1991]. Shown is the Na^+ breakthrough at two different locations (as indicated in Fig. A.3) for an instantaneous point injection. The initial concentration is 10^{-2} mol/l in the volume of injection.

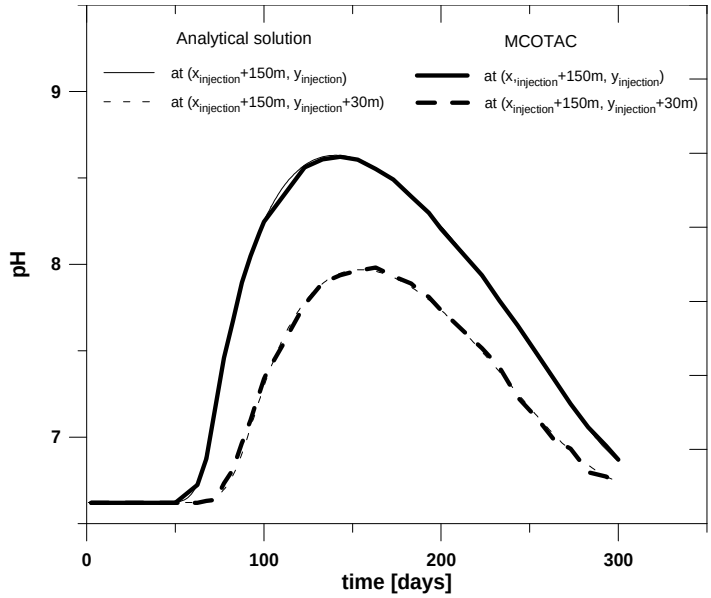

Fig. A.2: Comparison of MCOATC 2D-simulation (pure Random-Walk transport) and a related 2D-analytical solution for a special reactive transport problem proposed by [Read 1991]. Shown is the pH as a function of time at two different locations for an instantaneous point injection.

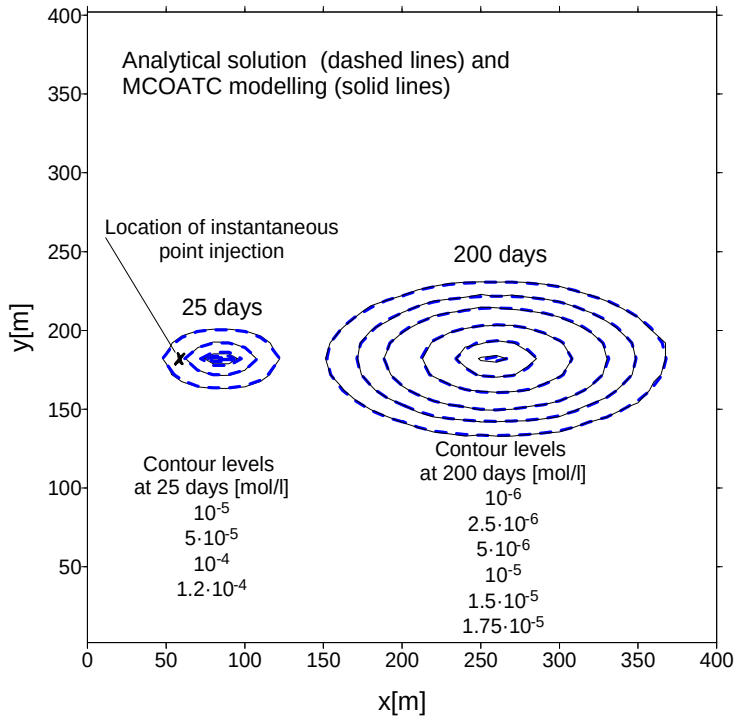

Fig. A.3: Comparison of MCOATC 2D-simulation (pure Random-Walk transport) and a related 2D-analytical solution for a special reactive transport problem proposed by [Read 1991]. Shown is the Na^+ concentration distribution at 25 and 200 days after an instantaneous point injection. Initial concentration is 10^{-2} mol/l in the volume of injection.

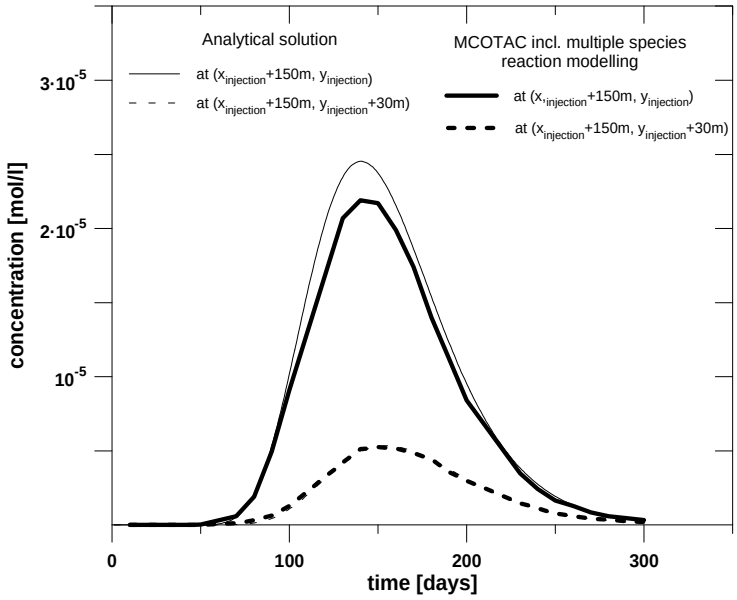

Fig. A.4: Comparison of MCOATC 2D-simulation including multiple species reaction modelling and a related 2D-analytical solution for a special reactive transport problem proposed by [Read 1991]. Shown is the Na^+ breakthrough at two different locations for an instantaneous point injection.

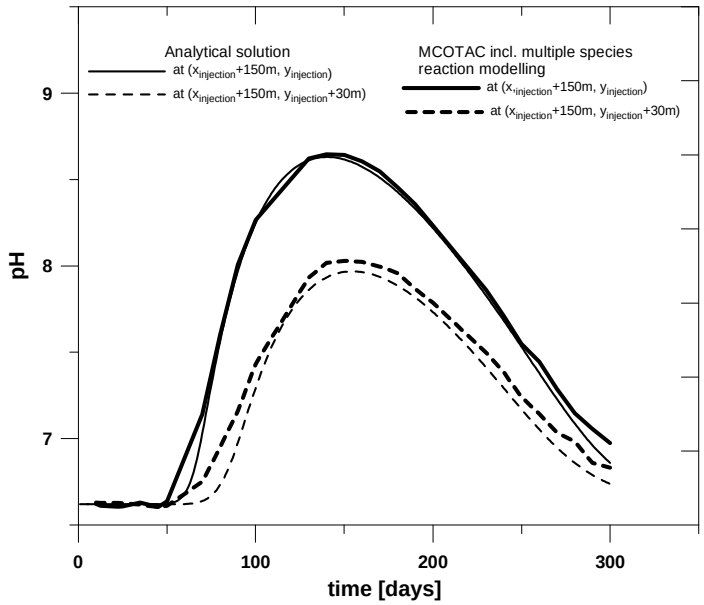

Fig. A.5: Comparison of MCOATC 2D-simulation including multiple species reaction modelling and a related 2D-analytical solution for a special reactive transport problem proposed by [Read 1991]. Shown is the pH as a function of time at two different locations for an instantaneous point injection.

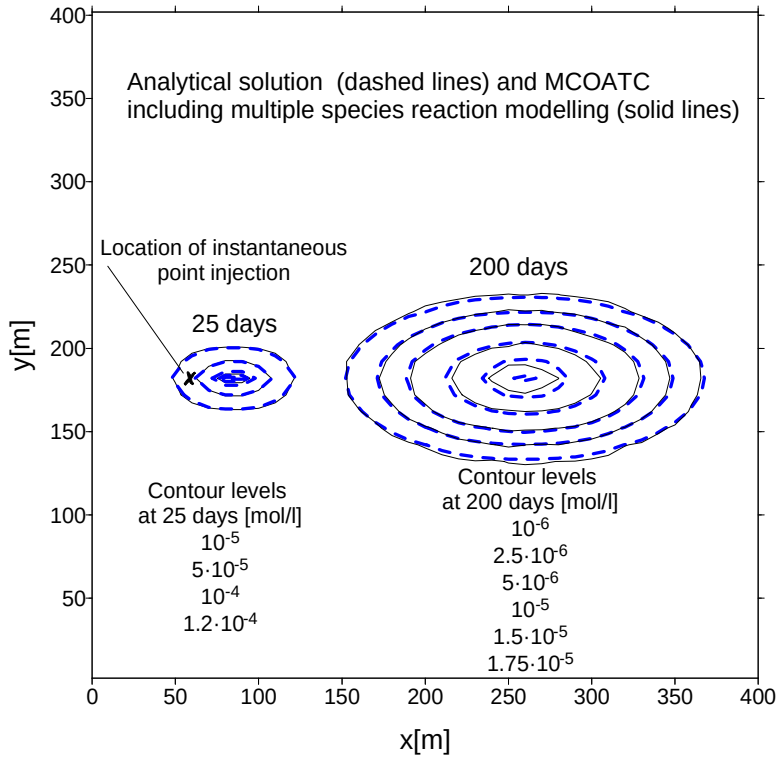

Fig. A.6: Comparison of MCOATC 2D-simulation including multiple species reaction modelling and a related 2D-analytical solution for a special reactive transport problem proposed by [Read 1991]. Shown is the Na^+ concentration distribution at 25 and 200 days after an instantaneous point injection.

APPENDIX B : INLFUENCE OF BOUNDARY CONDITIONS AND SYSTEM SET-UP FOR ONE-DIMENSIONAL COUPLED CODE APPLICATIONS

In order to investigate the cement-host rock interactions related to the potential L/ILW repository site at Wellenberg, a one-dimensional modelling approach was used, too. Such an approach is sufficient in some cases when, for example, looking at the influence of the chosen boundary conditions. The geochemical set-up is the same as described in Chap. 4 for the one-dimensional system modelled here. Transport parameters are given in Table B.1, where the water flow velocity and dispersion/diffusion parameter are assumed to be the same for all solutes.

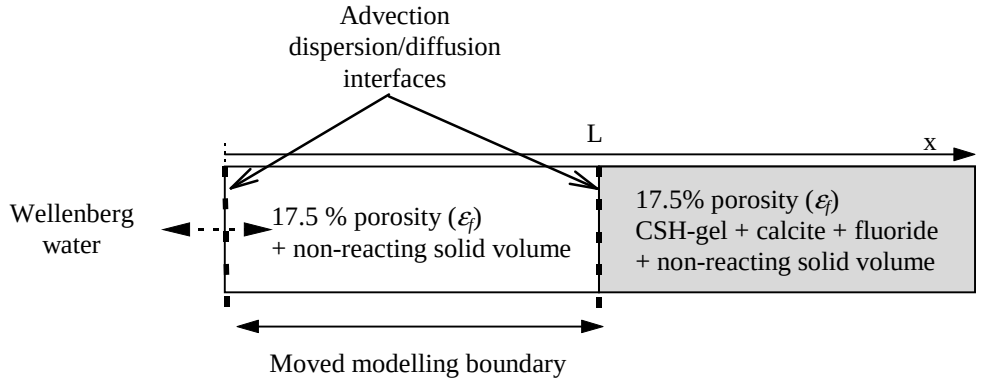

Fig. B.1: 1D model set-up for the degradation of hardened cement paste by rock water. Moving the boundary between cement paste and rock water in the modelling represents two scenarios: (a) boundary to the left with an assumed constant water composition induces a continuous steep chemical gradient directly at the boundary - degradation is accelerated, especially for diffusion dominated transport processes; (b) boundary in the middle of model area with an assumed constant water composition at the left (right) allows for chemical reactions at the interface. The rock/water area was assumed to have the same porosity as the CSH area with non-reacting solids (calcite is already present within the marl host rock, [Baeyens and Bradbury 1994]). For b) degradation is slower, especially for diffusion dominated transport processes because chemical gradients become smoother with increasing time.

Table B.1: Transport parameters used for one-dimensional modelling. Variations are given in parentheses.

Column length	1.0 m
Grid distance (20 cells)	0.05 m
Pore water velocity (Darcy flux/porosity)	$2.3 \cdot 10^{-12}$($2.3 \cdot 10^{-10}$,$2.3 \cdot 10^{-11}$)m/s
Hydrodynamic dispersion coefficient	0. ($5 \cdot 10^{-10}$) m^2/s
Initial porosity in the column	0.175
System solid	Cement (CSH-gel)

The modelling results for scenario (a) (see Fig. B.1) are shown in Figs. B.2 to 2.4 for different water flow velocities. In this pure advective driven scenario the chemical gradient is kept steep between the cement and Wellenberg water composition by using a constant inlet boundary condition with respect to water flux and composition. Mineral dissolution and precipitation scale linearly with the water velocity, i.e. slow water flow and related solute transport will take longer to reach the same mineral turnaround as for faster water flow. The precipitation dissolution fronts move about 0.1 - 0.2 m into the column for the calculated periods and their related water flow velocities. In each of the simulations all three model solids, representing CSH, are present within the transition zone. The model solids portlandite and CaH_2SiO_4 are dissolved by the Wellenberg groundwater to precipitate calcite. As calcite has a lower molar volume than assumed for the model solids portlandite and CaH_2SiO_4, the porosity increases at the inlet boundary because portlandite and CaH_2SiO_4 are successively replaced by calcite. Ca in solution and pH are directly related to the CSH dissolution and calcite precipitation fronts. Ca is at lower level in the Wellenberg water since it has been precipitated as calcite at locations where CSH has been dissolved. Further, pH is high where it is buffered by CSH and low at Wellenberg water level where $Ca(OH)_2$ and CaH_2SiO_4 have been dissolved. The peak jag in the porosity is the result of using the incongruent cement dissolution model together with values for molar volumes for the real solids. During the CSH degradation, the amount of Ca in the solid phase is partly transferred from $Ca(OH)_2$ to CaH_2SiO_4 due to the formulation of the CSH degradation model[33]. For this pure advective system, the location of the mineral front system might be extrapolated for larger times, because this simple system behaves linearly with respect

[33] Although the model for incongruent dissolution of cement paste is originally used to describe dissolution [Berner 1988], here it is also used to describe precipitation of the model solids. The reversibility of precipitation and dissolution processes is assumed within the chemical equilibrium model.

to water flow velocity and the related dissolution/precipitation front movement. A constant water flux is assumed although the hydraulic conductivity along the column may change according to the porosity changes. An increase of porosity would increase hydraulic conductivity and water flow, resulting in a faster degradation.

Model parameters at t=40000 years (Advection, v=2.3·10^{-10}[m/s])

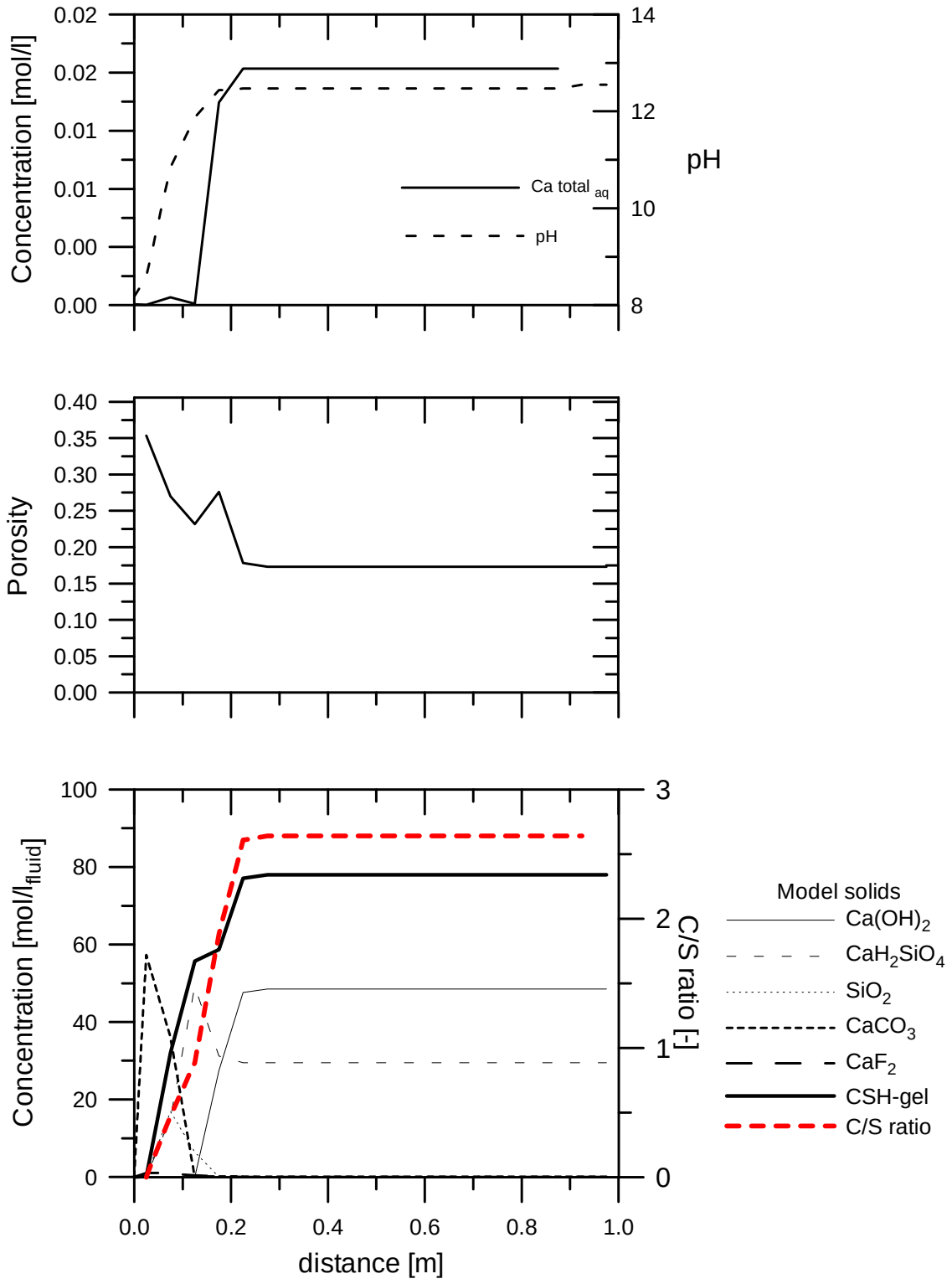

Fig. B.2: Concentration distribution for Ca_{total}, pH, porosity, model solids and C/S ratio along the column (scenario (a) - flow velocity: 2.3·10^{-10} m/s).

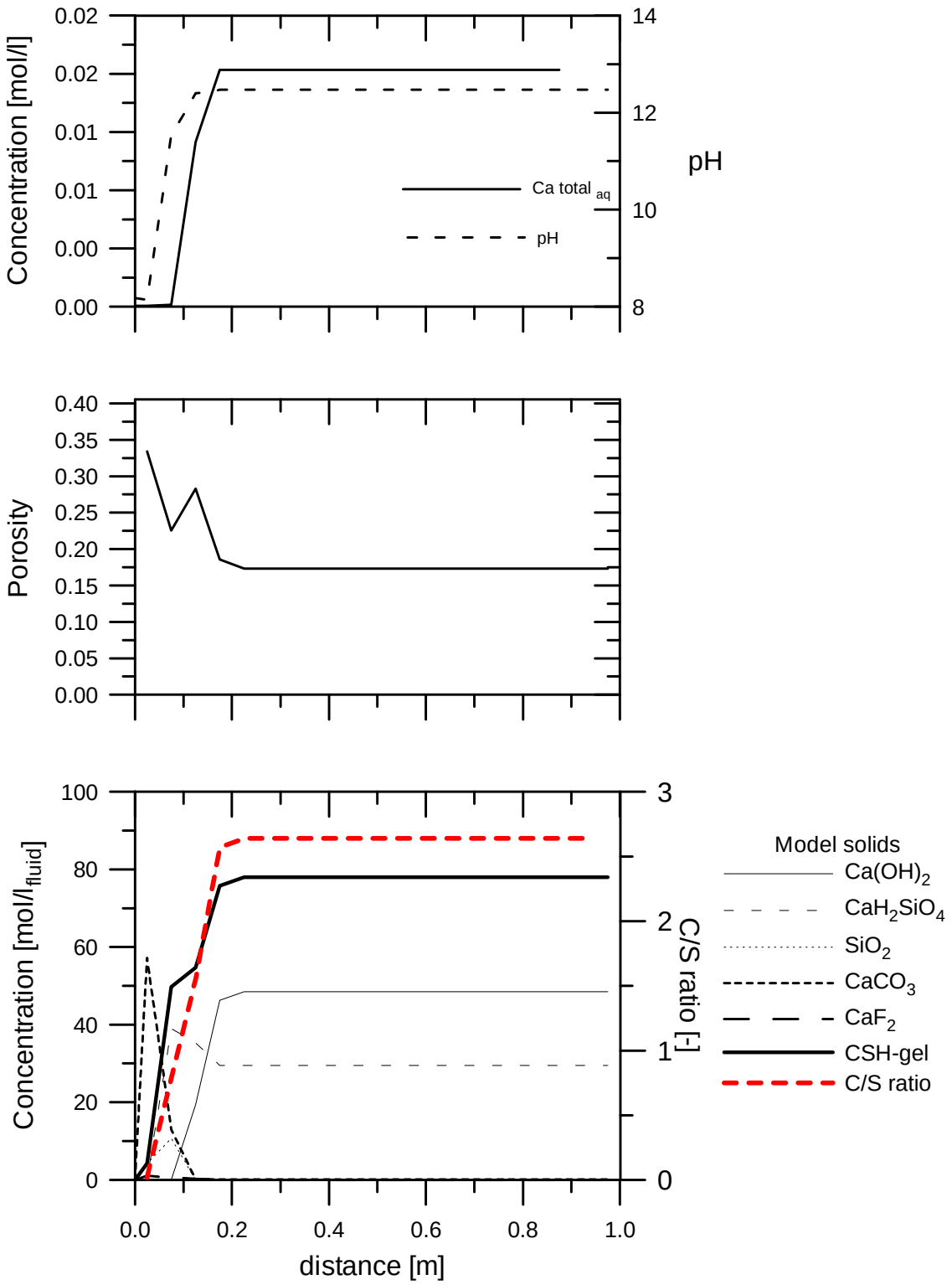

Fig. B.3: Concentration distribution for Ca_{total}, pH, porosity, model solids and C/S ratio along the column (scenario (a) - flow velocity: $2.3 \cdot 10^{-11}$ m/s).

Model parameters at $t=3\cdot10^{6}$years (Advection, $v=2.3\cdot10^{-12}$[m/s])

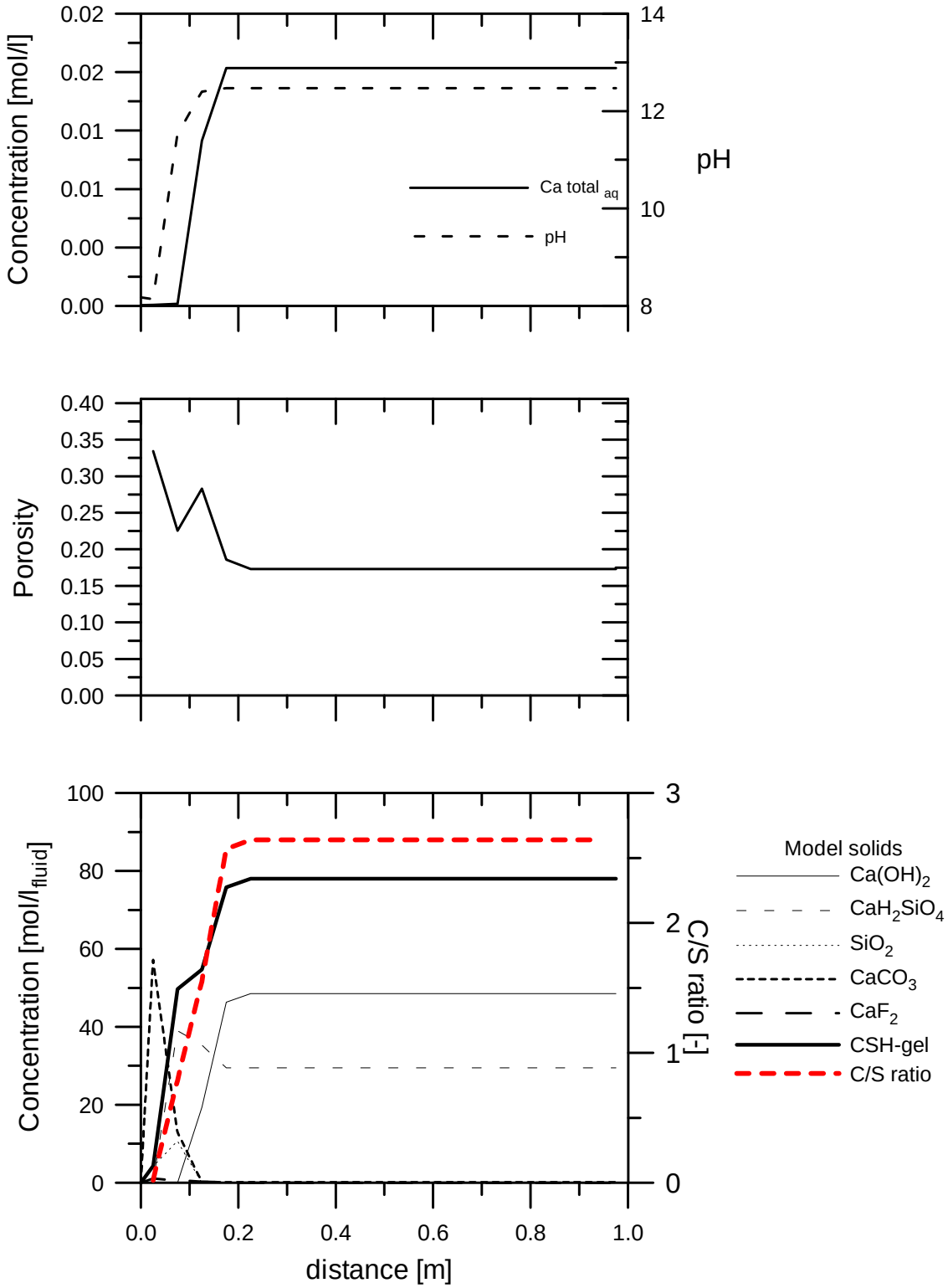

Fig. B.4: Concentration distribution for Ca_{total}, pH, porosity, model solids and C/S ratio along the column (scenario (a) - flow velocity: $2.3\cdot10^{-12}$ m/s).

Pure diffusion is also modelled for scenario (a) (Fig. B.1). The mineral fronts calculated are similar to those calculated for the advection-dispersion dominated scenario. The results might look like more diffusive, but now the calcite precipitation is limited to the inlet boundary since no driving force, as advection before, serves for calcite precipitation further within the column. Dissolving CSH inside the column increases the porosity there and generates higher Ca concentration compared to the inlet water composition at the boundary. A reverse gradient holds for the carbonate concentration resulting in locally precipitating calcite. The constant inlet water composition generates steep chemical gradients all the time which drives the mineral reactions inside the column. There are no such driving forces (gradients) for Ca or other 'CSH dissolution products' as pH to move into the column. Calcite precipitates inside the column and has to replace dissolving CSH there with the effect that a high amount of calcite is necessary first to replace CSH volume fraction and then to reduce the porosity as it can be seen in Fig. B.5. The modelling was stopped after 4000 years of interaction. That is, when porosity becomes nearly zero near the boundary and the diffusion coefficient will become very small and hence, transport processes are negligible.

To investigate the effect of the choice of the boundary or interface between Wellenberg water and cement, a scenario (b) was chosen, where the interface is in the middle of the model area (Fig. B.1). This scenario is of less interest for the advective systems described above, because there the dominant driving force for transport is always away from the inlet boundary into the column, being the same for all solutes, whereas it will be important for a diffusive scenario. There the transport driving forces are in the direction of the chemical gradients and, therefore, are acting in both directions different for individual solutes in the cement and Wellenberg water area. For modelling the initial composition of cement, cement water and Wellenberg water remains the same, but now the model solids are allowed to precipitate or dissolve also in the area with Wellenberg water.

The boundary conditions are now: constant concentration at the left (Wellenberg water) and right (cement water) of the column. The boundaries are now further away from the reacting interface cement - Wellenberg water and will have less influence on the reaction at the boundary. The results are shown in Fig. B.6. The differences to the scenario (a) are obvious. Calcite precipitation is now left to the interface in the Wellenberg water area and the CSH dissolution inside is less extended. The 60 mol/l_{fluid} level for CSH is about 0.2 m from the inlet for case (a) and only about 0.1 m for case (b). The reason is that now the chemical gradients across the interface are smoothed out

slightly slowing down the transport driving forces. Also the influence of the inlet boundary condition is less pregnant. The Ca concentration profile is still low along the model area, not only at the left boundary (a more flat Ca gradient between left boundary and cement area serves as the Ca source). Although less CSH was calculated to dissolve during 2000 years of interaction, the porosity in the Wellenberg water area was calculated to be nearly zero, lower than for the diffusion scenario (a). That is because location of dissolution and precipitation are separated from each other for model set-up (b). Calcite precipitate does not have to replace dissolved CSH volume fraction first to finally decrease the initial porosity. The amount of Ca from dissolved CSH is used at a different place, in the Wellenberg water area, to precipitate calcite. This causes a local porosity reduction, spatially separated from the dissolution area. The time used to reach a porosity nearly zero is shorter for this case (b) than for the above mentioned case (a) where calcite has first to replace dissolving CSH volume fraction and then reduce porosity.

The modelling of these two diffusion examples demonstrates, that the choice of the (appropriate) boundary condition and model domain will have an influence on the results of the apparently similar model set-ups. The decision, which is appropriate and applicable to a cementitious repository near-field, depends on the assumptions made with respect to hydrology, host rock and repository properties, geometry and heterogeneity of the near-field. It seems questionable that simple system set-ups, as described above, are sufficient to the needs of performance assessment which should include quantitatively the timescale for degradation of repository components, e.g. the temporal evolution of the 60 mol/l_{fluid} CSH level in the cement area. They might be adequate to describe sufficiently one-dimensional laboratory experiments as for example done by [Adenot and Buil 1992], who reported on an experiment where a cylinder of Ordinary Portland Cement (OPC) paste was immersed to de-ionised circulating water. Another one-dimensional example was described by [Pfingsten and Shiotsuki 1998] where de-ionised water was forced to degrade a hardened cement paste in a column like set-up under constant hydraulic head conditions. There, the degradation resulted in an increased porosity within the sample, increasing the water flow through the column. Experiment and modelling showed a coupling between reactive transport and hydraulic properties: the porosity and the hydraulic conductivity are related by a Kozeny-Carman relationship [Bear 1979]. This could be verified for the simple one-dimensional system. But here, the question arises, how to apply these one-dimensional approaches to realistic, three-dimensional scenarios?

The one-dimensional experiments with cement that will not be used for repository constructions, or experiments using pure water for the degradation process are not representative for a real cementitious repository. They might be a first step in gaining more understanding in processes that are ongoing. But these investigations should be continued to more realistic repository conditions - with respect to geochemistry and hydraulic conditions.

Comparison of cases a) and b) showed major differences for the diffusion scenario already for this one-dimensional modelling, due to the different boundary condition chosen. Therefore, a strict but artificial separation of, e.g. repository near-field and far-field seems questionable. On one hand, for repository degradation a simple one-dimensional modelling with constant water flow was used to estimate the period of pH buffering capacity of the repository, important for radionuclide retention. On the other hand, the cement host rock system consists of large chemical reactive potential that causes mineral reactions influencing hydraulic and transport through and from the repository. At least, a two-dimensional model approach is necessary to cover the above mentioned processes and to investigate their influence on the long-term behaviour of a cementitious repository.

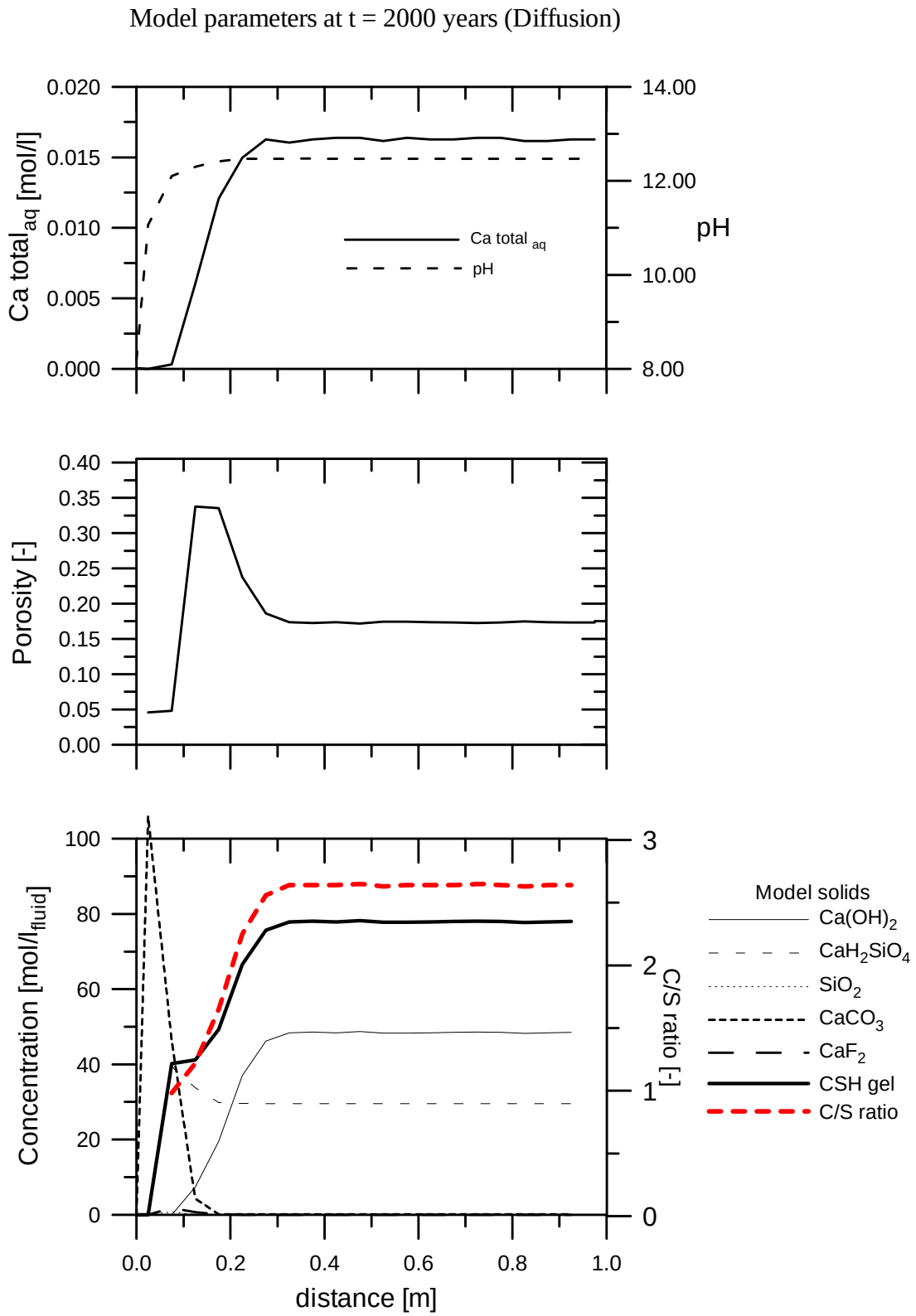

Fig. B.5: Concentration distribution for Ca_{total}, pH, porosity, model solids and C/S ratio along the column (scenario (a) - diffusion scenario).

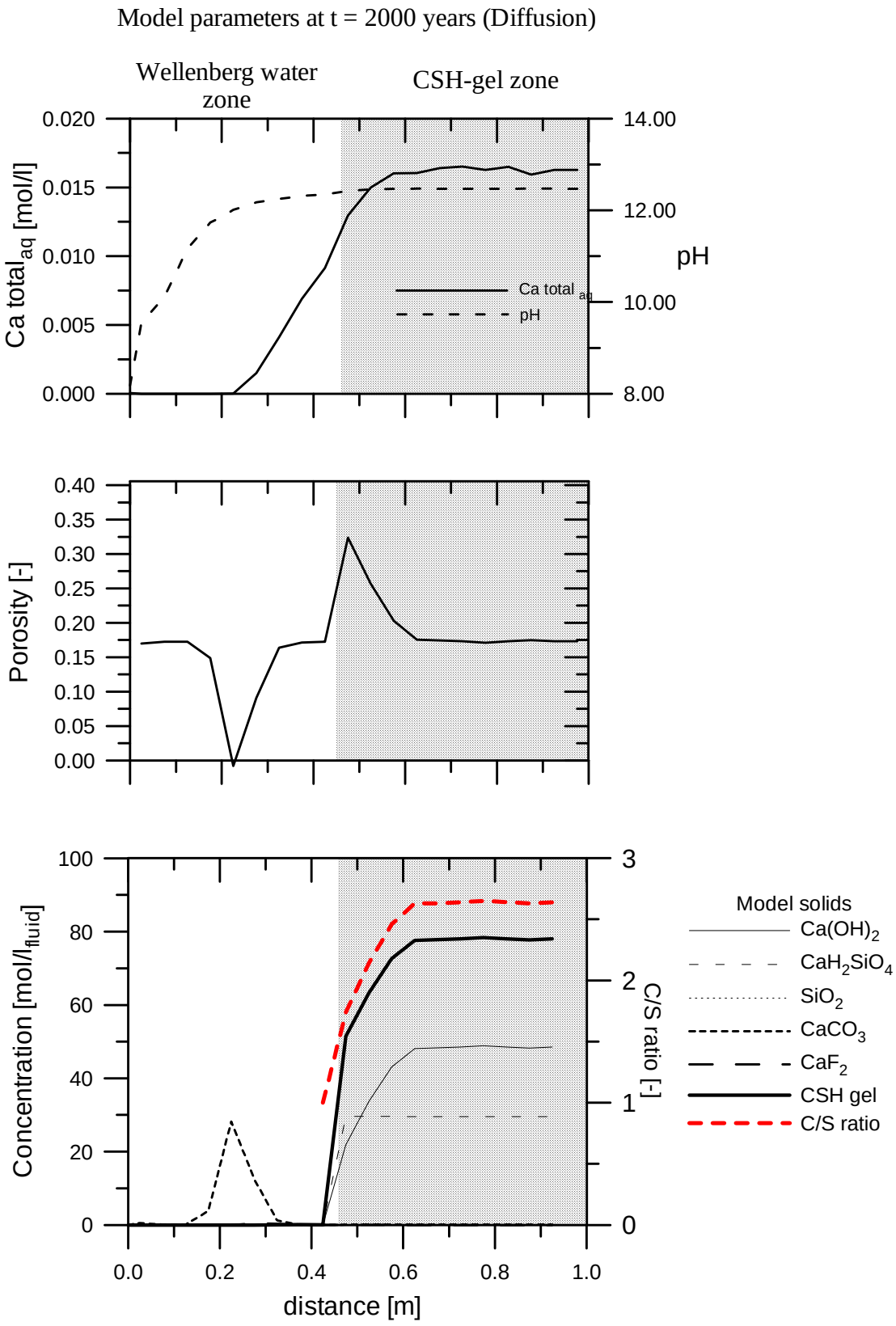

Fig. B.6: Concentration distribution for Ca_{total}, pH, porosity, model solids and C/S ratio along the column (scenario (b) - diffusion scenario).

APPENDIX C: 2D TRANSPORT DESCRIBED BY RANDOM-WALK OF PARTICLES

For application of the Random-Walk method to describe the tracer transport (Eq. 3.11) one has to keep in mind that the space- and time-dependent distribution $X(x,y,t)$ of a particle ensemble is an approximation for a particle ensemble carrying out single transport steps (with particle related parameters for velocity v and hydrodynamic dispersion D) given by the Ito-Fokker-Planck equation [Kinzelbach 1987, p. 229]:

$$\frac{\partial X}{\partial t} + v_x \frac{\partial X}{\partial x} + v_y \frac{\partial X}{\partial y} = \frac{\partial^2}{\partial x^2}\left(D_{xx}\, X\right) + \frac{\partial^2}{\partial x \partial y}\left(D_{xy}\, X\right) + \frac{\partial^2}{\partial y \partial x}\left(D_{xy}\, X\right) + \frac{\partial^2}{\partial y^2}\left(D_{yy}\, X\right), \quad \text{(C.1)}$$

which is not equal to the transport equation for a single tracer[34]:

$$\frac{\partial X}{\partial t} + v_x \frac{\partial X}{\partial x} + v_y \frac{\partial X}{\partial y} = \frac{\partial}{\partial x}\left(D_{xx} \frac{\partial X}{\partial x} + D_{xy} \frac{\partial X}{\partial y}\right) + \frac{\partial}{\partial y}\left(D_{xy} \frac{\partial X}{\partial x} + D_{yy} \frac{\partial X}{\partial y}\right) \quad . \quad \text{(C.2)}$$

Only a substitution of $\vec{v}$ by $\vec{v}'$:

$$\vec{v}'(x,y) \rightarrow \left(v_x + \frac{\partial D_{xx}}{\partial x} + \frac{\partial D_{xy}}{\partial y}, v_y + \frac{\partial D_{xy}}{\partial x} + \frac{\partial D_{yy}}{\partial y}\right) , \quad \text{(C.3)}$$

and neglecting second order derivative terms of the dispersion coefficients leads to an equivalent description of the transport Eq. C.2 and the time dependent particle ensemble distribution (Eq. C.1).

The terms in the transport equation C.2 can be expressed as:

[34] Decay, sources and sinks (and with them, the cross terms) are handled separately within the Random-Walk transport description. For simplicity of presentation, the index for the basis species j is omitted.

$$\frac{\partial X}{\partial t}+v_x\frac{\partial X}{\partial x}+v_y\frac{\partial c}{\partial y}=\frac{\partial}{\partial x}\left(D_{xx}\frac{\partial X}{\partial x}+D_{xy}\frac{\partial X}{\partial y}\right)+\frac{\partial}{\partial y}\left(D_{xy}\frac{\partial X}{\partial x}+D_{yy}\frac{\partial X}{\partial y}\right)$$
$$=\frac{\partial D_{xx}}{\partial x}\frac{\partial X}{\partial x}+D_{xx}\frac{\partial^2 X}{\partial x^2}+\frac{\partial D_{xy}}{\partial x}\frac{\partial X}{\partial y}+D_{xy}\frac{\partial^2 X}{\partial x\partial y}+\frac{\partial D_{xy}}{\partial y}\frac{\partial X}{\partial x}+D_{yx}\frac{\partial^2 X}{\partial y\partial x}+\frac{\partial D_{yy}}{\partial y}\frac{\partial X}{\partial y}+D_{yy}\frac{\partial^2 X}{\partial y^2} \quad (C.4)$$

The terms in the Ito-Fokker-Planck equation C.1 can be expressed as:

$$\frac{\partial X}{\partial t}+v_x\frac{\partial X}{\partial x}+v_y\frac{\partial X}{\partial y}=\frac{\partial^2}{\partial x^2}\left(D_{xx}X\right)+\frac{\partial^2}{\partial x\partial y}\left(D_{xy}X\right)+\frac{\partial^2}{\partial y\partial x}\left(D_{xy}X\right)+\frac{\partial^2}{\partial y^2}\left(D_{yy}X\right)$$
$$=\frac{\partial^2 D_{xx}}{\partial x^2}X+\frac{\partial D_{xx}}{\partial x}\frac{\partial X}{\partial x}+\frac{\partial D_{xx}}{\partial x}\frac{\partial X}{\partial x}+D_{xx}\frac{\partial^2 X}{\partial x^2}+\frac{\partial^2 D_{xy}}{\partial x\partial y}X+\frac{\partial D_{xy}}{\partial y}\frac{\partial X}{\partial x}+\frac{\partial D_{xy}}{\partial x}\frac{\partial X}{\partial y}+D_{xy}\frac{\partial^2 X}{\partial x\partial y} \quad (C.5)$$
$$+\frac{\partial^2 D_{yx}}{\partial y\partial x}X+\frac{\partial D_{xy}}{\partial x}\frac{\partial X}{\partial y}+\frac{\partial D_{xy}}{\partial y}\frac{\partial X}{\partial x}+D_{xy}\frac{\partial^2 X}{\partial y\partial x}+\frac{\partial^2 D_{yy}}{\partial y^2}X+\frac{\partial D_{yy}}{\partial y}\frac{\partial X}{\partial y}+\frac{\partial D_{yy}}{\partial y}\frac{\partial X}{\partial y}+D_{yy}\frac{\partial^2 X}{\partial y^2}$$

It can be seen that

$$(\mathrm{F}-1)=(\mathrm{F}-2)-\left[\frac{\partial D_{xx}}{\partial x}\frac{\partial X}{\partial x}+\frac{\partial D_{xy}}{\partial y}\frac{\partial X}{\partial x}+\frac{\partial D_{xy}}{\partial x}\frac{\partial X}{\partial y}+\frac{\partial D_{yy}}{\partial y}\frac{\partial X}{\partial y}\right]$$
$$-\left[\frac{\partial^2 D_{xx}}{\partial x^2}X+\frac{\partial^2 D_{xy}}{\partial x\partial y}X+\frac{\partial^2 D_{xy}}{\partial y\partial x}X+\frac{\partial^2 D_{yy}}{\partial y^2}X\right] \quad (C.6)$$

Neglecting terms including second order derivatives of the dispersion coefficients and substituting $\vec{v}$ by $\vec{v}'$ in (Eq. C.5), the Random-Walk description with parameters $\vec{v}'$ and **D** is equivalent to a transport description with parameters $\vec{v}$ and **D** in two dimensions.

For variable dispersion coefficient in space (e.g. by a variable velocity field or in case of explicit calculation of the spatial variable, porosity-dependent diffusion coefficient) it is necessary to apply a 'counter term' [Kinzelbach 1988] in the advective step to get consistency of the transport equation and the form of stochastic single steps. Also if advection is negligible, a “counter flow field” will result for a variable diffusion coefficient in space. It will be zero if $v = v'$, that is if:

$$\frac{\partial D_{xx}}{\partial x}+\frac{\partial D_{xy}}{\partial y}=0 \text{ and } \frac{\partial D_{xy}}{\partial x}+\frac{\partial D_{yy}}{\partial y}=0\ . \quad (C.7)$$

This means that the 'counter term' is negligible if the spatial gradients of *D* are small; otherwise this term has to be taken into account within Random-Walk transport modelling[35].

The Random-Walk description implies that at each location in space the transport parameters are known. They are calculated from the finite differences grid specific hydraulic heads and related Darcy velocities. Particle velocities as well as the hydrodynamic dispersion coefficient (dispersion and diffusion) will be interpolated to the particle location[36].

The "counter terms", yielding consistent description of advective dispersive transport (Eq. C.8) and the behaviour of a statistical ensemble, are calculated from a gradient field of the hydrodynamic dispersion coefficient field and then also interpolated to the particle location. This gives the "corrected" velocity in the two-dimensional case:

$$\vec{v}'(x,y)=\left(v_x + \frac{\partial D_{xx}}{\partial x}+\frac{\partial D_{xy}}{\partial y}, v_y + \frac{\partial D_{xy}}{\partial x}+\frac{\partial D_{yy}}{\partial y}\right) . \qquad \text{(C.8)}$$

In case of pure diffusion processes $\vec{v}(x,y) = (0,0)$ and a variable diffusion coefficient in space, a "counter term velocity" was introduced for the particle velocities in addition to the coupling terms (Eq. 3.31), that is:

$$\vec{v}'(x,y)= \left(\frac{\partial D_m}{\partial x}, \frac{\partial D_m}{\partial y}\right) . \qquad \text{(C.9)}$$

[35] These counter terms are meaningless if another numerical approach is used for the transport description, e.g. finite differences or finite elements methods.

[36] The porosity is, as a non primary variable within the transport calculation, calculated from the initially known porosity and the accumulated solid precipitation and dissolution reactions, and therefore space and time dependent.

Modification of the transport module - distribution of particles

For a Random-Walk transport description it is necessary to distribute solute mass to particles which will be moved during the transport calculation. The distribution of the particles in a two-dimensional model area is related to that used for the one-dimensional MCOTAC version that is:

A fixed number of particles, $N_{\max}$, is distributed in the model area, so that there are no particles directly on the boundary. Initially, they were set to have a fixed distance between each other, Δx_p, Δy_p, in *x*- and *y*-direction and particles nearest to the boundary have a distance $\Delta x_p / 2$, $\Delta y_p / 2$ to the boundary. Starting with the position for the first particle at ($partx_1$, $party_1$), the procedure for the initial particle distribution delivers positions (*partx(i)*, *party(i)*) for all particles $i>1$, where

$$partx(i) = partx(i-1) + \frac{\Delta x_p}{2} \qquad \text{(C.10)}$$

and

$$party(i) = party(i-1) + \frac{\Delta y_p}{2} \qquad \text{(C.11)}$$

An example for an initial particle distribution is given in Fig. C.1. Due to non-zero gradients of some transport parameters and the Random-Walk transport description, the number of particles per grid cell will vary. If the number of particles in a certain cell will be “too low”, a redistribution is foreseen for particles in the model area.

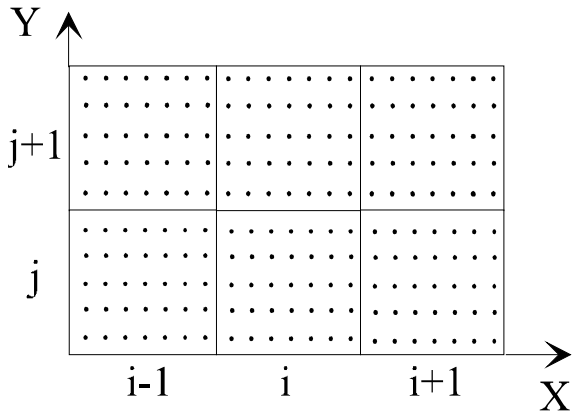

Fig. C.1: Representative particle distribution in the model area at the beginning of the Random-Walk transport calculation. The grid cells (*i, j*) represent the distribution of the immobile solids and related porosity, diffusion/dispersion coefficient, Darcy flux, hydraulic conductivity etc.

The initial system set-up in a heterogeneous medium, or, in cases of heterogeneously distributed sources within the model domain, can be adjusted by an initial particle distribution. It is related to chemical gradients and mineral fronts, where a higher particle density in space is necessary to have an appropriate representation of the species in solution. This is possible by defining a related initial particle distribution. As time evolves, a redistribution of particles is possible in cases of "too less particles in a grid cell" or in cases of time dependent external sources.

Because the Random-Walk transport description in principal is independent of the spatial grid used, the spatial grid can be chosen to match the system geometry. This can be an equidistant rectangular grid, grids with variable grid spacing and also grids with special geometry, e.g. cylinder geometry. This might be helpful for the system set-up if spatial hydraulic, transport and chemical heterogeneity have to be considered.

Interpolation of particle parameters

The Random-Walk transport description is possible if the velocity and/or the hydrodynamic dispersion coefficient is known, or can be calculated at each particle location in the two-dimensional model area. This will be no problem if, as for the one-dimensional version of MCOTAC, constant transport parameters were assumed. If variable transport parameters in time and space are assumed, an interpolation of the transport parameters from the grid to the location of each particle is necessary. (A finite

differences model is used to calculate the Darcy velocities related to the same grid used for the description of the solid concentrations and the porosity.) There are several procedures reported in the literature: [Prickett et al. 1982] proposed a quite thorough and expense one, which gives good values for areas near pumping wells where steep gradients in the flow field occur. But this procedure was recommended to be complicated, and more important here, slow because many calculations are needed for the interpolation. Here, a procedure proposed by [Roach 1972] was used. It was recommended to be simple and also fast. The principle of this procedure can be seen in Fig. C.2

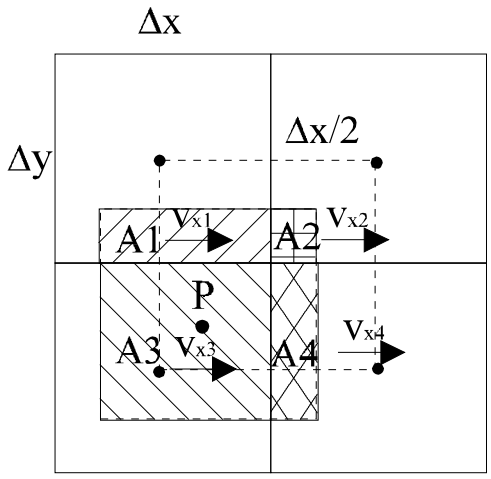

Fig. C.2: Sketch to visualise the interpolation procedure used to interpolate transport parameters, which are related to a spatial grid spacing $(\Delta x, \Delta y)$ as for example, water flow velocity, porosity and hydraulic conductivity, to transport parameters which are related to a particle at location P. Particle related transport parameters are weighted with respect to the relative position of the spatial $(\Delta x, \Delta y)$ grid to an equivalent grid element with centre P, the location of the particle, by their spatial overlap areas A1, A2, A3 and A4 .

For example, particle velocities are interpolated according to Fig. C.2 by:

$$v_{Px} = \frac{A1v_{x1} + A2v_{x2} + A3v_{x3} + A4v_{x4}}{\Delta x \Delta y} \qquad \text{(C.12)}$$

$$v_{Py} = \frac{A1v_{y1} + A2v_{yx2} + A3v_{y3} + A4v_{y4}}{\Delta x \Delta y} \qquad \text{(C.13)}$$

Same as for the velocity, the diffusion coefficient must be a known transport parameter for each particle. It is calculated by the same interpolation described above. Also the gradients of the dispersion coefficient were calculated by a similar interpolation procedure. These parameters are assumed to characterise spatial medium properties according to a finite differences grid. They are calculated to a central finite differences approach with A1=A2=A3=A4=Δx/2·Δy/2 (Fig. C.2). The calculation of the gradient is necessary to have an equivalent description of transport by the two-dimensional transport equation and the Random-Walk description by a statistical ensemble (see Chap.3.2).